



TÜBINGER GEOWISSENSCHAFTLICHE ARBEITEN (TGA)

Reihe C:
Hydro-, Ingenieur- und Umweltgeologie

Schriftleitung:
G. Teutsch, G. Einsele

Peter Merkel

Desorption and Release of Polycyclic Aromatic Hydrocarbons (PAHs) from Contaminated Aquifer Materials

TGA, C32, 1996

Desorption and Release of Polycyclic Aromatic Hydrocarbons (PAHs) from Contaminated Aquifer Materials

Peter Merkel

*Lehrstuhl für Angewandte Geologie
Institut für Geologie und Paläontologie
Universität Tübingen
Sigwartstraße 10
72076 Tübingen
FRG.*

Herausgeber:

Institut und Museum für Geologie und Paläontologie
der Universität Tübingen
Sigwartstraße 10, D-72076 Tübingen

Schriftleitung der Reihe C:

Lehrstuhl für Angewandte Geologie
Prof. Dr. G. Teutsch & Prof. Dr. G. Einsele

ISSN 0935-4948

Acknowledgements

This work was supported by PWAB (Projekt Abfall-Wasser-Boden PW 89 081; PW 92 113). I would like to thank Prof. Dr. emer. G. Einsele who started me off on this project and Prof. Dr. G. Teutsch for his continuing support. Special thanks go to my advisor Prof. Dr. P. Grathwohl for his constant interest and expertise, which are very much appreciated. Without my 'fellow inmates' at the MNF life could have been a bleak one; so thanks to everybody. Special thanks go to Sybille Kleineidam, Christoph Schüth and Willi Pyka for endless discussions, support and divergence.

The older I get, the more stupid I feel.....

Joe Jackson

Desorption and Release of Polycyclic Aromatic Hydrocarbons (PAHs) from Contaminated Aquifer Materials

PETER MERKEL¹

Abstract: Contaminations of aquifer material in the subsurface by PAHs are a widespread source of groundwater contaminations at practically all former manufactured gas plants and coking plants. Possible risks that arise for the groundwater quality in the vicinity of such sites depend largely on the release rates of contaminants from the site into the adjacent groundwater body. Recent field studies and laboratory experiments indicate that the emission of contaminants appears to be controlled by two major processes: dissolution of PAHs from residual coal tar and the desorption of PAHs from soil solids. Interaction of dissolved organic species with aquifer- or soil solids e.g. sorption and desorption, depend on the physical-chemical parameters of the contaminant as well as of those of the aquifer material. As the transfer of contaminants into the aqueous phase (from sorption sites in the intraparticle domain or out of residual phase) may be facilitated by molecular diffusion, the time scale that has to be considered for remediation actions is controlled by the effective transfer coefficients. The scope of this study was to measure the pollutant release rates in benchscale column experiments. The samples consisted of various aquifer materials either from aged contamination sites or aquifer materials that were contaminated under controlled laboratory conditions and left to interact for extended periods of time (hundreds of days). Desorption of PAHs from the contaminated aquifer sands appears to be completely reversible. The derived diffusion rate constants are in agreement with those achieved in sorption experiments. Increasing hydrophobicity of the PAHs is reflected by decreasing diffusion rate constants and is in accordance with the retarded pore diffusion model. Monitoring over extended periods of time may expose changing desorption regimes. An initial period of high release rates is followed by an extended period of slowly declining fluxes. Derived long-term rate constants facilitate predictions as to future release rates and times for contaminant removal. In any case the predicted release rates are a conservative estimate and represent maximum values. Diffusion rate constants are temperature dependent. Activation energies derived from temperature controlled experiments yield values that indicate hindrances other than retarded pore diffusion in an aqueous environment, e.g. rate limitation due to intrasorbent diffusion or constrictivity effects. The use of surfactants to increase release rates seems to have only limited effect on PAHs sorbed in the intraparticle domain. Samples containing residual tar phase show a correlation between release rates and flow velocities. Effluent concentrations can display maximum solubilities for the respective PAHs. The saturation distance needed to reach maximum saturation in the effluent was found to be on the order of decimeters for PAHs of a K_{ow} higher than 5.2, indicating that even small contaminated domains may cause max. effluent concentrations downgradient. PAH release rates from residual phase at nonequilibrium conditions depend on flow rates. PAH fluxes increase as flow velocities increase. In contrast to equilibrium release the increase is nonlinear.

¹ Dissertation an der Wissenschaftlichen Fakultät der Universität Tübingen
Anschrift des Verfassers: Peter Merkel, Ostpreußenstr. 22, 64367 Mühlital

Desorption und Freisetzung von polyzyklischen aromatischen Kohlenwasserstoffen (PAK) aus kontaminierten Aquifermaterialien

Kurzfassung: Durch PAK verursachte Untergrundverschmutzungen stellen eine weitverbreitete Ursache für Grundwasserverschmutzungen an fast sämtlichen ehemaligen Gaswerksstandorten dar. Mögliche Risiken für die Grundwasserqualität in der Umgebung solcher Standorte beruhen zum größten Teil auf den Freisetzungsraten der Schadstoffe in den umgebenden Grundwasserkörper. Neuere Feld- und Laborstudien deuten darauf hin, daß die Emission von Schadstoffen hauptsächlich von zwei Prozessen gesteuert wird: der Lösung von PAK aus residualen Teerölen und der Desorption aus Bodenpartikeln. Die Wechselwirkung zwischen gelösten organischen Wasserinhaltsstoffen und Aquifer- oder Bodenmatrix, wie z.B. Sorption und Desorption, hängt von den physikalisch-chemischen Parametern sowohl des Schadstoffs als auch der Bodenmatrix ab. Da der Transport gelöster Schadstoffe (von Sorptionsplätzen im Korninneren, wie auch aus der residualen Phase) der molekularen Diffusion unterliegt, sind die Zeiträume, die für Sanierungen angesetzt werden, von den Diffusionsratenkonstanten abhängig. Ziel dieser Arbeit war es, Schadstofffreisetzungsraten in Säulenversuchen im Labormaßstab zu ermitteln. Bei den Proben handelte es sich um Aquifermaterialien aus alten Schadensfällen oder Material, das unter Laborbedingungen kontaminiert und über lange Zeiträume equilibriert wurde (mehrere hundert Tage). Die Desorption von PAK aus kontaminierten Sanden ist nach diesen Ergebnissen völlig reversibel. Die erhaltenen Diffusionsratenkonstanten stimmen mit denen aus Sorptionsexperimenten unter Berücksichtigungen der Anfangsbedingungen überein. Zunehmende Hydrophobizität bei PAK spiegelt sich in abnehmenden Diffusionsratenkonstanten wieder, was für eine retardierte Porendiffusion spricht. Die Entwicklung der Austragsraten kann unterschiedliche Phasen durchlaufen. Anfänglich hohe Austragsraten werden von einer Periode mit nur langsam sinkenden Freisetzungsraten abgelöst. Die ermittelten Langzeitdiffusionsratenkonstanten ermöglichen Prognosen über zukünftig zu erwartende Freisetzungsraten und die voraussichtliche Dauer einer Dekontamination. Auf jeden Fall stellen die ermittelten Freisetzungsraten eine konservative Abschätzung dar und entsprechen den maximal zu erwartenden Raten. Die Diffusionsratenkonstanten sind temperaturabhängig. Aktivierungsenergien aus temperaturkontrollierten Experimenten ergeben Werte, die für einen weiteren limitierenden Prozess neben der retardierten Porendiffusion in wässriger Umgebung sprechen, wie z.B. Intrasorbentdiffusion. Die Anwendung von Tensiden scheint nur begrenzten Einfluß auf im Intrapartikelraum sorbierte PAK zu haben. Proben mit residualem Teerphase zeigen eine Korrelation zwischen Fuß und Freisetzungsraten. Konzentrationen können die maximale Löslichkeit erreichen. Die Fließstrecke zum Erreichen der Wassersättigung für PAK mit einem K_{ow} von 5.2 und mehr liegt im Dezimeterbereich, was bedeutet, daß selbst kleine Verschmutzungsherde abstromig zu Konzentrationen im Grundwasser im Bereich der Löslichkeit führen können. PAK-Freisetzung aus residualer Phase unter Nichtgleichgewichtsbedingungen sind abhängig von der Fließgeschwindigkeit und steigen mit zunehmender Fließgeschwindigkeit an. Im Gegensatz zu Freisetzung unter Gleichgewichtsbedingungen zeigt diese Zunahme keine lineare Korrelation zur Fließgeschwindigkeit.

Contents

1. Introduction	1
1.1 Research Significance	1
1.1.1 Tar Contaminated Sites	1
1.1.2 Migration Processes of Coal Tar	1
1.1.3 Physico-Chemical Properties of PAHs	1
1.1.4 Research Objectives	4
2. Physical and Chemical Principles	5
2.1 Solute Transport	5
2.2 Hydrodynamic Processes	
2.2.1 Advection	5
2.2.2 Hydrodynamic Dispersion	5
2.3 Sorption and Desorption Phenomena	6
2.3.1 Sorption Mechanisms	6
2.3.2 Sorption Isotherms	7
2.3.3 Natural Organic Matter Partitioning	8
2.3.4 Nonequilibrium Transport	8
2.3.5 Mass Transfer Rates	9
2.3.5.1 Film Diffusion	9
2.3.5.2 Pore Diffusion	10
2.3.5.3 Rate Limitations Due to Pore Geometry and Steric Hindrances	11
2.3.5.4 Intra-Organic Matter Diffusion	12
3. Modeling of Desorption and Contaminant Release	13
3.1 Desorption Limited by Spherical Intraparticle Diffusion	13
3.1.1 Desorption in Case of Prior Equilibration	13
3.1.2 Modeling Desorption for Heterogeneous Mixture	14
3.1.3 First-Order Kinetics	15
3.1.4 Concomitant First Order Kinetics and Intraparticle Diffusion	15
3.1.5 Determination of Diffusion Rate Constants from Column Experiments	16
3.1.6 Sensitivity Analysis of the Diffusion Model with Respect to Mass Recoveries	16
3.1.7 Desorption in Poorly Equilibrated Systems	17
3.2 Release of PAHs from Residual Coal Tar	18
3.2.1 Evaluating Equilibrium Release of PAHs in Column Experiments	18
3.2.2 Evaluating Nonequilibrium PAH Release from Coal Tar	19
4. Materials and Laboratory Methods	21
4.1 Materials	21
4.1.1 Aquifer Sands	22
4.1.2 Samples from Former MPG Sites	22
4.2 Sample Characterization	22
4.2.1 Carbonate Content	22
4.2.2 Density	22
4.2.3 Organic Carbon Content	22
4.2.4 Intraparticle Porosity and Internal Surface	23
4.2.5 Results	23

4.2.5.1 Density, Carbonate Content, Organic Matter Content	24
4.2.5.2 Internal Porosity and Internal Surfaces	24
4.3 Experimental Concept	26
4.3.1 Column Setup	26
4.3.2 Experimental Implementation and Sample Handling	26
4.3.3 Surfactants	27
4.4 Analytical Methods	27
4.4.2 Soil Samples	28
4.4.2.1 Soxhlet Extraction	28
4.4.2.2 Supercritical Fluid Extraction (SFE)	28
4.4.3 PAH Analysis	29
4.4.3.1 HPLC Chromatography	29
4.4.3.2 GC/MS Analysis	30
5. Desorption from Contaminated Aquifer Material	31
5.1 Desorption from Rhine Sand	31
5.1.1 Sorption History	31
5.1.2 Desorption Behavior of Rhine Sand (RS)	31
5.2 Desorption from Neckar Sand (NS)	34
5.2.1 Sorption History	34
5.2.2 Desorption Behavior of Neckar Sand	34
5.3 Desorption from Allgäusand (AS)	37
5.3.1 Sorption History	37
5.3.2 Effects of Nonequilibrium Conditions	37
5.3.3 Desorption Behavior of Allgäu Sand	37
5.3.3.1 Desorption of NAP and FTH	37
5.3.3.2 Desorption of PAH Mixture	39
5.4 Summary and Discussion	42
6. PAH Release from Gasworks Site Material	44
6.1 Desorption Experiments of the Heidenheim Materials	44
6.1.1 Desorption of PAH from the 'Light' Fraction (0.25-0.5 mm)	44
6.1.2 Temperature Effects on Desorption	46
6.1.2.1 Nature of Temperature Dependencies	47
6.1.2.2 Determination of Activation Energies	48
6.1.3 Desorption of the 'Dark' Fractions	50
6.1.3.1 Desorption from the 0.25- 0.5 mm Fraction	50
6.1.3.2 Desorption from the 1-2 mm Fraction	51
6.1.4 Summary	52
6.2 PAH Release from Materials Containing Residual Coal Tar	54
6.2.1 Validation of Equilibrium PAH Release	54
6.2.2 PAH Release from Karlsruhe Material	55
6.2.2.1 Modeling Equilibrium PAH Release	56
6.2.2.2 Nonequilibrium PAH Release from KA Material	58
6.2.3 Summary and Discussion	60
7. Conclusions	62
8. Bibliography	64
9. Appendices	70

Nomenclature

a	Radius of a Sphere	[L]
C	Concentration of a Compound in a Medium	[ML ⁻³]
C_{eq}	Uniform Equilibrium Concentration on Solids	[M/M]
C_w	Aqueous Concentration	[ML ⁻³]
C_w^{sat}	Aqueous Saturation Concentration of a Compound	[ML ⁻³]
C_w^{sat*}	Aqueous Saturation Concentration of a Compound from Complex Mixtures	[ML ⁻³]
C_s	Concentration Sorbed onto Solids	[M/M]
C_{max}	Max. Surface Concentration (Used in Langmuir Isotherm)	[M]
D_a	Apparent Diffusion Coefficient	[L ² T ⁻¹]
D_a/a^2	Diffusion Rate Constant	[T ⁻¹]
D_{aq}	Diffusion Coefficient in Water	[L ² T ⁻¹]
D_{eff}	Effective Diffusion Coefficient	[L ² T ⁻¹]
D_l	Longitudinal Dispersion Coefficient	[L ² T ⁻¹]
f_{oc}	Organic Carbon Content	[-]
E_a	Activation Energy	[Jmol ⁻¹]
F	Diffusive Flux	[MT ⁻¹]
F'	Dimensionless Flux ($F/(M_{eq}D_a/a^2)$)	[-]
F_w	Flow Velocity	[LT ⁻¹]
K_d	Distribution Coefficient Solid/Water	[L ⁻³ M ⁻¹]
K_f	Freundlich Partition Coefficient	[-]
k	Mass Transfer Coefficient	[LT ⁻¹]
K_l	Langmuir Sorption Coefficient	[-]
K_{oc}	Partition Coefficient with Respect to Organic Carbon	[L ³ M ⁻¹]
K_{ow}	Octanol/Water Partition Coefficient	[-]
L_{sat}	Saturation Distance	[L]
M	Remaining Mass Sorbed on Solids	[M]
M_{eq}	Total Mass Sorbed on Solids at Equilibrium	[M]
M_s	Initially Sorbed Mass	[M]
M_{te}	Total Mass Sorbed on Solids after an Exposure Time t_e	[M]
n_e	Effective Porosity	[-]
Pe	Peclet Number	[-]
R	Universal Gas Constant	[Jmol ⁻¹ K ⁻¹]
S_w	Molar Solubility	[Mol/L ³]
Sh	Sherwood Number	[-]
r	Radial Distance to the Center of a Sphere ($0 > r \leq a$)	[L]
T	Time	[T]
t_e	Period of Sample Exposure to Sorbate Prior to Desorption	[T]
t_{90}	Time to Reach 90 % of Desorption	[T]
V'_B	LeBas Molar Volume	[L ³ mol ⁻¹]
V_w	Volume of Water-Filled Pore Space	[L ³]
v_x	Pore Velocity	[LT ⁻¹]
X_i	Fraction of Fast Desorbing Mass with Respect to the Total Mass	[-]

Ancronyms

<i>ACE</i>	Acenaphthene
<i>ANY</i>	Acenaphthylene
<i>ANT</i>	Anthracene

AS	Allgäu Sand
<i>B(a)A</i>	Benzo(a)anthracene
<i>B(k)F</i>	Benzo(k)fluoranthene
CHR	Chrysene
DNAPL	Dense Nonaqueous Phase Liquid
FL	Fluorene
FTH	Fluoranthene
HH	Heidenheim
MGP	Manufactured Gas Plant
NAP	Naphthalene
NS	Neckar Sand
PAH	Polycyclic Aromatic Hydrocarbon
PHE	Phenanthrene
RS	Rhine Sand
TCE	Trichloroethene

Greek Symbols

α_l	Dispersivity	[L]
α	Capacity Factor	[-]
β	Ratio of Solute Mass Dissolved to Mass Sorbed in Equilibrium	[-]
χ	Molar Fraction of a Compound in a Complex Mixture of Organics	[-]
ρ	Bulk Density of Porous Media	[ML ⁻³]
γ	Activity Coefficient	[-]
δ	Constrictivity Factor	[-]
λ	First-Order Mass Transfer Coefficient	[T ⁻¹]
λ_p	Ratio Solute Diameter/Pore Diameter	[-]
ε	Total Porosity of a Media, Intraparticle Porosity	[-]
ε_t	Transport Effective Porosity (Interparticle Porosity)	[-]
τ_f	Tortuosity Factor	[-]
μ	Dynamic Viscosity	[ML ⁻¹ T ⁻¹]

1. Introduction

1.1 Research Significance

1.1.1 Tar Contaminated Sites

Massive subsurface contaminations caused by coal tar and tar related products are found at virtually every major gas manufacturing site. Coal tar is formed as a by-product during the carbonization of coal and is made up of a complex mixture of many hydrocarbons. PAHs (Polycyclic Aromatic Hydrocarbons) which are major constituents of these complex mixtures have been shown to act carcinogenic, toxic and mutagenic, thus creating a considerable hazard to the environment. The number of gasworks sites in former West Germany is estimated to be on the order of 1000 sites (GUTSCHE and HEIKE, 1990). Many of these production sites operated over extended periods of time (order of decades). Poor safety standards (leaking pipes and tanks) and sometimes deliberate introduction of coal tar into the subsurface led to a severe contamination of the subsurface environment. The costs involved in remediation of all former gasworks sites in West Germany are an estimated 10 billion DM (GUTSCHE and HEIKE, 1990).

In order to understand the fate and transport of coal tar constituents and the groundwater risk it is necessary to characterize the processes in the subsurface that are involved in the release of a contaminant into the groundwater. Knowledge of the specific behavior of a contaminant in the subsurface environment of a specific site is a prerequisite for the selection of cost effective remediation schemes.

1.1.2 Migration Processes of Coal Tar

The migration of complex DNAPL mixtures (Dense Non-Aqueous Phase Liquids), such as coal tar oils in the subsurface, depends on many factors. These include site specific parameters as well as material characteristics (CHERRY and FEENSTRA, 1988), such as:

- the volume of DNAPLs released per unit infiltration area
- the time frame of infiltration
- properties of the DNAPL constituents (e.g. density, viscosity).
- hydrodynamic characteristics of the subsurface

The mobility of DNAPLs in the subsurface is influenced by three forces (MERCER and COHEN, 1993):

- the pressure due to gravity
- capillary pressure
- hydrodynamic pressure

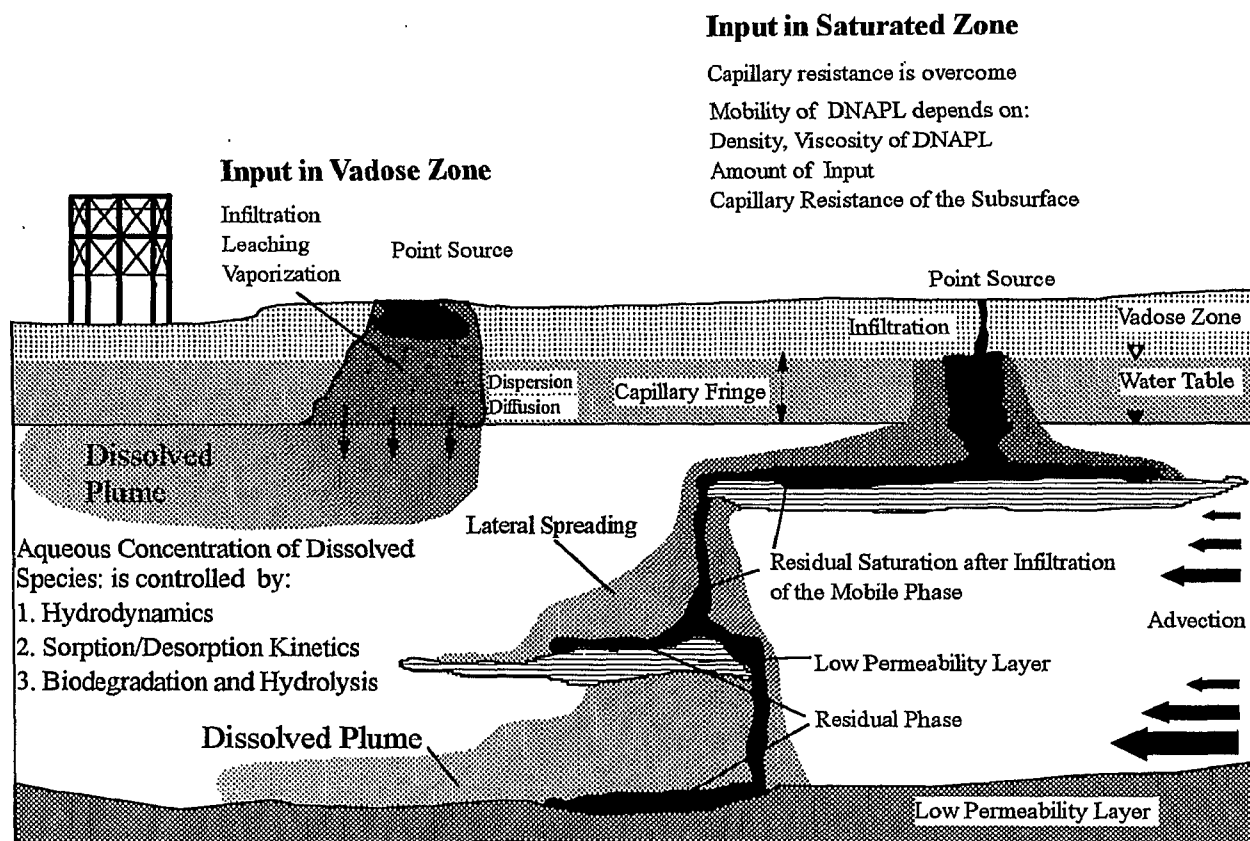
The interaction of all processes results in inherent migration patterns in the vadose as well as in the phreatic subsurface.

Although in most contaminated sites the release can be approximated as point inputs, the extent of subsurface spreading can be very complex and change substantially in lateral and vertical direction (see Fig. 1-1). Conceptual models of multiphase transport processes of DNAPLs in various hydrogeological settings have been given by several authors (e.g. KUEPER and FRIND, 1991; SCHWILLE, 1988; MACKAY and CHERRY, 1989). An understanding of the prevailing processes of emplacement is necessary to evaluate sites and locate possible areas of contamination.

1.1.3 Physico-Chemical Properties of PAHs

The smallest subunit of PAHs is the benzene ring. The ability of the electrons of forming π -bonds that cover regions of more than 1 atom in the ring (delocalization) results in a lower energy level of the molecule and thus in a greater stability (conjugated bonds) (SCHWARZENBACH, 1993). PAHs are formed by condensation of 2 or more benzene rings, where the benzene rings share carbon atoms (FETTER, 1993). This formation is linked to incomplete oxidation of organic matter. The

Conceptual Model of Tar Oil Contamination at Gasworks Sites



Input in Saturated Zone

Capillary resistance is overcome
 Mobility of DNAPL depends on:
 Density, Viscosity of DNAPL
 Amount of Input
 Capillary Resistance of the Subsurface

Figure 1-1: Schematic view of typical migration patterns of tar oil contaminations from point sources at gasworks sites. Depending on whether the capillary fringe can be overcome, the tar oil penetrates the saturated zone and is distributed in complex patterns. Once in the subsurface, the aqueous concentration depends on the various processes acting on the PAHs. Hydrodynamic processes and mass transfer rates at the water/tar interface control the release of PAHs into the groundwater. As the dissolved compounds move through the aquifer, they are subject to sorption and retardation with respect to the bulk groundwater movement. Different sorptive behavior will lead to a quasi-chromatographic separation of the compounds, as they move downgradient. In addition, the transport velocities of individual compounds depend on the rates at which they interact with the aquifer material (sorption rates and degradation rates).

minimum temperature for the formation of PAHs found in the literature ranges from 400°C (BJØRSETH, 1978) to 700°C (GRIMMER, 1983). The sources of PAHs are multiple and include distillation fractions from petroleum, asphalt, coal tar, and creosote (FETTER, 1993) to cigarette smoke (SEVERSON ET AL., 1976). Out of the large number of possible PAHs and their isomers, the U.S. Environmental Protection Agency (EPA) selected 16 PAHs for their priority list (see Tab. 1-2). Overviews of distillation methods and the resulting compounds (PAHs only make up a fraction of a coal tar; PYKA, 1994) are given e.g. in IARC (1985) and MERCER and COHEN (1993).

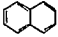
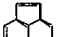
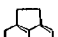
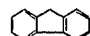
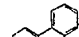
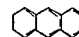
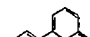
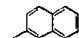

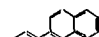
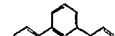

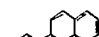

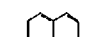
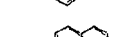
The PAH-related health hazards include carcinogenic and mutagenic effects (FREUDENTHAL and JONES EDS., 1976, 1978) which are caused by metabolites (epoxides) formed by the oxidation of the PAHs. The actual toxicity of PAHs however is considered to be low.

Especially important in this context is the bioaccumulation of PAHs in organisms due to their lipophilicity. Clams have been reported to have accumulated ¹⁴C-benzo[a]pyrene to reach a 236-fold tissue concentration with respect to the aqueous concentration in only 24 hours (ZANDER, 1980). Due to the substantial changes in important physico-chemical parameters, it is obvious that the PAHs will show varying transport behavior. Generally, it can be said that with increasing number of rings the mobility of PAH is reduced.

Table 1-1: Comparison of octanol-water partition coefficients (K_{ow}) of some environmentally relevant organic compounds (NIMMI, 1991) and some PAHs of equivalent hydrophobicity (SIMS and OVERCASH, 1983).

Compounds	K_{ow}	PAHs	K_{ow}
Lindane	3.59	Naphthalene	3.35
Endrin	4.48	Phenanthrene	4.46
PCB 15	5.27	Pyrene	5.32
o,p-DDT	5.75	Benzo(a)anthracene	5.61

Table 1-2: Physico-chemical parameters of the 16 EPA PAHs compiled from :¹ Mackay and Shiu, (1977); ^{2,5} Yalkowsky and Valvani, (1979); ³ Klevens (1950); ⁴ Loyek (pers. com., 1995); ⁶ Miller et al., (1985); ⁷ Sims and Overcash, (1983); # Walther and Luthy, (1984). K_{ow} denotes the octanol/water partition coefficient.

PAH/ Formula	Molar Weight (g/mol)	Vapor Pressure (torr) 20°C	Melting Point (°C)	Aqueous Solubility (mg/l) 25°C			Subcooled Liquid Sol. (mg/l)	log K_{ow}		
				1	2	3		4	5	6
 Naphthalene (C ₁₀ H ₈) (NAP)	128	4.92 · 10 ⁻²	80	30	30.59	12.5	119.43	3.35	3.35	3.37
 Acenaphthylene (C ₁₂ H ₈) (ANY)	154	2.90 · 10 ⁻²	92	#	16.1		84.49	#	4.07	
 Acenaphthene (C ₁₂ H ₁₀) (ACE)	154	2.00 · 10 ⁻²	96	3.47	3.93	4.03	19.96	3.92	4.33	
 Fluorene (C ₁₃ H ₁₀) (FL)	166	1.30 · 10 ⁻²	116	1.98	1.83		18.05	4.47	4.18	4.18
 Phenanthrene (C ₁₄ H ₁₀) (PHE)	178	6.80 · 10 ⁻⁴	101	1.29	1.18	1.6	8.32	4.63	4.57	4.46
 Anthracene (C ₁₄ H ₁₀) (ANT)	178	1.96 · 10 ⁻⁴	216	0.07	0.73	0.075	6.38	4.63	4.54	4.45
 Fluoranthene (C ₁₆ H ₁₀) (FTH)	202	6.00 · 10 ⁻⁶	111	0.26	0.26	0.265	2.11	5.22	5.22	5.33
 Pyrene (C ₁₆ H ₁₀) (PY)	202	6.85 · 10 ⁻⁷	149	0.14	0.13	0.175	2.72	5.22	5.18	5.32
 Benzo(a)anthracene (C ₁₈ H ₁₂) (B(a)A)	228	5.00 · 10 ⁻⁹	158	0.014	0.014	0.01	0.33	5.91	5.91	5.61
 Chrysene (C ₁₈ H ₁₂) (CHR)	228	6.30 · 10 ⁻⁷	255	0.002	0.002	0.006	0.44	5.91	5.79	5.61
 Benzo(b)fluoranthene (C ₂₀ H ₁₂) (B(b)F)	252	5.00 · 10 ⁻⁷	167	0.0012			0.035	6.57		
 Benzo(k)fluoranthene (C ₂₀ H ₁₂) (B(k)F)	252	5.00 · 10 ⁻⁷	217	0.00055			0.035	6.84		
 Benzo(a)pyrene (C ₂₀ H ₁₂) (B(a)P)	252	5.00 · 10 ⁻⁷	179	0.0038	0.0038		0.14	6.50	5.98	6.04
 Dibenzo(a,h)anthracene (C ₂₂ H ₁₄) (D(ah)A)	278	1.00 · 10 ⁻¹⁰	163	0.0005	0.0005		1.66	7.19	5.97	
 Indeno(1,2,3-cd)pyrene (C ₂₂ H ₁₂) (IP)	276	1.00 · 10 ⁻¹⁰	222	0.062			0.13	7.66		
 Benzo(g,h,i)perylene (C ₂₂ H ₁₂) (BP)	276	1.00 · 10 ⁻¹⁰	262	0.00026	0.00026		0.027	7.10	7.10	7.23

This is documented by a decrease of the water solubilities of 6 orders of magnitude and increases of $\log K_{ow}$ of 4 orders of magnitude from Naphthalene (2-rings) to Indeno (1,2,3-cd)pyrene (6-rings). Covering this wide range of parameters, a comparison between other environmentally relevant toxic organic compounds of similar properties is possible (see Table 1-1).

1.1.4 Research Objectives

Once *In-Situ*, the release of contaminants from the residual phase into the groundwater is controlled by several factors, e.g. the interfacial area available for mass transfer and the mass transfer coefficients of the contaminant into the aqueous system. In contrast to nonreactive species (conservative tracers), which are subject to retardation due to diffusion into low permeability domains, the PAHs in the hydrogeological cycle are also subject of interactions between the porous aquifer material and the aqueous phase resulting in sorption and thus retardation. The sorption and desorption processes of a solute in aquifer material are the controlling factors that determine the spreading behavior of contaminants in the groundwater. Recent investigations show that the time required for sorptive uptake and/or desorption processes can reach days to years depending on the aquifer material and the contaminant under consideration (BALL, 1991; SCHÜTH, 1994; SCHÜTH and GRATHWOHL; 1994; GRATHWOHL ET AL., 1994).

For a better understanding of the desorption processes it is necessary to quantify the dynamics of interactions between sorbate and sorbent. Therefore, this investigation addressed several aspects of sorbate and sorbent interaction, which included:

1. Release rates of PAHs from several contaminated materials
2. Dependency of the desorption kinetics on pollutant as well as soil properties
3. Desorption kinetics of PAHs compared with sorption data to check for reversibility

4. Temperature effects on the desorption rates
5. Effects of surfactants on the contaminant release
6. Dissolution/release kinetics of PAHs from residual coal tar
7. Prediction of long-term release rates

To monitor the desorption rates, long-term column desorption experiments were conducted at laboratory scale using aquifer material from two contaminated manufactured gas plants (MGP) sites and aquifer sands commonly found in Southern Germany, which were contaminated in the laboratory. The equilibration time for the laboratory samples exceeded several hundred days to reach a high degree of equilibrium between sorbate and sorbent. The time frame of the experiments allowed to check for possible changes in release rates and to derive long-term estimates of transfer rates of PAHs into the groundwater in contrast to short-term release rates from batch experiments. To evaluate reversibility of diffusive uptake, samples loaded in the laboratory were desorbed and the obtained rate constants were compared. By simultaneously monitoring the release of several PAHs covering a wide range of octanol-water partition coefficients (K_{ow}), the variability of desorption rates for a single aquifer material was evaluated. With the high variability in hydrophobicity the monitored PAHs can be used to estimate the behavior of other nonpolar, hydrophobic contaminants.

As possible ways to enhance the PAH release in the experiments, temperature dependency of desorption was evaluated in controlled experiments and the effect of surfactants on release rates was monitored.

Knowing effective long-term release rates should lead to a better risk assessment of contaminated sites with respect to their influence on the groundwater quality and yield an additional measure to improve remediation schemes.

2. Physical and Chemical Principles

2.1 Solute Transport

The transport of solutes in porous media is affected by several processes, some of which are due to the hydrodynamic conditions imposed on a solute volume by the properties of the aquifer material. Parameters such as the effective porosity and transmissivity control the hydrodynamical processes and thus the bulk movement of groundwater. Superimposed on this bulk movement are processes that include several interactions between the aquifer material and the dissolved reactive species. These processes include sorption and desorption of solute onto and from aquifer material, as well as processes that influence the original concentration of a solute per unit volume such as biodegradation or radioactive decay. Depending on the specific characteristics of both the aquifer material and the physico-chemical characteristics of the reactive species, the transport behavior can differ substantially from that of the bulk movement of groundwater. As all processes may take place simultaneously and lead to similar results (e.g. spreading of a solute plume and decrease of concentrations), it is sometimes difficult to assign the effective processes to an observed transport behavior. In order to investigate the consequences of a process of interest in the laboratory, it is essential to rule out sources that could lead to nonunique interpretations of the observed phenomena.

2.2 Hydrodynamic Processes

Hydrodynamic processes include all effects in a flow system that have an immediate influence on the transport behavior of water particles and nonreactive species. The combined hydrodynamic effects can be subdivided into two basic processes, advection and dispersion.

2.1.1 Advection

Advection is the portion of solute movement that is solely attributed to the transport by the

bulk motion of flowing groundwater. The average linear velocity in advective transport can readily be obtained using Darcy's law couched in terms of

$$v = \frac{k}{n_e} \frac{\partial h}{\partial l} \quad (2-1)$$

where k is the hydraulic conductivity [LT^{-1}], n_e the transport effective porosity [-], and $\partial h/\partial l$ the hydraulic gradient [-].

2.2.2 Hydrodynamic Dispersion

Hydrodynamic dispersion consists of two processes which both lead to a spreading of a solute during transport. Mechanical dispersion is caused by mixing processes resulting from different flow trajectories of individual water and solute particles in a porous media. The varying flow velocities spread around the average linear velocity, as different particles "see" irregular paths in the media. The degree of spreading around the advective front is a function of both the media and the pore velocity and is described by the dispersion coefficient

$$D_l = \alpha v \quad (2-2)$$

with α being equal to the dispersivity [L], an empirical material constant, and the linear velocity v [LT^{-1}]. Dispersivity is closely related to the scale under consideration. At large scales α reflects aquifer heterogeneities, at the pore scale diffusion and differential pore velocities. Upscaling generally leads to increasing values of D_l , as more and more inhomogeneities are encountered by the particles.

In addition to Darcy's law, where solute movement is due to a gradient in the hydraulic heads, there is also transport of solutes due to a concentration gradient. Molecular diffusion is caused by random movement of molecules (Brownian Motion) due to their thermal

kinetic energy. For molecular diffusion the movement of solute under steady-state conditions is described by Fick's 1st Law

$$F = -D_p \frac{\partial C}{\partial l} \quad (2-3)$$

where F is the diffusive flux [ML⁻²T⁻¹], D_p the pore diffusion coefficient [L²T⁻¹], and $\partial C / \partial l$ [-] the concentration gradient. The pore diffusion coefficient takes into account the tortuous pathways in a porous media which effect diffusive fluxes. D_p is expressed as

$$D_p = \frac{D_{aq}}{\tau_f} \quad (2-4)$$

where D_{aq} [L²T⁻¹] is the diffusion coefficient in water. The tortuosity factor (τ_f) is the squared tortuosity, which accounts for the geometrical structure of the pore space (dividing the diffusive path length in the porous media by the fictional straight line distance in case of diffusion in a nontortuous media).

The hydrodynamical dispersion coefficient in a porous media for transient conditions incorporating both a diffusive and a dispersive process can be written as

$$D_l = \frac{(\alpha_l v + D_p)}{R} \quad (2-5)$$

where R is the retardation factor [-] which corrects for the altered transport behavior of a solute that interacts with the aquifer matrix in comparison to a conservative species in solution.

Although diffusive fluxes are generally small and advective transport, if present, accounts for the bulk share of solute movement, diffusion plays an important role in the mass transfer from low permeability zones, aquifer solids, and residual DNAPLs to the mobile aqueous phase.

2.3 Sorption and Desorption Phenomena

The effectiveness of solute transport in the subsurface depends largely on the degree, to which solutes are exposed to advective and dispersive processes. Sorptive processes will tend to remove dissolved species from the mobile phase and therefore alter their transport behavior with respect to the bulk groundwater movement.

The general term of sorption includes attractive processes that take place at surfaces (adsorption), as well as the movement of solute into an immobile phase, e.g. organic matter (absorption). Sorption of neutral organic compounds, in contrast to chemisorption, which alters the sorbed constituents in a chemical reaction, is regarded to be due to establish only weak intermolecular attractions between sorbate and sorbent. These bondings are considered to be reversible (KARICKHOFF, 1979; SCHWARZENBACH ET AL., 1993; CHIOU ET AL., 1983) and therefore imply that the desorption of organic solutes tends to follow similar processes as the sorptive uptake.

However, the effect of any sorptive process on the transport behavior of a solute is controlled by the rate at which these processes take place with respect to advection. To evaluate sorptive uptake and desorption, sorption mechanisms must be described and classified for respective solid phase/mobile phase systems. The superposition of this mass transfer between aquifer solids and the mobile phase will result in the specific transport characteristics of a solute in the subsurface.

2.3.1 Sorption Mechanisms

The transfer of dissolved species out of a solution and the subsequent accumulation in or on solids (sorption) can be due to several processes. As PAHs are nonpolar molecules and lack polar functional groups, sorption mechanisms such as ion-pair bondings and ion exchange between sorbate and sorbent are not possible. The attractive forces between nonpolar molecules and solid surfaces are weak London and van der Waal forces. As

solute molecules approach a surface, the electrons of both the surface molecules and the solute interact inducing dipole-dipole and quadrupole-quadrupole moments which result in weak electrostatic attractive forces (VOICE and WEBER, 1983). These forces have a very limited range and decrease in amplitude following power laws (sixth to tenth power), as the distance between the surface and the solute molecules increases (WEBER ET AL., 1991).

The main reason for the sorption of hydrophobic molecules, however, is due to interactions between the water molecules and the hydrophobic molecules. The solution of water-borne hydrophobic molecules can only be achieved by an arrangement of water molecules of ice-like structured crystals (FRANK and EVANS, 1945). The coordination of water molecules around a dissolved molecule is generally exothermic, leading to a decrease of the systems enthalpy. The solution's entropy, however, changes, as the solvent (water) molecules achieve a greater degree of order. Hydrophobic bonding leads to a gain in entropy upon the breakup of the ordered structure around dissolved hydrophobic molecules (PIGNATELLO, 1989; HASSETT and BANWART, 1989). The tendency of a solute to undergo hydrophobic bonding will depend on the amount of entropy gained by the removal of the hydrophobic compound from the solution. As the amount of entropy gained increases with the size of the nonpolar molecule (large molecules need more structured water molecules to be kept in solution), larger molecules have higher tendency to undergo sorption and therefore show decreasing mobility in the subsurface.

2.3.2 Sorption Isotherms

In order to determine the relative abundance of a particular species in a solution at equilibrium condition, it is necessary to quantify the concentration on the solid with respect to a defined volume of water. The distribution of a solute between solid phase and aqueous phase can simply be visualized by plotting the concentrations on solids vs. the corresponding aqueous concentrations at constant temperature. Such sorption isotherms may show dif-

ferent shapes depending on the sorption processes involved.

Langmuir isotherms describe surface sorption and are based on the assumption that only a limited number of sorption sites are available. The equilibrium concentration on the solid phase is calculated using

$$C_s = \frac{K_l C_{max} C_{aq}}{1 + K_l C_{aq}} \quad (2-6)$$

with K_l the Langmuir coefficient and C_{max} the maximum surface concentration.

A commonly used relationship to fit experimental data in soils is the Freundlich isotherm (FREUNDLICH, 1903)

$$C_s = K_F C_w^{1/n} \quad (2-7)$$

where C_s [MM^{-1}] is the concentration on the solid, C_w [ML^{-3}] the concentration in the aqueous phase, and K_F [-] the Freundlich coefficient. The exponent $1/n$ is used to describe the degree of nonlinearity over the measured concentration range.

In the special case of $1/n = 1$, the distribution becomes independent of the concentration range and results in a linear isotherm. The slope of this isotherm defines the distribution coefficient K_d [L^3M^{-1}], and the isotherm is

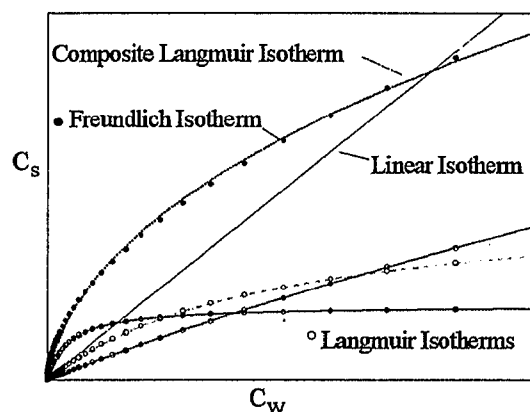


Fig. 2-1: Plot of Langmuir- and Freundlich isotherms in contrast to a linear sorption isotherm. The three Langmuir isotherms represent different populations of a mixed sample that show different sorption behavior. The composite Langmuir isotherm delineates the resulting isotherm of the mixture. Note that over a limited concentration range the three superimposed Langmuir isotherms seem to add up to a Freundlich type isotherm.

given by

$$C_s = K_d C_w \quad (2-8)$$

In heterogeneous media, the superposition of several Langmuir-type sites can add up to form a Freundlich-type isotherm over a limited concentration range (Fig. 2-1). A Freundlich isotherm would then be the result of a mixture of components having different sorption capacities. For the description of a concentration dependent sorption (desorption) it is possible to use a Freundlich isotherm with an exponent other than 1, or isotherm models such as the Langmuir-, BET- (BRUNAUER ET AL., 1938) isotherms.

2.3.3 Natural Organic Matter Partitioning

Sorption of nonpolar compounds onto aquifer material is closely correlated to the content and nature of organic matter (LAMBERT, 1965; CHIOU ET AL., 1983; KARICKHOFF, 1984; GRATHWOHL, 1990; RUTHERFORD ET AL., 1992). If there are non- or less polar sorption sites in an aqueous system, e.g. humic acids or soil organic matter, it is thermodynamically of advantage to drive out the solute from the water phase. The hydrophobic molecules will be sorbed in this "nonpolar" environment.

Therefore, the distribution coefficient for specific aquifer material/solute combination can be normalized with respect to the organic carbon content and is defined as (KARICKHOFF ET AL., 1979)

$$K_{oc} = \frac{K_d}{f_{oc}} \quad (2-9)$$

with f_{oc} being equal to fraction of the soil's organic carbon content [-]. The various types of soil organic matter (SOM) form 3-dimensional "networklike porous" macromolecules (SCHWARZENBACH, 1993). CAROLL ET AL. (1994) hypothesize that organic matter is composed of swollen and condensed humic polymers which show a distinct bimodality in desorption rates. These structures can physically incorporate smaller molecules and absorb them at sorption sites within the SOM. The wide range of composition in SOM is reflected by varying K_{oc} s (GRATHWOHL, 1990; GARBARINI and LION, 1985).

In order to estimate the behavior of various organic compounds in aquifer materials, several authors have introduced a relationship between K_{oc} and the octanol-water partition coefficient K_{ow} (CHIOU ET AL., 1983; KARICKHOFF ET AL., 1979), with

$$K_{ow} = \frac{C_{octanol}}{C_{water}} \quad (2-10)$$

Octanol has been a widely used reference phase for the partitioning of organic compounds in an organic phase/water system leading to a large data base for environmental relevant organic chemicals (e.g. NIIMI, 1991). Using

$$\log K_{oc} = a \log K_{ow} + b \quad (2-11)$$

can give an estimate of the equilibrium sorptive capacity of a material. Depending on the reference cited the values of the constants a and b may vary and lead to a range of possible K_{oc} s. Tab. 2-1 shows several empirically derived K_{oc} relationships

The affinity for organic matter cannot only lead to considerable retardation, but organic contaminants may experience fast transport velocities when sorbed onto dissolved organic macromolecules such as humic acids or fulvic acids (MAGGEE ET AL., 1991). PYKA (1994), however, considers enhanced transport due to the presence of e.g. humic acids to be of minor importance for natural groundwaters and compounds with $\log K_{ow} < 5.5$.

2.3.4 Nonequilibrium Transport

Recent studies indicate that sorption of organic contaminants in subsurface systems is limited by low transfer rates to sorption sites rather than by sorption reactions *per se* (e.g. WEBER ET AL., 1991, BALL and ROBERTS, 1991; GRATHWOHL, 1994; SCHÜTH, 1994). Nonequilibrium in batch sorption experiments

Table 2-1: Empirically derived constants for the calculation of K_{oc} (Eq. 2-11).

Reference	a	b
Karickhoff et al. (1979)	1	-0.21
Sontheimer et al. (1983)	0.807	0.068
Chiou et al. (1983)	0.904	-0.542

e.g. is documented by prolonged times of sorptive uptake (BALL and ROBERTS, 1991; KLEINEIDAM, 1992; GRATHWOHL, 1992). Column purge experiments show typically enhanced asymmetrical breakthrough curve (BTC) characteristics which also depend on the purge velocities. The degree of asymmetry of a BTC decreases with growing contact times in the solute/solid system (SCHWARZENBACH AND WESTALL, 1981; SCHÜTH, 1994b; PIGNATELLO ET AL., 1993). These processes are also active in groundwater flow, as aquifer geometries with high/low velocity domains result in regions of long and short contact times. Depending on the amount and the capacity of the available sorption sites in these zones, nonequilibrium transport will be more or less pronounced.

The Local Equilibrium Assumption (LEA) which assumes instantaneous equilibrium between the stationary phase (aquifer solids) and the mobile phase (VALOCCHI, 1985; BAHR, J.M. and RUBIN, J., 1987) will lead, when incorporated in transport considerations, to unrealistically high retardation factors.

As sorptive processes are taking place at a microscale (grain-scale) level, it is necessary to consider the inherent physical characteristics of the aquifer components (GRATHWOHL and KLEINEIDAM, 1995; WEBER ET AL., 1992). The physico-chemical parameters of the individual components give important clues regarding the sorption kinetics and thus transfer characteristics of contaminants.

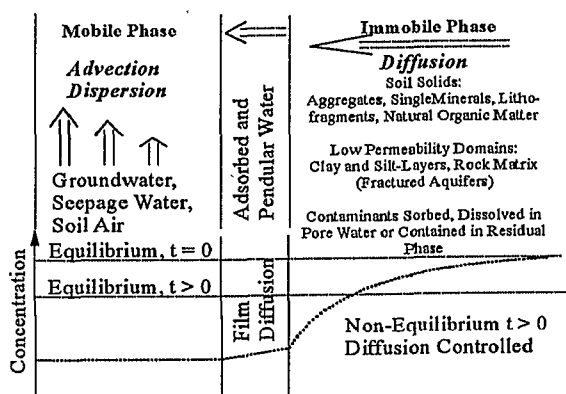


Figure 2-2: Scheme of nonequilibrium desorption of contaminants in the subsurface environment (from GRATHWOHL, 1994).

2.3.5 Mass Transfer Rates

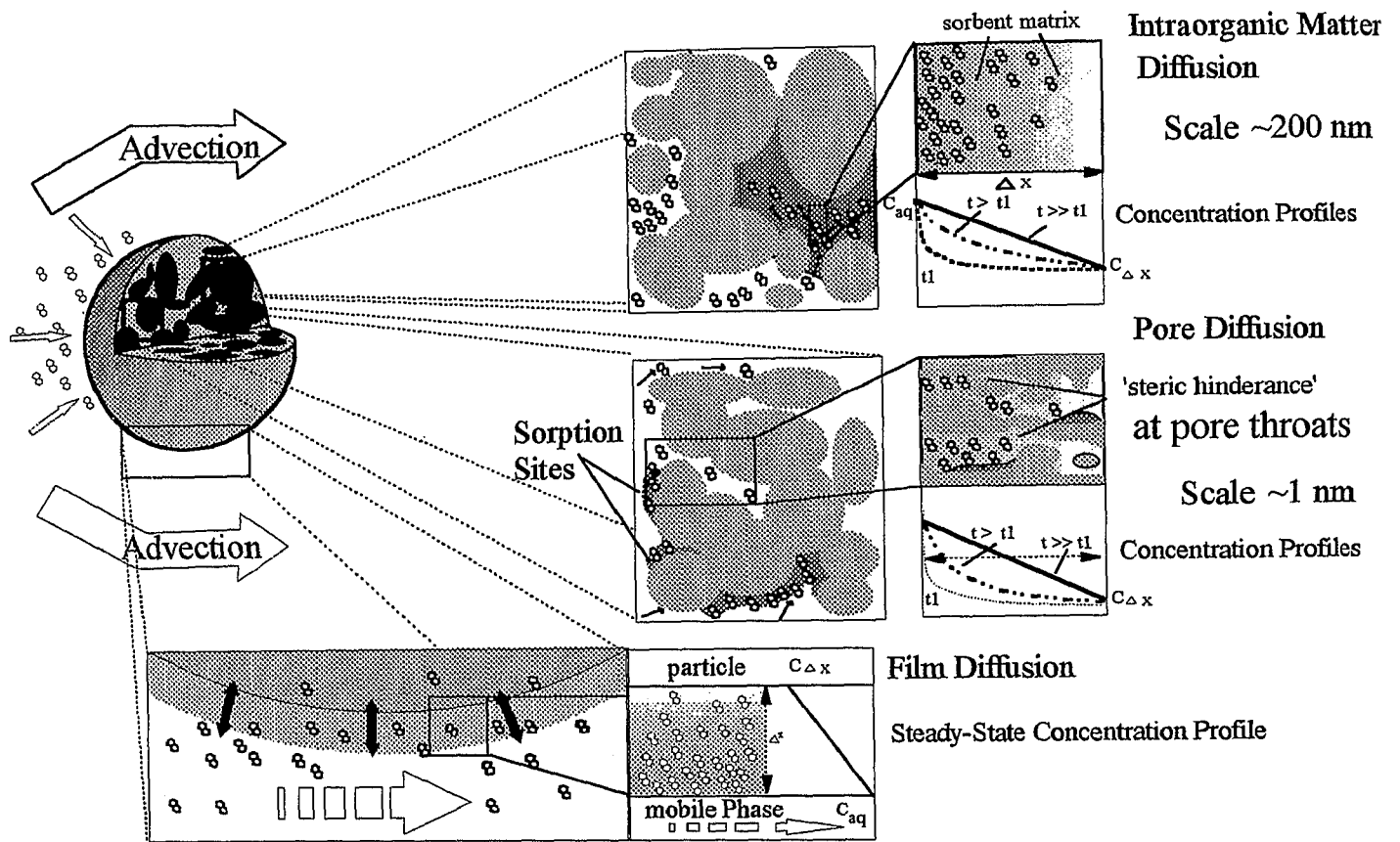
As the process of hydrophobic sorption and desorption of organic compounds is considered to be instantaneous and fully reversible, kinetic effects may be due to a delayed transport to and from the immobilization sites. At the microscale, diffusive processes can limit the transfer rates into the mobile phase (NKEDI-KIZZA ET AL., 1984; WU and GSCHWEND, 1986). Several types of diffusive limitations are discussed in the literature which, due to their nature, result in different diffusional resistances (see Figs. 2-2 and 2-3).

2.3.5.1 Film Diffusion

Generally, the bulk movement of molecules in the mobile phase is considered to be fast (see Fig. 2-3). At the interface mobile phase-solid however, a more or less stagnant boundary zone of water molecules is assumed, due to increased viscosity at the microscale as well as immobilized water molecules which form an adsorbed film around aquifer particles. The mass transfer across this zone is limited by the compounds' ability to diffuse across this stagnant boundary layer (SCHWARZENBACH ET AL, 1993). However, its effect as a limiting factor on overall mass transfer is considered to be of little importance compared to intragranular limitations (BRUSSEAU and RAO, 1989), as the thickness of this layer is too small to act as restriction to mass transfer across it, and the capacity of such a "film" is small compared to the adsorbent's particle capacity (KÄRGER and RUTHVEN, 1992). A mathematical description similar to Darcy's law can be used to describe steady flux across such a film. Introducing a mass transfer coefficient $D_{aq}/\Delta x$ (LT^{-1}), the flux F , [$ML^{-2}T^{-1}$] is consequently expressed as

$$F = \frac{D_{aq}}{\Delta x} (C_w - (C_s / K_d)) \quad (2-12)$$

where C_w [ML^{-3}] is the equilibrium aqueous concentration, C_s [MM^{-1}] the equilibrium concentration on the solid phase at the surface of the particle, K_d the partition coefficient [L^3M^{-1}], and Δx is the film thickness [L] (KÄRGER and RUTHVEN, 1992). The concentration gradient is given by $(C_w - (C_s/K_d))/\Delta x$.



Relative Comparison of Physico-Chemical Parameters

Diffusion type	Sorption Capacity	Diffusion Rate Constant	Equilibration Time
Film	Low	High	Negligible
Intraparticle	Intermediate	Intermediate	Short
Intrasorbent	Very High	Low	Very Long

Figure 2-3: Schematic view of three diffusive mechanisms that affect mass transfer of contaminants from the advective domain into and out of a porous particle. Each diffusive process is linked to specific sites of the grain and induces different resistances to diffusive flux at the grainscale. **Intraorganic matter diffusion** (upper right panel): Diffusion in a quasi organic phase of SOM. **Intrapore diffusion** (central panel): Diffusion inside porous aquifer particles. With respect to aqueous diffusion, diffusion is hindered by tortuous diffusion paths and the limited intraparticle porosity. **Film diffusion** (lower panels): Diffusion across a "stagnant" water layer at the grain surface forms an external resistance to mass transfer into the mobile phase.

In contrast to other types of diffusion resistances, which affect the desorption of organic contaminants from soil solids, film diffusion plays an important part for the dissolution kinetics of PAHs from residual phase. With changing flow velocities the thickness of this stagnant water film changes, thus changing the gradient between the immobile and the mobile phase. A reduction of the film thickness at high flow velocities would lead to an increase of the fluxes. EBERHARDT (1995) found an inversely correlated relation between flow rate and film thickness.

2.3.5.2 Pore Diffusion

Aquifer materials may offer internal sorption sites that can only be reached by diffusive

transport into the porous grain. Mass transfer rates depend on the limitations that the internal pore geometries impose on the diffusive transport (BALL and ROBERTS, 1991b; GRATHWOHL ET AL., 1992). The pore diffusion coefficients inside porous grains are considerably lower than those of a non-restricted media. By approximating aquifer particles as spheres, Fick's 2nd Law for transient conditions is expressed in radial coordinates as (CRANK, 1975)

$$\frac{\partial C}{\partial t} = \frac{D_p}{R} \frac{1}{r^2} \frac{\partial}{\partial r} \left(r^2 \frac{\partial c}{\partial r} \right) \quad (2-13)$$

where D_p is the pore diffusion coefficient, r the radial distance from the sphere's center, and R the retardation factor. D_p/R is also

known as the apparent diffusion coefficient D_a . D_a incorporates the physical effects of diffusive restriction due to tortuosity τ and the effective intraparticle porosity ε , as well as retardation of solutes due to sorption. For a constant partition coefficient K_d (linear isotherm), D_a is defined as

$$D_a = \frac{D_{aq} \varepsilon_i \delta}{(\varepsilon + K_d \rho) \tau} = \frac{D_e}{\alpha} \quad (2-14)$$

where ε_i is the transport-effective porosity, δ (≤ 1) the constrictivity. The nature of δ is more thoroughly addressed in Chap. 2.3.5.3 Eq. 2-14 can also be expressed in terms of D_e and α which denote the effective diffusion coefficient ($D_{aq} \varepsilon_i / \tau$) and the rock capacity factor ($\varepsilon + K_d \rho$).

2.3.5.3 Rate Limitations Due To Pore Geometry and Steric Hindrances

Additional diffusion limitation can be caused by the shape and dimension of the available pore space, thus being of a purely physical nature (depending on the inherent geometry of the intraparticle pores).

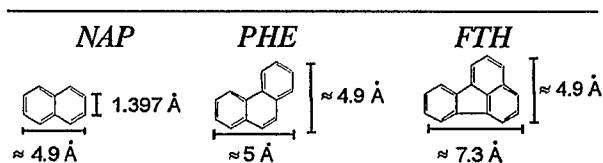
At a microscopic level, the size of pores and their interconnectivity starts to effect the rate of diffusive mass transfer. The tortuosity factor in Eq. 2-14 is used to evaluate the effect of the flow paths at the intragrain scale as compared to the shortest distance possible. It is defined as

$$\tau_f = \left(\frac{l_{eff}}{l} \right)^2 \quad (2-15)$$

with l_{eff} being the actual distance travelled and l the straight line distance between two points. Tortuosity τ is used to describe the influence of pore geometries on the flow length.

Higher tortuosities thus lead to smaller apparent diffusion coefficients (see Eq. 2-14) in aquifer material. However, the values obtained for the tortuosity may be unrealistically high. SCHÜTH (1994) calculated tortuosity factors in the hundreds to ten thousands, using data fitted for apparent diffusion coef-

Figure 2-4: Structural formulae and approx. sizes of 3 selected PAHs (after Herbert, 1992).



ficients. GEWALD (1995) found tortuosities up to 2700 for aquifer sands and HARMON and BALL (1994) estimated even higher tortuosities. Very high tortuosity factors are an indication that the pore diffusion model may not be appropriate for the material tested. Possible causes for unrealistic values include a heterogeneous sample or organic matter diffusion.

As the molecular diameter of the solute approaches such narrow pore- or pore throat diameters, diffusion becomes further restricted. This has to be corrected for by introducing a constrictivity factor δ . The constrictivity factor depends on the molecule/pore diameter ratio (λ_p). For the constrictivity factor δ CHANTONG and MASSOTH (1983) derived the following equation

$$\delta = 1.03 \exp(-4.5 \lambda_p) \quad (2-16)$$

with λ_p being the diameter ratio solute molecule/pore, for $\lambda_p < 1$.

From the above equation it becomes evident that for large values of λ_p the numerator in Eq. 2-14 becomes smaller. For PAHs constrictivity effects start to become important at

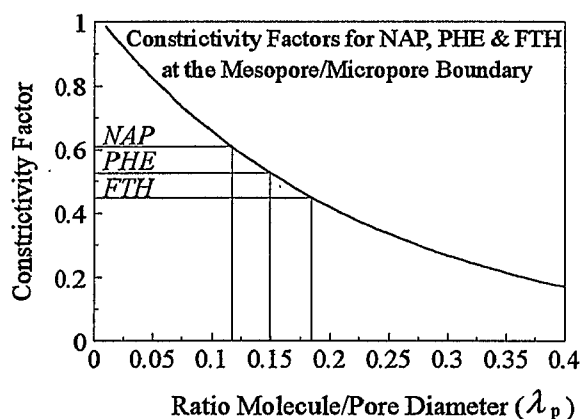


Figure 2-5: Constrictivity factors of 0.4 to 0.6 for the respective PAHs in pores of 2 nm radius lower the expected diffusion coefficients to 40% - 60% of the original value.

the lower mesopore to micropore range (approx. 2-3 nm).

Figure 2-5 shows the effect of constrictivity on 3 PAHs (*NAP*, *PHE* and *FTH*) at the meso-micropore boundary (radius 2 nm). The respective molecule sizes of these three PAHs is given in Figure 2-4.

If constrictivity considerations are not taken into account, tortuosity factors might be overestimated. However, unrealistically large tortuosities cannot be accounted for by the steric hindrance concept.

2.3.5.4 Intra-Organic Matter Diffusion

Soil organic matter (SOM) can be considered the primary location of sorption for nonpolar constituents (see 2.1.2.2). Solute transport of hydrophobic constituents into and out of such complex three dimensional polymer-like structures (RUTHERFORD ET AL., 1992),

forming a quasi nonaqueous phase (LIU and AMY, 1993) can also be important for sorption kinetics. The partitioning kinetics of organic contaminants into organic matter and their subsequent distribution is affected by the intrasorbent diffusion. Organic matter can be located in intraparticle regions of the grains or form individual aggregates. Diffusion coefficients in organic matter depend on the inherent nature of this natural polymer.

At the grain scale, all three types of diffusion processes may be active concomitantly (see Fig. 2-3). If e.g. SOM is present in intraparticle domains, the mass transfer in and out of aquifer particles will be affected by diffusion into two regions: the water-filled intraparticle pores and the organic matter-filled pore space. The desorption rates will be limited by the lowest diffusion coefficient active combined with the largest diffusion distance in such a system.

3. Modeling of Desorption and Contaminant Release

The modeling of mass transfer between a mobile and a stationary phase has been approached in different ways. In order to portray this "non-ideal" behavior of mass transfer between two phases, various approaches were introduced. Some are able to mimic the experimental data and at the same time offer a physical process (e.g. intraparticle diffusion) explaining the data, in contrast to approaches that fit data, yet do not readily lead to the "true" involved physical processes (first-order processes). This chapter introduces the modeling approaches that were used subsequently to simulate the desorption data obtained from the column experiments with various materials.

3.1 Desorption Limited by Spherical Intraparticle Diffusion

If the geometry of aquifer particles is approximated assuming a spherical shape, it is possible to express Fick's 2nd Law in 1-D, and analytical solutions to Eq. 2-13 for certain initial and boundary conditions are available. Depending on the initial concentration distribution in the grains, several desorption schemes can be applied to describe the desorption behavior of a contaminant out of the intraparticle domain.

3.1.1 Desorption in Case of Prior Equilibration

The time between the formation of PAH contaminations in the subsurface and the subsequent remediation is usually on the order of decades. Thus aquifer material can be assumed to have reached a high degree of equilibration with respect to adjacent aqueous concentrations. In case of a sudden drop of aqueous concentrations (e.g. pump-and-treat remediation) the desorption of PAHs from aquifer particles begins. This scheme is approximated by the following initial and boundary conditions

$$\begin{aligned} C &= C_{eq} & t &= 0 & 0 < r < a \\ C &= 0 & t &> 0 & r = a \\ \partial C / \partial r &= 0 & t &> 0 & r = 0 \end{aligned}$$

C_{eq} is the equilibrium concentration, C the concentration of the contaminant in the pore water, which is kept close to zero, and a is the radius of the particle.

For these conditions the cumulative mass (M) desorbed after a time t with respect to the equilibrium mass M_{eq} is given by CRANK (1975)

$$\frac{M}{M_{eq}} = 1 - \frac{6}{\pi^2} \sum_{n=1}^{\infty} \frac{1}{n^2} \exp \left[-n^2 \pi^2 \frac{D_a}{a^2} t \right] \quad (3-1)$$

The solute flux F out of a spherical grain is given by the time derivative of (3-1)

$$\frac{F}{M_{eq}} = 6 \frac{D_a}{a^2} \sum_{n=1}^{\infty} \exp \left[-n^2 \pi^2 \frac{D_a}{a^2} t \right] \quad (3-2)$$

As the series expansions of Eqs. 3-1 and 3-2 may require many terms to reach a sufficiently exact solution for early times, it can be useful to subdivide the time period that is to be modeled into two time domains. GRATHWOHL (1994) gives short-term and long-term approximations for the above Eqs.. The range in which either one can be applied is given by

$$\begin{aligned} D_a t / a^2 &\leq 0.15 && \text{for short-term approx.} \\ D_a t / a^2 &\geq 0.15 && \text{for long-term approx.} \end{aligned}$$

where $D_a t / a^2$ denotes dimensionless time.

The short-term approximation for the mass released can be expressed as

$$\frac{M}{M_{eq}} = 6 \sqrt{\frac{D_a t}{\pi a^2}} - 3 \frac{D_a t}{a^2} \quad (3-3)$$

and the corresponding flux is

$$\frac{F}{M_{eq}} = 3 \sqrt{\frac{D_a}{\pi a^2}} \frac{1}{\sqrt{t}} - 3 \frac{D_a}{a^2} \quad (3-4)$$

The long-term approximations are given by

$$\frac{M}{M_{eq}} = 1 - \frac{6}{\pi^2} \exp \left[-\pi^2 \frac{D_a}{a^2} t \right] \quad (3-5)$$

and

$$\frac{F}{M_{eq}} = 6 \frac{D_a}{a^2} \exp \left[-\pi^2 \frac{D_a}{a^2} t \right] \quad (3-6)$$

In the case of diffusion-controlled desorption, the plots of the approximated fluxes using a log-log chart show characteristic slopes. The short-term approximation will depend on the inverse of the square root of time, the long-term approximation will behave like a first-order process and display a slope of $-\pi^2 D_a/a^2$ in a semi-log plot (GRATHWOHL and REINHARD, 1993).

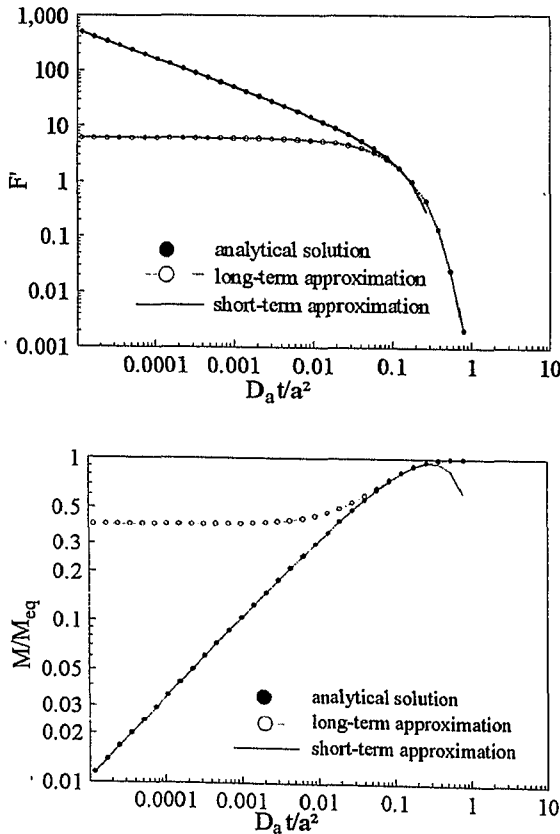


Figure 3-1: Comparison between the series expansion (200 terms) and the respective long-term and short-term solutions for M/M_{eq} (lower frame) and for fluxes (upper frame) (normalized as dimensionless fluxes, with $F' = F/M_{eq} D_a/a^2$) for desorption from a sphere in an infinite bath (equilibrium concentration throughout the grain prior to desorption and constant ("quasi zero") concentration in the mobile phase).

3.1.2 Modeling Desorption for Heterogeneous Mixture

Aquifer material can be made up of various lithological components of varying sizes. Depending on the relative amounts of specific components in a mixture and their desorptive characteristics, each component will show its own desorption kinetics (GRATHWOHL and KLEINEIDAM, 1995). Monitoring the contaminant release of mixed components, this heterogeneity can cause distinct phases in the log-log plot of M/M_{eq} and the fluxes with respect to time. As natural aquifer materials generally include a range of sizes and components (depending on transport distances and source lithology), the effects of single components will tend to be masked or subdued. To describe multicomponent systems, Eqs. 3-1 and 3-2 need to be extended to

$$\frac{M}{M_{eq}} = 1 - \sum_i X_i \frac{6}{\pi^2} \sum_{n=1}^{\infty} \frac{1}{n^2} \exp \left[-n^2 \pi^2 \frac{D_{a,i}}{a_i^2} t \right] \quad (3-7)$$

and

$$\frac{F}{M_{eq}} = \sum_i X_i \frac{D_{a,i}}{a_i^2} \sum_{n=1}^{\infty} \exp \left[-n^2 \pi^2 \frac{D_{a,i}}{a_i^2} t \right] \quad (3-8)$$

where X_i is the fraction of each component i of M_{eq} , $D_{a,i}$ and a_i^2 refer to the individual rate constants and particle radii.

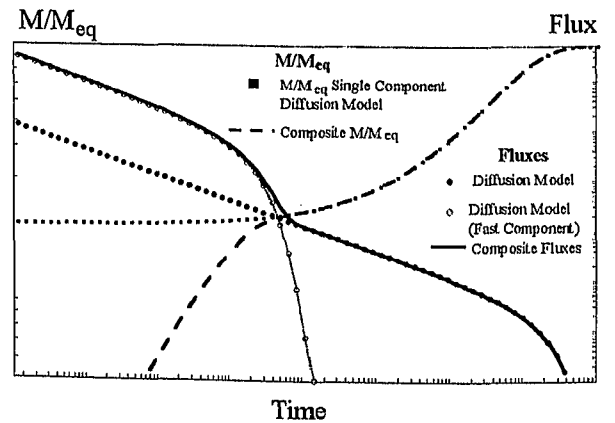


Figure 3-2: Desorption behavior of a dual component material having two diffusion rate constants (D_a/a^2 of component 1 = 10,000 x D_a/a^2 of component 2). Both branches of the flux curve show the typical slope of -1/2 in the log-log plot. As one fraction is depleted with time, the fraction with the higher diffusion rate constant becomes insignificant and the rates at late times will eventually be governed by the slowly releasing fraction.

GRATHWOHL (1994) showed that the effects of complex mixtures depend on the degree of variability in their relative abundances and kinetic characteristics, as well as on correlations between D_a/a^2 s and sorption capacity. Theoretically, superposition of data of various components can plot similar as in a homogeneous case.

3.1.3 First-Order Kinetics

Another scheme used for describing nonequilibrium conditions assumes that the rate of desorption is solely a function of the concentration of the species yet remaining on (in) the particle. This process describes the release of contaminants in a similar manner as for example radioactive decay or hydrolysis. This approach is commonly used in the modeling of contaminant release. FARRELL (1993) uses a first-order approach to describe the release of contaminants from high energy sites or restricted transport through small pores. The release of originally sorbed mass M_s [M] on (in) a soil particle with respect to time can be expressed as

$$\frac{\partial M_s}{\partial t} = -\lambda M_s \quad (3-9)$$

with λ [T⁻¹] being the first-order rate coefficient. The mass still sorbed after a time M_t is given by

$$M_t = M_s \cdot e^{-\lambda t} \quad (3-10)$$

A comparison between intraparticle diffusion and a first-order approach shows distinct differences with respect to contaminant releases at early time scales. In order to model intraparticle diffusion using a first-order approach, a time-variant first-order rate coefficient would be needed for early time data (GRATHWOHL, 1994).

3.1.4 Concomitant First Order Kinetics and Intraparticle Diffusion

Data obtained from desorption experiments often show initially high fluxes of contaminant followed by a period of persistent but low release rates, which decrease slowly with time (CAROLL ET AL., 1994; GRATHWOHL ET AL.,

1994). This first phase appears to be in contradiction to a single component intraparticle diffusion model, which cannot accommodate for the observed initial fluxes and their rapid decline. Possible reasons for this behavior could be the heterogeneity of the sample or the desorption of compounds near the surface of particles.

Without the influence of intragranular limitations to diffusion, this fraction of sorbed contaminant will be released fast (with respect to hindered pore diffusion) showing high initial fluxes and a rapid decrease in concentrations.

In order to model such early time experimental data, first-order kinetic models can be used. Eqs. 3-1 and 3-2 are changed to

$$\frac{M}{M_{eq}} = (1 - X_i) \left(1 - \frac{6}{\pi^2} \sum_{n=1}^{\infty} \frac{1}{n^2} \left[-n^2 \pi^2 \frac{D_a}{a^2} t \right] \right) + X_i (1 - \exp[-\lambda t]) \quad (3-11)$$

$$\frac{F}{M_{eq}} = (1 - X_i) \left(6 \frac{D_a}{a^2} \sum_{n=1}^{\infty} \exp \left[-n^2 \pi^2 \frac{D_a}{a^2} t \right] \right) + X_i \lambda (1 - \exp[-\lambda t]) \quad (3-12)$$

where X_i denotes the fraction of the component which is governed by a fast first-order process.

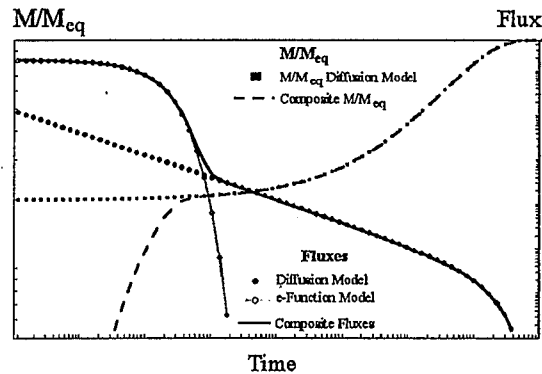


Figure 3-3: Modeling of desorption with a dual component approach. The model shows high initial fluxes of a fast desorbing fraction (X_i) described by a simple first-order approach. In comparison to the two-site diffusion model (Fig. 3-2), the fluxes for the fast component initially do not exhibit the $-1/2$ slope, but a rather constant level of fluxes followed a dramatic drop of the fluxes.

The introduction of first-order processes for the instantaneously desorbing fraction of a sorbed contaminant, however, does not render a physico-chemical analogy, as does the concept of retarded pore diffusion at the grain scale, and needs further investigation (PEDIT and MILLER, 1994).

3.1.5 Determination of Diffusion Rate Constants from Column Experiments

The sensible determination of diffusion rate constants from column experiments using the diffusion model depends on whether the assumptions inherent to the model actually reflect the processes active at the grain scale.

These assumptions include that:

- the aquifer material had enough time to reach equilibrium conditions with respect to the aqueous concentrations, to assure that the mass sorbed in the particles is equal to M_{eq}
- the diffusion rate constant is not a function of the aqueous concentration of the compound under consideration (= linear sorption isotherm)
- aquifer particles can be approximated by spheres of an average radius
- the physical characteristics of the spherical aquifer particles are homogeneously distributed throughout their volume

To compare the experimental results with the diffusion model, the data were plotted in terms of mass released vs. total mass retained in the column (M/M_{eq}) vs. time and contaminant flux (MT^{-1}) vs. time. In order to account for a fraction of the contaminant that is quickly released a combined first-order/diffusion model was used (Eqs. 3-11 and 3-12). Fitting parameters for matching the data with the model are X_i (the fraction of M_{eq} involved in fast desorption), the first-order coefficient λ , and the diffusion rate constant D_a/a^2 for the slowly desorbing fraction. Best fit between the data and the model was achieved by minimizing the weighted squared error of model and data values using

$$\sum \left(\frac{\text{measured value} - \text{model value}}{\text{measured value}} \right)^2$$

3.1.6 Sensitivity Analysis of the Diffusion Model with Respect to Mass Recoveries

Arriving at meaningful diffusion rate constants strongly depends on the mass balance achieved in the column experiment. Looking at the short-term solution of the spherical diffusion model (Eq. 3-4), it is readily demonstrated that in the case of erroneous mass recoveries, the diffusion rate constant derived from the curve fitting procedure can deviate considerably from the true value, although the data and model exhibit an optimal fit. A mistake in underestimating M_{eq} by some factor x will lead to a diffusion rate constant differing from the true value by a factor of x^2 (as D_a/a^2 in Eq. 3-3 enters in the square root).

However, at late times incomplete mass recoveries result in a rapid decline of the fluxes in the model, in contrast to the acquired data. Once this deviation is visible, an insufficient extraction can be assumed. As the degree of removal of the initially sorbed mass must be on the order of 90 % to notice this deviation, long purging periods are needed (especially for high K_{ow} compounds), which are rarely in an experimental time frame (see Figure 3-4).

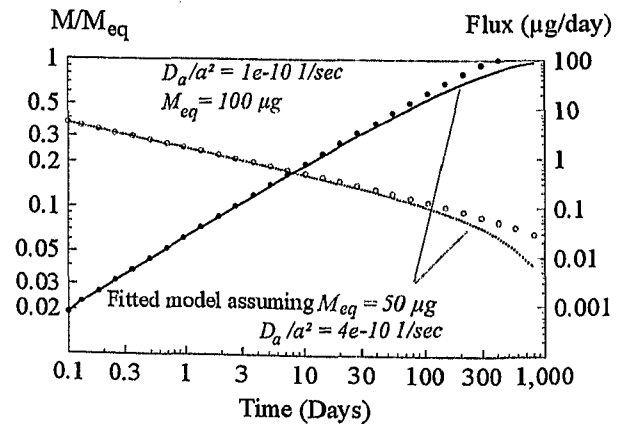


Figure 3-4: The data depict the desorption of a compound (symbols) of a D_a/a^2 of $1e^{-10}$ 1/s and a M_{eq} of $100\mu\text{g}$. The erroneous fit assuming a M_{eq} of only $50\mu\text{g}$. An underestimation of M_{eq} by a factor of 2 will lead to an overestimation of the diffusion rate constant of a factor of 4. Late time data would show the deviation of the data from the model, but is rarely in the time frame of desorption experiments.

Performing mass balances for PAHs with their wide range of octanol-water partition coefficients can also lead to an underestimation of sorbed mass of high K_{ow} compounds with their tendency to resist extraction (slow release from sorbing sites). So considerable caution must be taken to assure best possible mass recoveries especially when dealing with high- K_{ow} compounds.

3.1.7 Desorption in Poorly Equilibrated Systems

In order to describe desorption processes using the above diffusion model, it is necessary to start with an equilibrated system. Its applicability therefore depends on both

- the exposure time and
- the rates of sorptive uptake

of a sorbed compound. The effects of exposure time on the release of contaminants is stressed by several authors (e.g. PIGNATELLO ET AL., 1993; GRATHWOHL, 1993). GRATHWOHL (1994) reasons that observed hysteresis of sorption/desorption experiments could be due to insufficient degrees of equilibrium achieved in aquifer particles. In such cases, a diffusive front would still be moving towards

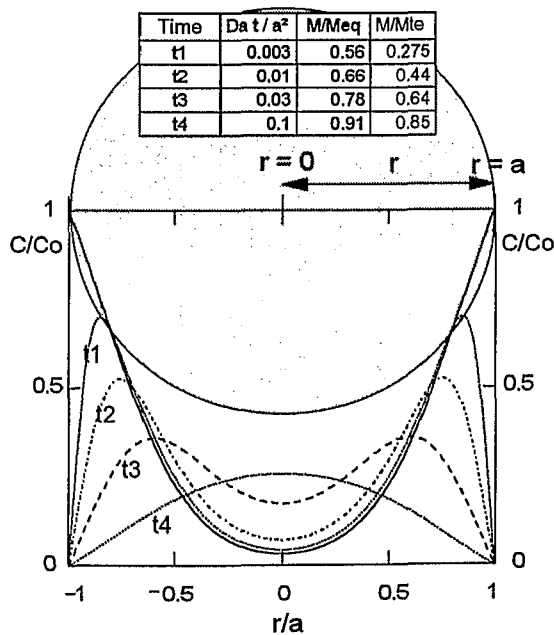


Figure 3-5: Concentration profiles in a sphere if desorption is started before sorption equilibrium is reached. Solid line: concentration after exposure for $Da t/a^2 = 0.05$; dashed lines: concentration profiles during desorption (from GRATHWOHL, 1995).

the center of a particle, while mass is already desorbing into the mobile phase again due to the bidirectional concentration gradient (one towards the center of the sphere and one towards the mobile phase (see Fig. 3-5).

A solution to the distribution of concentration in a sphere after being exposed to a constant concentration for a limited period of time t_e (CRANK 1975) is

$$\frac{C}{C_0} = 1 + \frac{2a}{\pi r} \sum_{n=1}^{\infty} \frac{(-1)^n}{n} \sin \left[\frac{n \pi r}{a} \right] \exp \left[\frac{-n^2 \pi^2 D_a t_e}{a^2} \right] \quad (3-13)$$

For starting desorption by reducing the mobile phase concentration to zero after t_e , the concentration profile is given by (LIEDL, 1994)

$$\frac{C}{C_0} = -\frac{2a}{\pi r} \sum_{n=1}^{\infty} \frac{(-1)^n}{n} \sin \left[\frac{n \pi r}{a} \right] \exp \left[\frac{-n^2 \pi^2 D_a t}{a^2} \right] \left(\frac{-n^2 \pi^2 D_a t_e}{a^2} \right) \quad (3-14)$$

The corresponding flux leaving the sphere is

$$F = 6 M_{eq} \frac{D_a}{a^2} \sum_{n=1}^{\infty} \exp \left[\frac{-n^2 \pi^2 D_a t}{a^2} \right] \left(1 - \exp \left[\frac{-n^2 \pi^2 D_a t_e}{a^2} \right] \right) \quad (3-15)$$

The masses released with respect to M_{eq} are

$$\frac{M}{M_{eq}} = \left(1 - \frac{6}{\pi^2} \sum_{n=1}^{\infty} n^{-2} \exp \left[\frac{-n^2 \pi^2 D_a t}{a^2} \right] \right) \left(1 - \exp \left[\frac{-n^2 \pi^2 D_a t_e}{a^2} \right] \right) \quad (3-16)$$

Assuming constant concentrations in the mobile phase and knowing the exposure time and the sorbed mass after t_e (M_{te}), it is possible to fit diffusion rate constants without

specifying the equilibrium mass sorbed by using Eq. 3-17. In order to evaluate the fluxes, it is however necessary to know the mass sorbed at equilibrium.

$$\frac{M}{M_{te}} = \left(1 - \frac{6}{\pi^2} \sum_{n=1}^{\infty} n^{-2} \exp \left[\frac{-n^2 \pi^2 D_a t}{a^2} \right] \right) \left(1 - \exp \left[\frac{-n^2 \pi^2 D_a t_e}{a^2} \right] \right) / \left(1 - \frac{6}{\pi^2} \sum_{n=1}^{\infty} n^{-2} \exp \left[\frac{-n^2 \pi^2 D_a t_e}{a^2} \right] \right) \quad (3-17)$$

The comparison between the evolution of fluxes and released masses derived from an equilibrated sample and from samples of varying degrees of equilibration is documented in Fig. 3-6.

In the case of low degrees of equilibrium, the amount of mass released to the total mass sorbed (M_{te}) will be very high, as the diffusive concentration front has not penetrated the grain very far. Thus, there is a large gradient close to the grain surface, which results in high diffusive fluxes. The closer a system is to the state of equilibrium (i.e. the more evenly distributed the concentrations are throughout the grain), the more similar are the slopes of the fluxes of the equilibrium and nonequilibrium case in the log-log plot. Ob-

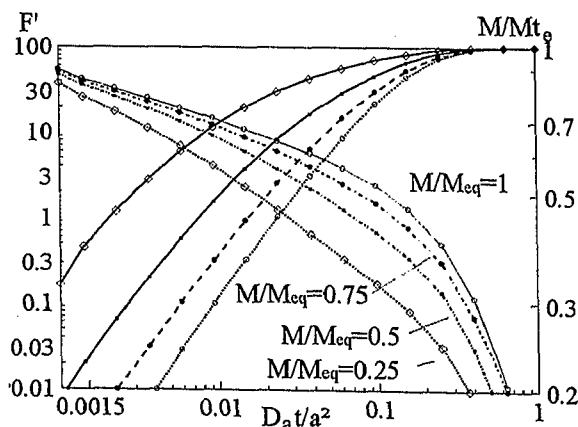


Figure 3-6: The influence of nonequilibrium starting conditions on the release of sorbed compounds is plotted as dimensionless flux ($F' = F / (M_{eq} D_a / a^2)$) and M/M_{te} vs. dimensionless time ($D_a t / a^2$). At low values of M/M_{eq} high amounts of relative masses M/M_{te} are released at early times. Fluxes show increasingly negative slopes (-1/2 to -3/2), as one moves away from the state of initial equilibrium.

served fluxes for nonequilibrated systems are smaller and show increasingly higher negative slopes (-1/2 to -3/2), as the fraction of M/M_{eq} reached after t_e approaches smaller values (see Fig. 3-6).

3.2 Release of PAHs from Residual Coal Tar

The mechanisms controlling the release of PAHs from residual tar phase into the groundwater are of a different nature with respect to the previously described nonequilibrium processes. For the release of PAHs from coal tar in phase, film diffusion plays an important role. If the residual tar phase and the aqueous phase share a common interface, a stagnant film forms which acts as an external diffusion resistance limiting the mass transfer of PAHs into the mobile phase.

If contact times are sufficient, equilibrium conditions between the residual phase and the aqueous phase are established. The equilibrium aqueous concentrations for the respective PAHs depend on the composition of the complex tar mixture. Solubilities in mixtures can be considerably smaller than estimated from the solubility of the pure compounds and are described by Raoult's Law

$$C_{i,W}^{sat*} = \chi_i \gamma_i S_{i,W_{sat}} \quad (3-18)$$

with $C_{i,W}^{sat*}$ [ML^{-3}] the aqueous solubility of a compound out of a mixture, $S_{i,W_{sat}}$ the subcooled liquid solubility of a compound, χ_i [-] the molar fraction of a compound, and γ_i the activity coefficient [-]. With a changing composition of a tar, as it is depleted during the differential release of PAHs, the mole fraction of a compound in a mixture changes and $C_{i,W}^{sat*}$ can become time-variant.

3.2.1 Evaluating Equilibrium Release of PAHs in Column Experiments

As pristine water enters a contaminated domain (column), the concentrations in the aqueous phase increases with growing contact time. Assuming a short saturation distance L_{Sat} [L] compared to the length of the

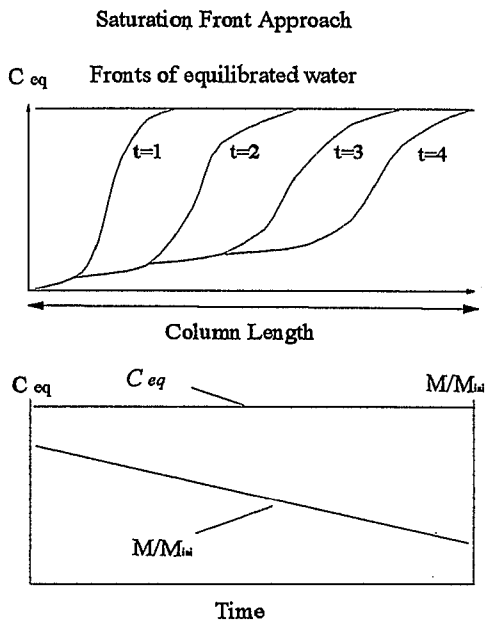


Figure 3-7: Schematic view of a prograding saturation front in a column experiment. The saturation front approach assumes that after pristine water enters a column it increasingly reaches equilibrium conditions.

observed domain, the effluent leaving the domain will reach equilibrium concentrations corresponding to those derived from Raoult's Law. For such an advancing saturation front effluent fluxes will be linearly correlated with the flow rate, as long as the saturation front has not yet reached the end of the domain. Figure 3-7 shows plots fluxes vs. time, where the steps in the fluxes correspond decreasing flow velocities.

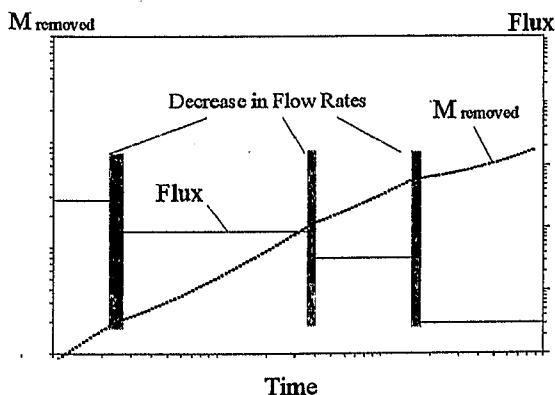


Figure 3-8: Schematic release of a compound from residual tar phase, assuming equilibrium conditions in the column during the experiment. The prominent steps in fluxes and the changes in the slope of the cumulative mass plot are due to decreasing flow velocities. In contrast to the saturation front approach, the equilibrium partition model yields decreasing concentrations.

For equilibrium conditions the contaminant fluxes can easily be calculated as all necessary parameters can be experimentally determined (flow velocity F_w and saturation concentration C_w^{sat*}). The release rates of PAHs at changing flow velocities and estimations as to the time needed to reach removal are therefore a straight-forward problem.

Strictly speaking, the above saturation front approach is only valid for a time-invariant C_w^{sat*} . The time range over which this simplifying assumption is valid depends on the inherent molar fractions of the individual compounds in the mixture. As C_w^{sat*} decreases with time, the above assumptions describe the worst possible case of contaminant release.

3.2.2 Evaluating Nonequilibrium PAH Release from Coal Tar

If the saturation conditions are not reached due to e.g. higher flow velocities, kinetic effects will start to influence the mass transfer between aqueous phase and the residual coal tar.

In order to describe nonequilibrium conditions, the stagnant two-film model is used. The model approximates the tar-water interface by introducing 2 layers, one of which resembles a stagnant water film due to increasing viscosity at the microscale, the other one resembles a "skin"-type domain at the interface in the tar phase, where the tar has been depleted with respect to PAHs (see Fig. 3-9). At the boundary layer between the two films PAHs leave the tar phase and enter the aqueous phase under equilibrium conditions. The concentrations on either side of each film are controlled by the tar-water partition coefficient K_{TW} defined as

$$K_{TW} = \frac{C_{i,T}}{C_{i,W}} \quad (3-19)$$

where $C_{i,T}$ is the concentration of a compound i in coal tar and $C_{i,W}$ the aqueous solubility of the same compound i .

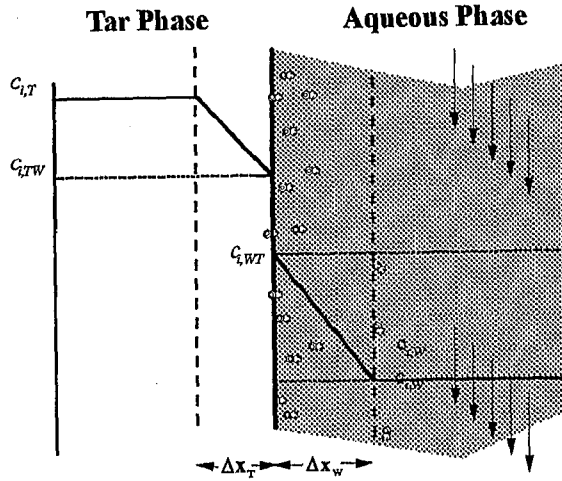


Figure 3-9: Schematic view of a stagnant two-film model. Mass transfer across either film is assumed to be controlled by Fick's 1st Law. At the interface equilibrium is assumed, and concentrations on either side are controlled by the tar-water partition coefficient. Δx_T and Δx_W refer to the respective film thicknesses, C_{iT} and C_{iW} are the concentrations in the tar and aqueous phase (after EBERHARDT, 1995).

In contrast to equilibrium mass transfer, the mass transfer across the film is limited by film diffusion.

The fluxes across both films can be evaluated using Fick's 1st Law (Eq. 2-3). Assuming a steady-state mass transfer across the two films, fluxes across both films are equal.

$$F_{iW} = \frac{-D_{iW}}{\Delta x_W} (C_{iWT} - C_{iW}) =$$

$$F_{iT} = \frac{-D_{iT}}{\Delta x_T} (C_{iTW} - C_{iT}) \quad (3-20)$$

where F_W and F_T are the fluxes in the layers of the film, Δx_T and Δx_W are the respective film thicknesses, $C_{i,T}$ is the concentration of a compound i in coal tar, $C_{i,W}$ the solubility of the compound i , and D_T and D_W are the respective diffusion coefficients.

The total flux can then be written as

$$F = \frac{1}{\frac{\Delta x_T}{D_T} + \frac{\Delta x_W C_{i,T}}{D_W C_{i,W}}} C_T \quad (3-21)$$

If both films have about the same thickness, the flux will only depend on K_{TW}/D_W and on $1/D_T$. As C_{iT}/C_{iW} is much larger than one thousand and $D_T > 0.1 D_W$, the flux will be controlled solely the water film. Contaminant flux can therefore be approximated by

$$F = \frac{D_W}{\Delta x_W} C_{i,W} \quad (3-22)$$

The mass transfer coefficient $D_W/\Delta x_W$ is therefore proportional to the diffusion coefficient and inversely proportional to the film thickness.

4. Materials and Laboratory Methods

4.1 Materials

One of the premises of the study was to investigate the desorption characteristics of contaminated materials that have reached equilibrium. The materials used include contaminated samples from two manufactured gas plant (MGP) sites in Southern Germany (Heidenheim and Karlsruhe) and 3 typical aquifer sands that have been exposed to PAHs in either column experiments to determine the

transfer characteristics of PAHs out of residual coal tar phase (WILHELM, 1992) or were used to derive sorption characteristics of the sands with respect to selected PAHs (SCHÜTH, 1994). The aquifer sands cover a wide range of physico-chemical parameters due to their various source rocks. SANNS (1992), HERBERT (1992), SCHÜTH (1994), KLEINEIDAM (1992), and others have used some of these sands for their sorption studies.

Table 4-1: Sand samples used for desorption studies. Capital letters denote the origin of the samples. NS=Neckar Sand, AS= Allgäu Sand, RS=Rhine Sand, KA=Karlsruhe, and HH=Heidenheim. Indexes to the abbreviations denote previous workers of the sample. (S=Schüth, W=Wilhelm). T_e = approx. exposure time (days) of the samples.

Sample	PAHs monitored	Grain size	T_e	Gauss-Krüger Coordinates	
Single Component Samples					
RS _S	NAP/FTH	0.315-1 mm	500	34273-53903	used by Schüth/ (1994) stored in batch vial until used
AS _S	NAP/FTH	0.315-1 mm	500	35706-52939	used by Schüth (1994) stored in batch vial until used
Multicomponent Samples					
NS	FL/PHE/ANT/ FTH/PY/B(a)A/ CHR	0.25-1 mm	700	35002-53730	used by Wilhelm (1992) air-dried and dry-sieved prior to use/ exposed to surfactant flushing
AS ₁	FL/PHE/ANT FTH/PY	0.25-1 mm	700	35706-52939	used by Wilhelm (1992). air-dried and dry-sieved prior to use
AS ₂	FTH/PY/B(a)A/ CHR	0.25-1 mm	700	35706-52939	
HH _{light}	FL/PHE/FTH B(a)A/B(k)F	0.25-0.5 mm	dec*	35854-59944	
HH _{dark}	FL/PHE/FTH B(a)A/B(k)F	0.25-0.5 mm	dec*	35854-59944	air-dried and dry sieved; subject to on-site surfactant treatment
HH _{dark}	FTH/PY	1-2 mm	dec*	35854-59944	
KA 1	ACE/FL/PHE/ ANT/FTH/PY/ B(a)A/CHR	<0.5 mm	sou ⁺	34585-54297	
KA 2	ACE/FL/PHE/ ANT/FTH/PY/ B(a)A/CHR	0.5-1 mm	sou ⁺	34585-54297	sediment samples containing residual coal tar in phase, air-dried, dry-sieved and stored until use
KA 3	ACE/FL/PHE/ ANT/FTH/PY/ B(a)A/CHR	1-2 mm	sou ⁺	34585-54297	
KA 4	ACE/FL/PHE/ ANT/FTH/PY/ B(a)A/CHR	1-2 mm	sou ⁺	34585-54297	isolated coal tar aggregates,

* dec = decades

⁺ sou = material from contaminated sites, containing residual phase

4.1.1 Aquifer Sands

Sedimentologically, the aquifer sands can be classified as follows:

Rhine Sand: fluvial deposit;
Source rock area: Black Forest and Alpine Regions
Components: quartz, mica and high content of igneous and metamorphic rocks

Neckar Sand: fluvial deposit;
Source rock areas: Mostly Sedimentary Rocks from Southern Germany
Components: Triassic Carbonates (Muschelkalk), Jurassic Carbonates (Oxford and Kimmeridge) and Bunter Sandstone

Allgäu Sand : fluvio-glacial deposit
Source rock area: Austrian Alps
Components: Mostly Cretaceous and Jurassic Carbonates

The aquifer sands can be subdivided into two batches:

- The samples used by Schüth (1994) in sorption experiments were left in the glass vials until use. Prior to the desorption the concentration in the aqueous phase was measured.
- The Allgäu Sand and Neckar Sand samples used in PAH transport experiments from WILHELM (1992) were removed from the column and air-dried, sieved and stored in dark glass vessels prior to use.

4.1.2 Samples from former MPG Sites

One set of samples was taken after an on-site soil washing of the contaminated soil, using a special surfactant (proprietary process), at the former MPG site in Heidenheim (HH) (Southern Germany). The wet samples were taken immediately after finishing the cleaning cycles. After the treatment the sand fraction of the material showed no visible traces of residual phase (coal tar). It was air-dried and sieved. The soil sample consisted mostly of carbonate rock fragments, but each size fraction contained considerable amounts of cinders, soot and coal particles as well as brick and glassy components. The 'dark' components (HH_d) were removed for the most part from the bulk matrix by use of a ferromagnetic separator. Until their use, the

materials were stored in dark glass containers.

A second set of samples was taken at the former MPG site in Karlsruhe. The samples were taken from a boring. The material was air-dried and dry-sieved. It consisted of quartz sand and also contained residual tar phase, present in small spherical aggregates mixed and covered with sand and silt. Table 4-1 summarizes the samples used in desorption experiments, their origin, size fractions, and the PAHs monitored in the experiments.

4.2 Sample Characterization

4.2.1 Carbonate Content

The carbonate content of the samples was measured by dissolution in *HCl* and back titration of the unused amount of *HCl* with 0.5 *N* caustic soda; phenolphthalein was used as indicator.

4.2.2 Density

The density was determined using a helium pycnometer Accu Pyc 1330 from Micromeritics.

4.2.3 Organic Carbon Content

The organic carbon content was determined using catalytic combustion of the materials. Prior to the measurements, inorganic carbon sources (e.g. $CaCO_3$) were removed using *HCl*. To remove the *Cl* from the gas stream, it was purged over silver threads. The system components are summarized in Table 4-2.

Table 4-2: System components and analysis conditions for organic carbon measurements.

Method	Catalytic combustion Infra-red detector
Oven	Rosemount/Dohrmann Model 183 Boat Sampling Modul
Detector	Horiba PIR-2000, NDIR in Dohrmann DC-90
Temperatur	800-1000 °C
Catalysts	Cobalt oxide, copper granules
Scrubbers	Silver threads
Concentration Range	0.5 - 160 µg C

4.2.4 Intraparticle Porosity and Internal Surface

The internal surface, intraparticle porosity, and the pore radii distribution were measured using nitrogen adsorption/desorption (BET-Method). This method is based on measuring the amount of N_2 adsorbed on an adsorbent by successively increasing the N_2 partial pressures, starting at low pressure (at a constant temperature of 77° Kelvin), until saturation vapor pressure is reached. As the pressure is increased, the coverage of the internal surfaces with N_2 changes from a monolayer to a multilayer and finally to capillary condensation of N_2 in the pores, as saturation vapor pressure is approached.

The sorption isotherm branch is used to calculate the internal surface of a sample using the BET model (BRUNAUER ET AL, 1938). As the pressure is decreased step by step, the release of N_2 reveals the distribution of pore radii in a range from 2 nm to 25 nm, which corresponds with IUPAC classification of mesopores. In the presence of such mesopores the sorption and the desorption branch show a characteristic hysteresis loop and form a type 4b isotherm (GREGG and SINGH, 1982). The lower detection limit is due to the loss of tensile strength of N_2 , as desorbing pores reach radii in the order of 1.7 nm - 2.0 nm (at $P/P_0 \cong 0.42$). On the sorption/desorption plot this is identical with the lower closure point of the hysteresis loop (see

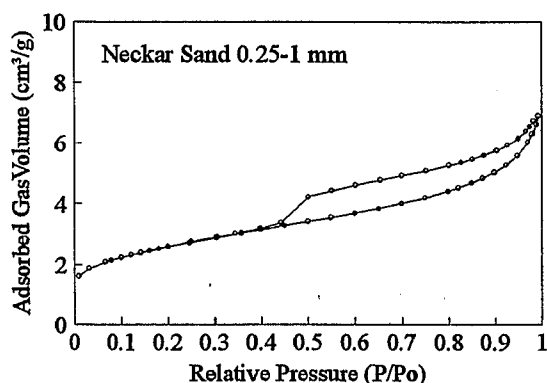


Figure 4-1: Nitrogen sorption and desorption isotherm showing the typical hysteresis for mesopores. The methodological resolution with respect to the pore size distribution is limited to the range of 2 - 25 nm.

Fig. 4-1). Applying a Kelvin type analysis would erroneously imply a prominent pore fraction with a sudden cut-off in radii at 1.7 nm. A physically meaningful interpretation of the sudden N_2 release can only give clues as to the amount of pore space filled with N_2 that is at and smaller than 2 nm. The upper detection limit of N_2 is limited by the ability in measuring partial pressures close to 1 and is reached at pore radii of about approx. 25 nm.

4.2.5 Results

In order to interpret the contaminant release characteristics of the various materials with respect to their inherent particle parameters and to determine their effect on release behaviors, the most relevant physico-chemical

Table: 4-3: Characterization of physico-chemical parameters of the used samples. The subscripts S=Schüth and W=Wilhelm refer to prior use of the material, d and l to 'dark' and 'light' fractions of the Heidenheim samples.

Sample	Grain size [mm]	Density [g/cm³]	CaCO ₃ [%]	C _{org} [%]	BET Surface [m²/g]	Internal Porosity [%]
AS _s *	0.315-1	2.70	32.4	0.057	2.12	1.01
RS _s *	0.315-1	2.65	1.9	0.015	1.19	0.80
NS _w	0.25-1	2.69	24.5	0.48 (0.089*)	9.22	2.50
AS _w	0.25-1	2.72	33.0	0.074	1.59	0.72
HH _l	0.25-0.5	2.67	34.0	2.72	0.98	1.10
HH _d	0.25-0.5	2.67	12.0	9.87	7.82	3.89
HH _d	1-2	2.39	7.5	45.63	5.88	1.06
KA 1	< 0.5	2.62	4.10	0.62	1)	1)
KA 2	0.5-1	2.61	3.27	0.63	1)	1)
KA 3	1-2	2.61	5.18	0.62	1)	1)

* Values from SCHÜTH (1994)

1) not measured, as samples contain residual phase

parameters were measured. The results document the variability between the materials. They give a basis for a subsequent interpretation and are compiled in Table 4-3.

4.2.5.1 Density, Carbonate Content, Organic Matter Content

Density reflects the lithological differences in the composition of the various sands. Increasing carbonate content leads to higher values, and RS with its mostly quartzitic composition shows the lowest density as well as carbonate and organic matter content. The AS and NS reach considerably higher values.

With respect to the organic carbon contents of the various samples it must be considered that some of the samples were subject to prior surfactant treatment that might have had considerable effect on this parameter. All samples that were subject to surfactant treatment (see Tab. 4-1) are expected to show higher OM contents due to sorbed surfactant. Similar samples used by other workers (e.g. SCHÜTH, 1994) show considerably lower values in the NS for example. AS with no prior treatment correlates fairly well with prior measurements of Schüth and Wilhelm. Sample variability, as observed e.g. in the HH_d material, where the composition is subject to considerable heterogeneity, can lead to varying contents of OM from sample to sample.

4.2.5.2 Internal Porosity and Internal Surfaces

Internal porosity and internal surfaces were measured with nitrogen adsorption/desorption BET method, which covers the range of mesopores (\varnothing 2-50 nm). Pore spaces with less than 2 nm diameter cannot be evaluated using this method (see 4.2.4). All samples showed typical IVb isotherms which document the presence of mesopores (see Fig. 4-1). With the exception of RS (SCHÜTH, 1994), all samples showed considerable intraparticle porosity in the mesopore range.

Fig. 4-2 shows the volume distribution of the intraparticle pores for changing pore radii for three materials. The characteristic spike at approx. 2 nm, which is a prominent feature

Table 4-4: Summary of intraparticle porosities and internal surfaces. (Evaluation methods: SP= Single Point N₂ adsorption, BET=BET N₂ Adsorption Isotherm, BJH =N₂ Desorption Isotherm).

Sample \varnothing (mm)	Int. Surface [m ² /g]			Int. Porosity [%]	
	SP	BET	BJH	SP	BJH
AS (0.25-0.5)	1.55	1.59	1.40	0.59	0.72
AS*	1.35	1.39	1.68	0.72	1.04
NS (0.25-0.5)	8.97	9.22	7.38	2.44	2.50
NS*	9.38	9.69	11.31	3.12	3.62
HH ₁ (0.25-0.5)	0.92	0.98	1.26	0.65	1.08
HH ₁ *	0.77	0.78	0.97	0.64	1.10
HH _d (0.25-0.5)	7.61	7.82	7.79	2.96	3.89
HH _d *	7.12	7.40	9.60	3.39	4.21
HH _d (1-2)	5.68	5.88	4.74	0.64	1.06

*Samples remeasured after heat treatment (550 °C)

present in all samples (see Appendix II), does not correspond with a distinct pore radius (see 4.2.4), but can be considered as an instantaneous release of the remaining nitrogen that can be detected with this methodology. Fig. 4-3 shows the cumulative plots of the internal surfaces and volumes vs. pore radii. T-plots used to check for microporosity did show only minor y axis intercept indicating virtually no microporous domain. Table 4-4 gives a summary of the derived internal surfaces and internal porosities. Note that due to different evaluation methods values for both internal surface and intraparticle porosity in one sample might differ. In Tab. 4-5, BET surfaces and porosities based on the BJH-desorption isotherm are listed. The results from NS and AS generally compare well with those from SCHÜTH (1994) and GEWALD (1995), considering that the samples contained different grain sizes.

The most prominent result derived from the analysis of the intraparticle porosity is the fact that for the NS and AS small pores, at the micro-mesopore boundary contribute major fractions of both the internal surface as well as the pore volume. Although the HH samples also show this peak in the lower mesopore range, the relative amount of pore volume and specific surfaces is much less

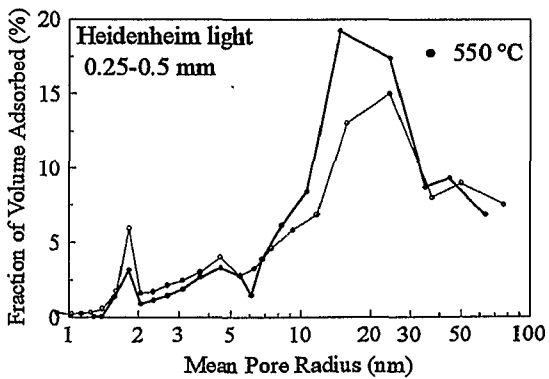
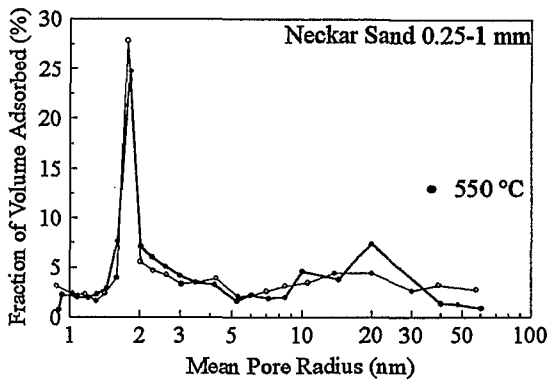
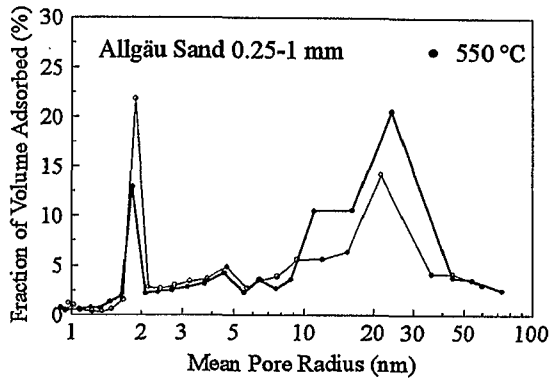


Figure 4-2: Fractions of total pore volume (%) plotted vs. pore radii of three materials. Peaks at 2 nm correspond to the integrated instantaneous release of N_2 at the lower end of the detection limit. The curves represent samples which were oven-dried at 105°C and 550°C respectively.

dominant. For all samples both parameters (pore volume and internal surfaces) are, as expected, highly correlated (simultaneous increases in porosity and surfaces). Pore volume and internal surface distributions of the samples were remeasured after heat treatment of 550°C over 6 hours. At these temperatures carbonate alteration should not yet occur, but organic matter should undergo combustion. Possible changes in pore volume and internal surface might therefore be due to the removal of organic matter and indicates

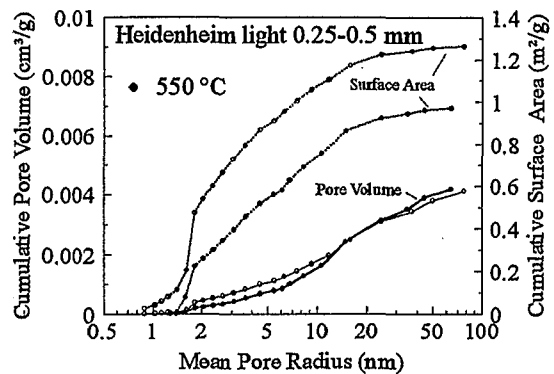
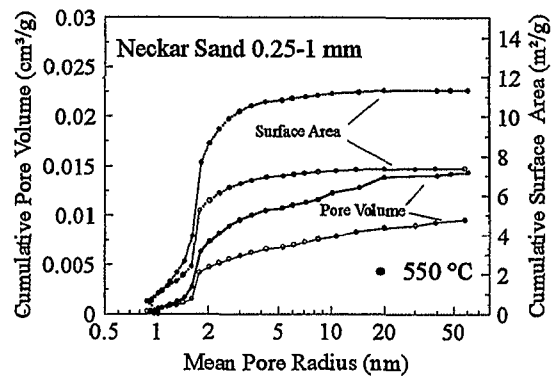
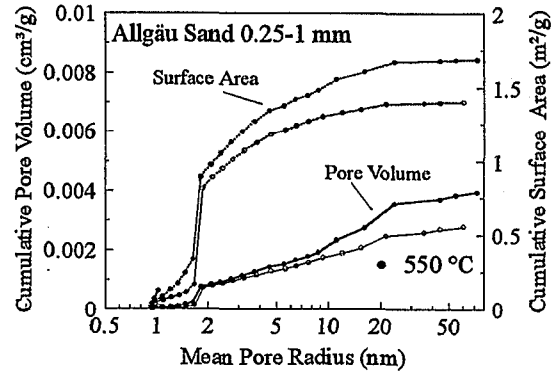


Figure 4-3: Cumulative plots of the internal surfaces and pore volumes vs. pore radii. Steep slopes manifest domains that account for substantial amounts of either surface area or volume. The prominent slopes at approx. 2 nm do not correspond with an available surface or volume at that specific pore radius, but stand for integrated surfaces and volumes measured at the lower end of the detection limit.

that the distribution of organic matter varies with changing pore domains.

The obtained data show marked differences between the values obtained at 105°C and 550°C (Tab. 4-4). The samples follow a general trend of decreasing fraction of pore volume at 2 nm and an increasing fraction at about 20-30 nm (see Figures 4-2 and 4-3). At the same time, intraparticle porosities

Table 4-5: Comparison of intraparticle porosities and internal surfaces from Allgäu Sand and Neckar Sand obtained by various workers (SCHÜTH, 1994 ; GEWALD, 1995). * denotes sample values after heat treatment (550° C).

Sample/Grain Size [mm]	BET Surface [m ² /g]			Internal Porosity [%]		
	Schüth	Gewald	this work	Schüth	Gewald	this work
Allgäu Sand						
(0.315-1)	2.12			1.01		
(0.25-0.5)			1.59/*1.39			0.72/*1.04
(1-2)		1.79/*1.53			0.92/*1.14	
(0.08-0.315)		2.52/*1.52			1.34/*1.24	
Neckar Sand						
(0.315-1)	8.68			3.11		
(0.25-0.5)			9.22/*9.69			2.50/*3.62
(1-2)		11.29/*9.13			3.83/*3.41	
(0.08-0.315)		1.51/*11.29			1.26/*4.79	

increase noticeably, with the exception of sample HH₁.

An interpretation of the observed deviations as being caused by the removal of organic matter, however, is somewhat speculative, as the thermal treatment could also cause additional cracks that add to a grain's porosity, and incomplete combustion would spare domains containing organic matter which would then not show up in the comparison between heat treated and untreated sample.

However, finding samples such as AS and NS, where large fractions of the total porosity belong to pore sizes at the lower mesopore range would cause PAHs diffusing into these domains to undergo constrictivity effects (see 2.3.5.3), a mechanism that would lead to low apparent diffusion coefficients. If constrictivity is not taken into account, the observed low diffusion rate constants might erroneously be corrected by a tortuosity factor that does not reflect the actual pore geometry.

4.3 Experimental Concept

4.3.1 Column Setup

The aim of the experiments was to test various sample matrices under laboratory conditions with respect to their desorption characteristics for strongly sorbing organic contaminants. The column setup was chosen, because it allows to create a maximum concentration gradient from the immobile into the mobile phase by a constant removal of the contaminants from the aqueous phase

(Fig. 4-4). This boundary condition (quasi zero concentration of PAHs in the water) results in maximum flux and allows simple analytical solutions to spherical diffusion problems (see Chap. 3.1).

The samples were packed into stainless steel columns. All other system components (fittings, screens, tubing) were also made of stainless steel. The use of stainless steel and glass components guarantees that the system sorption is kept at a minimum.

4.3.2 Experimental Implementation and Sample Handling

The columns were filled from the top, as water entered the column at the bottom. The material was filled in simultaneously with a rising water level in the column. This ensured that the columns were water saturated at all times. In order to achieve a homogeneous packing and to remove captured air, the column was intermittently shaken to allow for successive compaction of the material. Using material of a very narrow grain size range

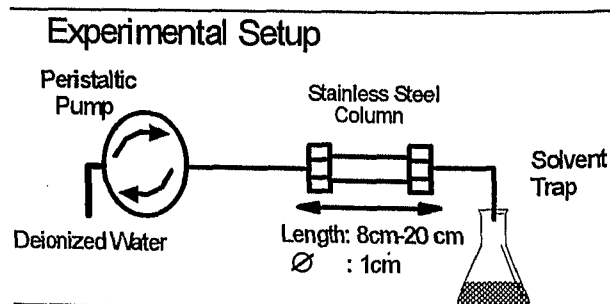


Figure 4-4: Experimental setup of the desorption experiments using only stainless steel and glass components. Flow conditions are controlled by a peristaltic pump.

also helped to achieve uniform flow conditions.

In experiments with materials from previous batch experiments, the first pore volumes do also not picture the sorptive release of contaminants but the aqueous concentrations at the end of the batch experiments.

In the final stages of the experiments some columns were purged with a surfactant (see Chap. 4.3.3). Their dispersive properties sometimes cause sediment fines to pass the screens in the effluent (screen \varnothing 63.5 μm). These fines are "extracted" in the solvent trap. Therefore, the contaminant mass of these samples does not reflect a diffusive release, but an advective removal of aquifer solids (along with their extraction). As aquifer fines can contain high amounts of contaminants, high concentrations of contaminant masses can be released.

4.3.3 Surfactants

Surface active agents have received increasing interest with regard to their application in subsurface *In-situ* remediation. (e.g. KILE and CHIOU, 1989; ABDUL ET AL., 1990, EDWARDS ET AL., 1991; FOUNTAIN, 1992; SHIAU ET AL., 1992). The main focus has been put on the surfactants' ability of the solubilization of hydrophobic compounds. This ability is due to the amphiphilic nature of surfactant molecules (possessing 2 functional groups (hydrophobic and hydrophilic) (see Fig. 4-5), generating two moieties of contrasting tendencies to go into solution (ROSEN, 1979).

As the concentrations of a surfactant are raised above a critical concentration threshold

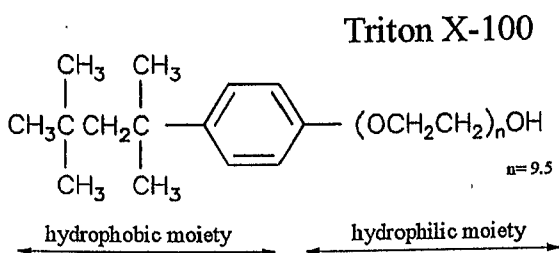


Figure 4-5: Structure of the nonionic surfactant Triton X-100. Triton has a hydrophilic moiety made up of a polyoxyethylene chain of $n = 9.5$ in average (after EDWARDS ET AL., 1991).

Table 4-6: Structure, molar weight and critical micelle concentration (CMC) of Triton X-100, a nonionic surfactant (from KILE and CHIOU, 1989).

Structure:	$\text{C}_8\text{H}_{17}\text{C}_6\text{H}_4\text{O}(\text{OCH}_2\text{CH}_2)_{9.5}\text{OH}$
Molar Weight:	628
CMC: (mg/l)	130

(CMC), the monomers form 3-dimensional structures (micelles) where the ionic or polar groups face the aqueous phase and the hydrophobic ends form a pseudo-organic phase. The surfactant used in the final stages of the desorption experiments was Triton X-100, a nonionic surfactant (see Fig. 4-5; Tab. 4-6).

Dissolved PAHs show a high affinity towards this 'hydrophobic' core of micelles and exhibit increased apparent solubilities in the presence of micelles. High molecular PAHs are more prone to this effect. In addition to mobilization and solubilization, surfactants are also utilized in sorption barrier concepts (BURRIS and ANTWRTH, 1992; BROWN ET AL., 1992).

4.4 Analytical Methods

4.4.1 Water Samples

The effluent water was collected in glass vials containing cyclohexane as solvent trap for the extraction of PAHs and an internal standard. The flow rate was controlled using a peristaltic pump. The effluent was completely collected for complete recovery of the desorbed PAHs. The complete sampling of the effluent of course limits the flow rates through the columns at extended sampling intervals (severals days). In the course of the desorption experiment the fluxes were reduced as the release rates dropped.

Following initially high sampling frequencies at the beginning of the experiment, the flux of the peristaltic pumps is reduced. After removing a sample, the glass container was placed in a horizontal shaker for 30 minutes to allow for complete extraction of the effluent with the cyclohexane. The volume-ratio solvent trap/sample needed for complete extraction is a function of the K_{ow} . No ratio less than

1/100 was used. Fluorene with a $\log K_{ow}$ 4.18 (YALKOWSKY and VALVANI, 1979) will have a 10,000 fold higher concentration in the cyclohexane phase than in water. At the above 1:100 ratio 99% of the fluorene will be concentrated in the solvent trap. For a $\log K_{ow}$ larger than those of fluorene the extraction will be even more effective.

The samples that were analyzed using HPLC were reduced in N_2 to near dryness and resolved in acetonitrile (100 μ l). For subsequent GC/MS analysis, the cyclohexane phase was reduced to approx. 1 ml.

4.4.2 Soil Samples

In order to evaluate desorption processes, it is of prime interest to quantify the total amount of sorbed contaminant on the aquifer material. Next to highly sorbing sample matrixes (e.g. high organic carbon content) the variability of concentrations in "natural" samples imposes large problems on calculating mass balances. The extraction methods used involve two different techniques which are treated in detail in two diploma theses (WALZ, 1994; ANDERS, 1995).

4.4.2.1 Soxhlet Extraction

For the extraction of PAHs, a method was used as optimized by WALZ (1994). WALZ compared several extraction solvents including cyclohexane/acetone mixtures, toluene, and dichloromethane. Extractions using dichloromethane as solvent performed best. Extraction times needed to be extended to at least two days in order to remove high- K_{ow} PAHs from soil matrixes. To remove polar groups and soil particles from the dichloromethane extract, several clean-up steps are needed (see WALZ, 1994). After being transferred from dichloromethane to a cyclohexane phase, the latter was reduced in a N_2 stream near to dryness and picked up in acetonitrile for later analysis.

4.4.2.2 Supercritical Fluid Extraction (SFE)

Commonly used extraction methods involve large amounts of solvents, time, and labor consuming clean-up and handling procedures (e.g. transfer between different solvents). In

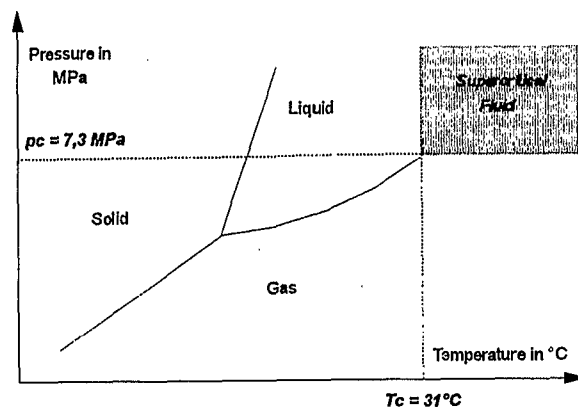


Figure 4-6: CO_2 phase diagram. The supercritical pressure/temperature range for CO_2 is above 31.1 °C and 7.3 MPa (after ANDERS, 1995)

order to reduce the use of solvents and to limit analyte loss during cleanup steps, aquifer materials were extracted using SFE. SFE is based on the changed physical properties of supercritical CO_2 . Supercritical conditions for CO_2 are reached at 31.1 °C and at a critical pressure of 7.37 MPa (REID ET AL., 1987) (see Fig. 4-6). At pressures and temperatures above these critical values the phase boundary between liquid and gaseous phase disappears.

Supercritical CO_2 is compressible, but cannot be liquified by further pressure increase. It has densities of three orders of magnitude higher than those of gases. Due to diffusion coefficients 1000x higher than in liquids and its nonpolarity it is an excellent extraction media for nonpolar compounds. A detailed introduction in the physical background of SFE is given by KNIPES ET AL. (1993).

Table 4-7: System components of the SFE and extraction methods of soil samples.

Extraction Unit	HP 7680 T
Trap	Hypersil ODS (40 μ m)
Thimble Volume	7 ml
Total Void Volume (Trap + Tubing)	1 ml
Extract Volume	1.8 ml
Total extraction time	2 hours
Extraction Pressure	37.9 MPa
Extraction Temperature	80 °C
Trap Temperature	25 °C
Rinse Rate	0.6 ml/min
Rinse Solvent	n-Hexane/Acetonitrile
Internal Standards	Deuterized PAHs Bromo-Phenanthrene

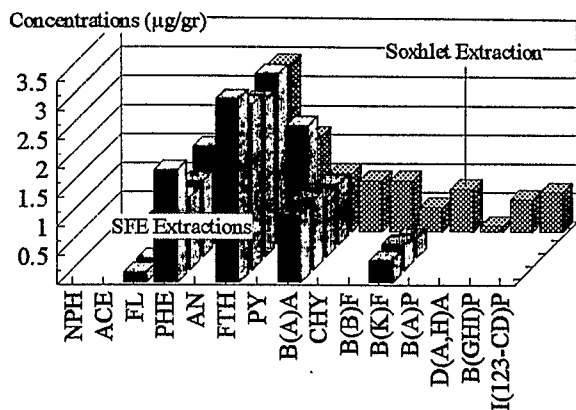


Figure 4-7: A comparison of mass balances of 1 Soxhlet extraction of HH₁ 0.25-0.5 mm and mass balances of 4 column experiments in which 5 PAHs were monitored, using SFE extractions.

Instrumentation and extraction method of the samples is given in Table 4-7. Prior to extraction the samples were freeze-dried, as high water contents could lower the recovery and may cause plugging problems at the restrictor unit of the SFE system.

ANDERS (1994) tested SFE in comparison to Soxhlet extraction and a method using an acetone-cyclohexane mixture, finding SFE to be equally or more efficient than the other two methods. Fig. 4-7 shows a comparison of column extractions and a Soxhlet extraction of the HH₁ 0.25-0.5mm.

4.4.3 PAH Analysis

Quantitative analysis of the water samples was performed using liquid chromatography (HPLC) implemented with fluorescence/UV detectors or gaschromatography (GC) with a mass spectrometry. As both analytical methods are well established, only a short introduction in the background and instrumental implementation is given. Details on e.g. HPLC can be found in MEYER (1979).

Table 4-8: HPLC system components

Detectors	Perkin Elmer LS-3b
HPLC Pumps	Waters 501
Injection valve	Rheodyne Six Port , 20 µl sample volume
A/D Interface	Waters System Interface Module
Software	Waters Maxima (1987)
Flow Media	Water/acetonitrile mixture of varying portions (non isocratic)
Column	Grom PAH, 250mm x 4mm, 5µm

Chromatographic methods are based on the separation of various compounds in multicomponent samples which is caused by different partitioning behaviors of components in a mobile phase with respect to a stationary phase. The mobile phase can be a liquid (e.g. acetonitrile/water mixture in HPLC) or a gas (e.g. helium in GC/MS). After separation in a column, the different compounds are queued up for subsequent detection.

All water samples were quantified using internal standards. Internal standards were chosen, such that the physico-chemical parameters were comparable to, or similar to those of PAHs. Methods and components used are listed in Tables 4-8 - 4-10 and in Appendix I. Soxhlet soil extractions (using dichloromethane as extraction solvent) that were analyzed with the HPLC were quantified using an external standard.

4.4.3.1 HPLC Chromatography

The components of the High Pressure Liquid Chromatography (HPLC) System using acetonitrile/water mixtures as flow media are listed in Table 4-8. Quantification of the samples was done by integration of the signal area and internal standards. System handling and data evaluation was performed with the Maxima chromatography software package.

Due to the various analytes (single compounds or more complex mixtures) several chromatographic methods were used. One of the methods is described below, for a complete listing of methods see Appendix I.

Table 4-9: Components and analysis conditions of HPLC method 1

Method 1 6 PAHs		
Internal Standard: Benzo(b)naphto(2,1-d)thiophene		
Wavelength (nm)	Extinction	Emission
Naphthalene	275	350
Fluorene	275	350
Phenanthrene	275	350
Fluoranthene	284	463
Benzo(a)anthracene	286	387
Int. Standard	284	463
Benzo(k)fluoranthene	305	366
UV detection	254	

Method 1 was used with complex samples (e.g. Heidenheim samples). The selected analytes were chosen to monitor a range of K_{ow} s (see Tab. 1-2) and also with respect to their relative abundances in soil extractions (chromatographic fingerprint). To achieve sufficient separation, a non-isocratic flow regime was used (0% - 40%).

4.4.3.2 GC/MS Analysis

For some samples PAH concentrations were quantified by gas chromatography (GC) combined with a mass selective detector (quadrupole mass spectrometer). Mass spectrometry is based on the fact, that molecules, after being exposed to an electron source, are shattered to fractions of characteristic masses. Quantification is possible by integrating the number of characteristic mass counts/time in the MS unit and by using internal standards. In contrast to fluorometry

detectors that exhibit varying sensibility with respect to different compounds (generally increasing sensibility with increasing number of rings), mass spectrometry has similar detection limits for all PAHs. The system qualifications are listed in Table 4-10.

Table 4-10: GC/MS system components

Gas Chromatograph	HP 5890 Series II
Mass Spectrometer	HP 5972 A
Autosampler	HP 7673
Software	HP G 1304 C
Column	HP 5.25m x 0.25mm, 025 μ m
Gas	Helium
Flux	30 cm/min (constant)
Temperature	65°C 4min; 10°C/min \Rightarrow 270°C;
Program	270°C 10 min; 10 °C/min \Rightarrow 310°C 310°C 6.5 min
Target Ions	128, 152, 154, 166, 178, 202, 228 252, 276, 278

5. Desorption from Contaminated Aquifer Material

The environmental impact of a contaminated site depends largely on the release characteristics of the compounds of interest. This chapter deals with the desorption behavior of several contaminated materials. These include samples of three aquifer materials. Continuous monitoring during column experiments makes it possible to discriminate between fluctuations in release rates and can give insights on the mechanisms active at various times scales. The time frame for the desorption experiments depends on the kinetics and the capacity of a material and ranged from 30 to more than 100 days. The PAHs monitored depend on their initial concentrations in the material which controls the time period over which they can be monitored.

In order to evaluate whether the sorption and desorption behavior of natural aquifer materials is fully reversible several samples from SCHÜTH (1994) were used in desorption purge experiments. The direct comparison of sorption and desorption data should give an indication as to whether uptake and release of hydrophobic compounds can be described by the same processes and whether the entire mass of sorbed solute is subject to subsequent desorption.

5.1 Desorption from Rhine Sand (RS)

5.1.1 Sorption History

The RS samples used were monitored during their sorptive uptake and reached equilibrium conditions after approx. 20 and 40 days for *NAP* and *FTH* (SCHÜTH, 1994).

5.1.2 Desorption Behavior of Rhine Sand

Figure 5-1 depicts the desorption of *NAP* and *FTH*. For *FTH*, two experiments were conducted to check for consistency. A surfactant (Triton X-100) was used to evaluate the possible impact on late-time release rates in one of the experiments (*FTH* II).

The RS shows a biphasic release behavior, consisting of an initial period of rapid desorption followed by a period of low, but more persisting release rates (see Fig. 5-1).

An interpretation of this biphasic behavior in terms of physical processes is nonunique, as fast fractions could be due to several reasons:

- mixed samples with several different desorption rates
- different grain sizes
- sorption sites on the outside of the grains, where no intraparticle resistance to diffusive transport affects the mass transfer between the mobile and immobile phase
- the mobilization of fines from the column content at the beginning of the experiment or possible flow conditioning effects of the column.

As the material used was limited to a narrow range of grain sizes, size effects are expected to be negligible. Initial mobilization of fines was not observed. Instead, the high value of the instantaneously or fast desorbing fraction for the RS seems to be closely related to release of PAHs from sites on or close to the grain surface.

Of all aquifer materials used, the quartzitic RS has the lowest organic carbon content which is accompanied by smallest intraparticle porosity in the mesopore range (SCHÜTH, 1994). This results in a low sorption capacity. A combination of the above characteristics fosters the emergence of a prominent fast fraction (in terms of mass released/total mass sorbed), most likely due to desorption from sites close to or on the surface of the grains.

To address the nature of these fast sites in terms of surface sorption vs. hydrophobic partitioning is somewhat indecisive. To determine the relative importance of surface sorption vs. hydrophobic partitioning into soil organic matter (SOM), MCCARTY ET AL. (1991) introduce the critical level of organic

matter for a specific solute/solid combination f_{oc}^* , which is defined as

$$f_{oc}^* = \frac{S}{200} \frac{1}{(K_{ow})^{0.84}} \quad (5-1)$$

where S is the specific surface area (L^2/M). If the measured f_{oc} is higher than the f_{oc}^* surface sorption is most likely not the ruling sorptive process. Eq. 5-1 readily shows that the amount of surface sorption is effected by the octanol/water partition coefficient, leaving less hydrophobic compounds prone to sorption on mineralic surfaces in contrast to the higher affinity of more hydrophobic compounds to partitioning into soil organic matter.

Calculating the f_{oc}^* for the RS and *FTH* leads to a f_{oc}^* well below the measured f_{oc} and supports the idea of exposed organic matter at the grain surface. More support for this interpretation is given by SCHÜTH and GRATHWOHL (1996), finding a drop of 90 % in sorption capacity for heat treated RS material ($550^\circ C$). The fast desorbing X_i fraction is therefore considered to be due to organic matter close to the surface.

The marked influence of the fast fraction in the RS is only due to the limited sorption capacity of the intraparticle domain. The relative amount of mass contributed by such a fraction would otherwise be considerably smaller, as surface- or near-surface desorption would be dwarfed by subsequent release from the intraparticle domain. In the case of the RS, the mass distribution of PAHs between the fast and slowly desorbing sites is more or less similar (see Table 5-1).

The observed results correspond well with the

Table 5-1: Diffusion rate constants (D_a/a^2) and fractions of instantaneously desorption (X_i) obtained from sorption (SCHÜTH, 1994) and desorption experiments (this work).

	Sorption		Desorption	
	D_a/a^2	X_i	D_a/a^2	X_i
	[1/s]	[-]	[1/s]	[-]
<i>NAP</i>	$1.8e-7$	0.58	$1.5e-7$	0.80
<i>FTH</i>	$9.2e-8$	0.49	$1.6e-8$	0.41
			$1.8e-8$	0.45

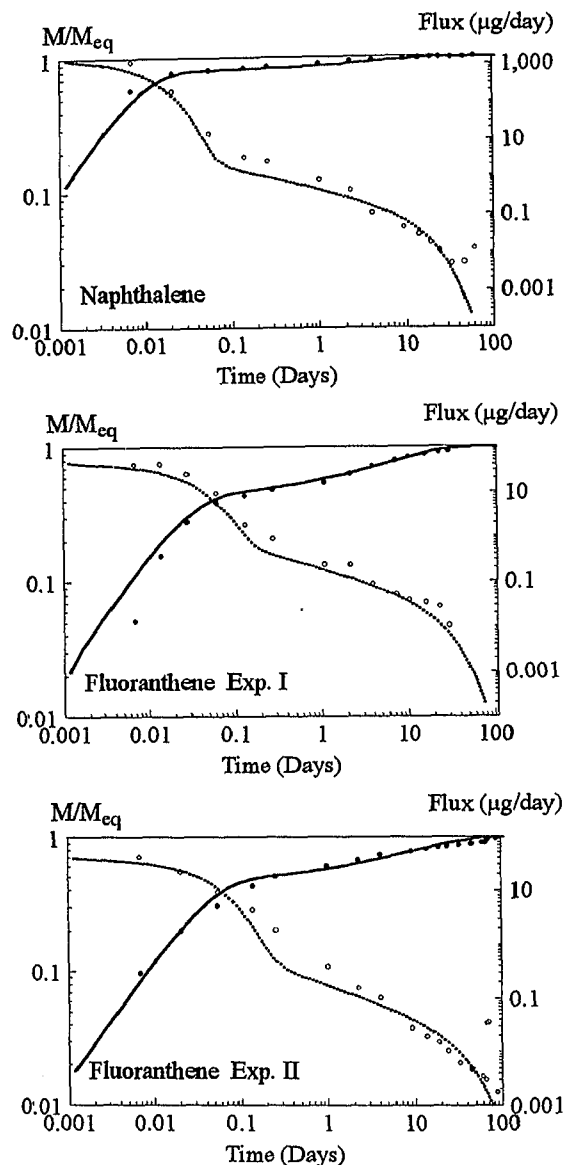


Figure 5-1: Desorption kinetics of Rhine Sand. Solid lines and dotted lines: M/M_{eq} and fluxes fitted with a two-site model. For the fast desorbing fraction (X_i), a simple first-order term is used to describe the desorption kinetics; the long-term desorption is modelled using the intraparticle diffusion model. The increase of *FTH* release rates in the lowermost frame at 60 days is due to the use of a surfactant (Triton X-100 at 2g/l) in the final stage of the experiment.

findings from the sorption data obtained by SCHÜTH (1994) (see Tab. 5-1) for the same samples. The diffusion rate constants from batch and column experiments are in close agreement with a deviation only in the amount of instantaneously removed fraction for *NAP*. Repeated experiments (*FTH I* and *FTH II*) showed that the procedure results in good reproducibility.

At the end of the *FTH II* experiment a surfactant (Triton X-100) at 2g/l was purged

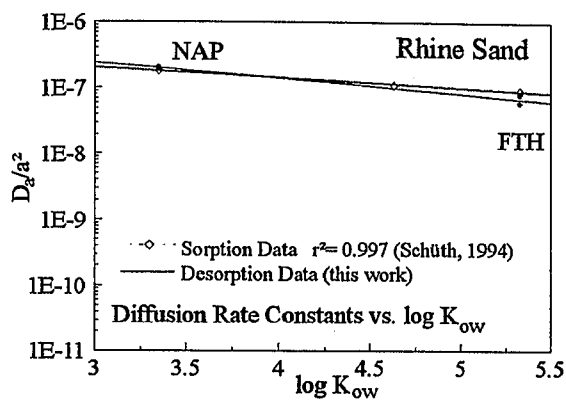


Fig. 5-2: Dependency of the diffusion rate constant on the octanol/water partition coefficient. The diffusion rate constants decrease with increasing K_{ow} . Values derived from sorption experiments (Schüth, 1994) and desorption experiments are in close agreement.

through the columns to evaluate its effect on the remaining sorbed PAHs. In the *FTH II* experiment a short peak in the release rates was observed, after which the release rates again dropped to a level predicted by the diffusion model.

An interpretation of this increased flux is not readily available. One possible reason for this behavior could be the removal of sediment fines due to the dispersing characteristics of surfactants. The fines would consequently undergo a solid phase extraction in the solute trap. Once this fraction is removed, the limiting factor on the release rates again is the diffusive mass transfer out of the intraparticle domain. Therefore, the increased solubility of *FTH* in the mobile phase has no further impact on the release rates.

Another possible explanation is that, next to the surfactant monomers, micelles enter those parts of the intraparticle domain which are accessible for them, before size exclusion occurs. Micelles with an approx. size of 5 nm ROSEN (1979) might be able to enter some

Table 5-2: Summary of the obtained diffusion rate constants, fractions of the fast components X_i , λ the first-order rate coefficient used to model the fast fraction, and t_{90} the time until 90 % of the sorbed mass is removed by mere purging.

Rhine Sand	λ [1/s]	X_i [-]	D_d/a^2 [1/s]	t_{90} (d)
<i>NAP</i>	1.5e-3	0.8	1.5e-7	2.6
<i>FTH I</i>	4e-4	0.41	6e-8	24.7
<i>FTH II</i>	2e-4	0.45	8e-8	19.1

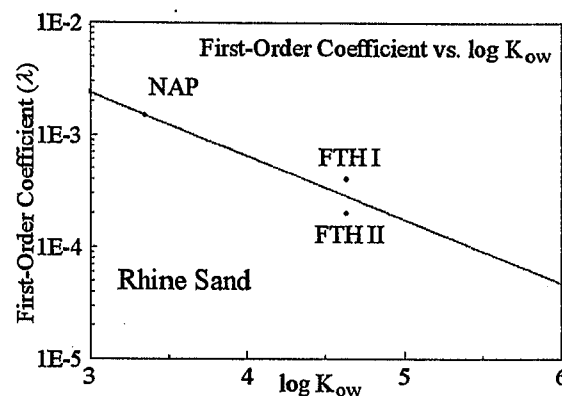


Figure 5-3: Dependency of the first-order rate constant of the fast desorbing fraction on the octanol/water partition coefficient. The first-order coefficients decrease with increasing K_{ow} .

intraparticle domains of the RS, as much of its porosity is associated with pore radii considerably larger than 5 nm. Access of micelles to some of these domains could cause increased release of PAHs into the mobile phase.

Plotting the diffusion rate constants vs. $\log K_{ow}$ s shows the dependency of the rate constants on chemical characteristics of the different compounds (see Fig. 5-2). Decreasing aqueous solubilities are expected to result in decreasing diffusion rate constants (BALL, 1989), as the apparent diffusion coefficient D_d depends on the K_d of the compounds of interest (see Eq. 2-14). The monomineralic RS also follows this behavior.

A similar correlation is found for the first-order rate constants of the fast desorbing fraction (Fig. 5-3). As the long-term approximation of diffusive fluxes out of a grain is a first-order process (Eqs. 3-5 and 3-6), the fast fractions could also indicate a very fast desorbing lithological component in the RS, which is depleted within the initial phase of the experiment.

Table 5-2 summarizes the results of the Rhine Sand experiments. Times to reach 90% removal of *NAP* and *FTH* from RS by desorption are on the order of days to weeks, indicating that PAH release from sandy material dominated by quartz is fast even for PAHs of a higher octanol/water partition coefficient such as *FTH*.

5.2 Desorption from Neckar Sand (NS)

5.2.1 Sorption History

The Neckar Sand sample was loaded with PAHs using a coal tar from the MPG Geislingen. The material was used in a column experiment where liquid coal tar phase was poured on the aquifer material and was subsequently purged with water (WILHELM, 1992). In the course of the experiment, the column was also purged with a surfactant. Prior to purging the material had approx. 700 days to equilibrate. From the bulk material the 0.25-1 mm fraction was used in the experiment. According to SCHÜTH (1994), NS samples (0.315 - 1 mm) reach 95 % of their equilibrium K_d values for *PHE* and *FTH* within 150 respectively 860 days. This implies a high degree of equilibrium for the samples used. The use of the diffusion model with its equi-

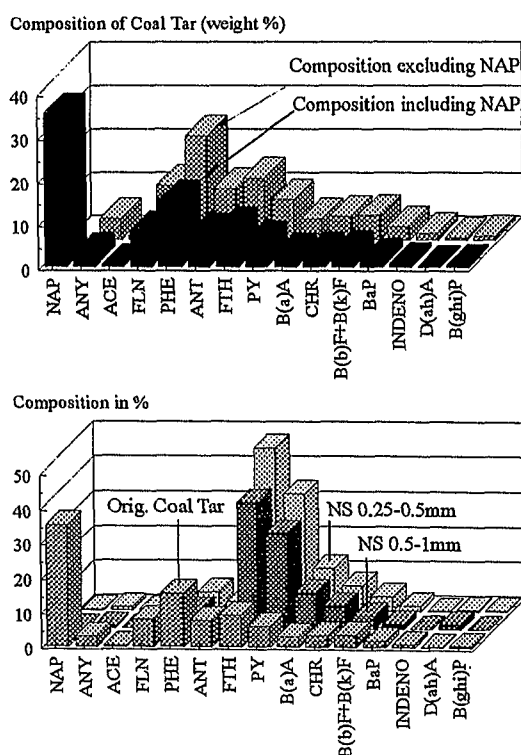


Figure 5-4: Upper frame shows the distribution of the 16 EPA PAHs in the Geislingen coal tar (fingerprint) (Eberhardt, 1995) and their respective weight percentages. The original tar is rich in *NAP* and shows a second maximum at *PHE*. Lower frame shows the marked differences in the relative abundances of PAHs and the fingerprint between the coal tar and 2 fractions of the NS samples. Both grain size fractions show a peak shift in the relative abundance from *PHE* to *FTH*.

rium boundary conditions (see Chap. 3.1.1) seems to be an appropriate way to describe its desorption behavior.

Fig. 5-4 shows the initial concentrations of the 16 EPA PAHs in the NS sample and the original composition of the coal tar from Geislingen. Compared to the relative abundance of PAHs from the Geislingen coal tar (EBERHARDT, 1995), the NS sample shows a shift in the relative abundances of the PAHs sorbed prior to the experiment. This difference in the 'finger printing' could be due to several reasons. The application of surfactants could have caused a partial desorption of the sand during the purging, where the more soluble compounds (*NAP* and 3-ring PAHs) with higher diffusion rate constants would show a higher degree of removal with respect to higher-ring PAHs. At the same time, 3-ring PAHs are more prone to degradation processes (e.g. possible biodegradation). The virtual absence of *NAP* is not surprising as *NAP* (2 rings) has been shown to be subject to considerable volatilization. All of the above mentioned processes would lead to the observed shift in relative amounts towards the 4- and 5-ring PAHs (see Fig. 5-4).

5.2.2 Desorption Behavior of Neckar Sand

In contrast to RS, the mass transfer of PAHs from NS into the aqueous phase can be attributed to release from the intraparticle domain, as most components did not show a fast desorbing fraction. Even for *FTH* and *PY* needing a fast desorbing fraction of 30 % of the M_{eq} in order to be fitted, the bulk of the sorbed mass followed the retarded pore diffusion model. This is in accordance with the higher intraparticle porosity and the higher organic carbon content of NS as compared to RS. The fast desorbing fraction for *FTH* and *PY* cannot be explained.

Figure 5-5 shows the desorption kinetics of four PAHs (*FTH*, *PY*, *B(a)A*, and *CHR*). As expected, the derived diffusion rate constants (D_a/a^2) for the intraparticle domain show a similar correlation as for RS. Declining diffusion rate constants correlate with increasing octanol/water partition coefficients (see Tab. 5-3).

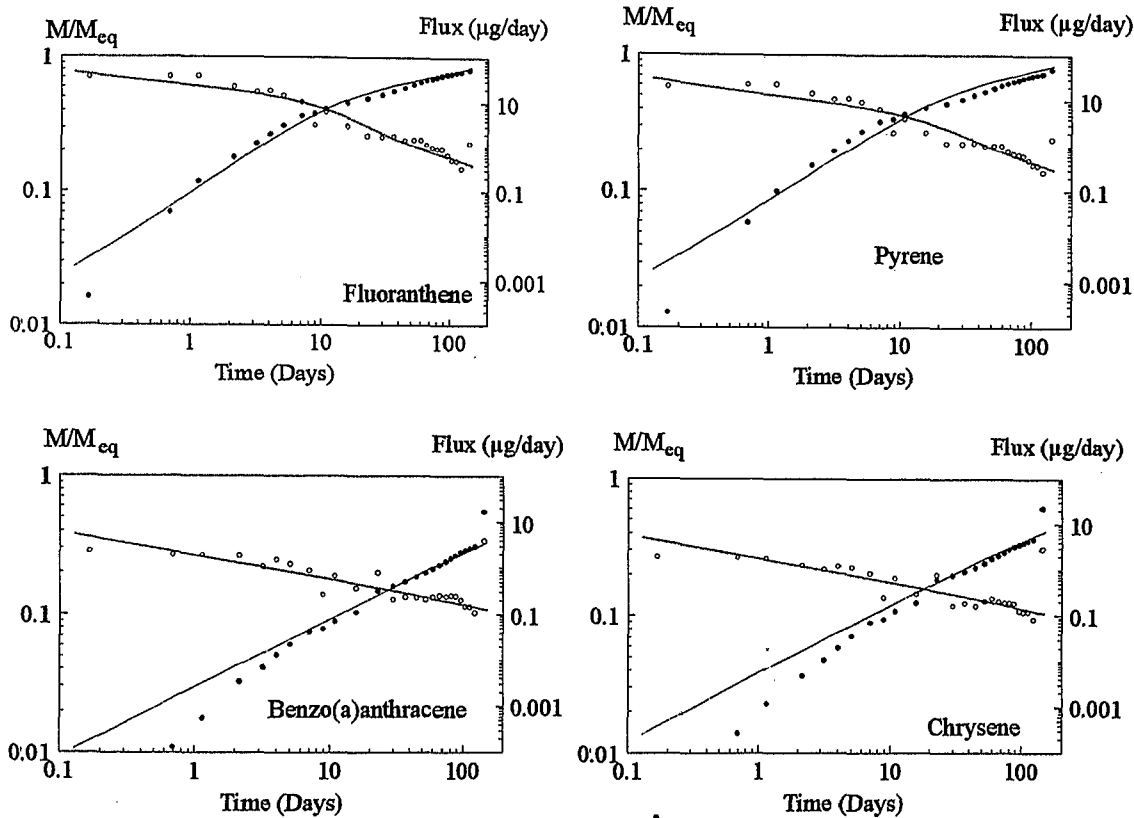


Figure 5-5: Desorption kinetics of Neckar Sand for 4 PAHs. Solid lines and dotted lines: M/M_{eq} and fluxes fitted with the two-site model. The increase in the release rates at the end of the experiment is due to the application of a surfactant (Triton X-100 at 2 g/l).

A comparison with data obtained by SCHÜTH (1994) for sorption shows a good agreement of the obtained rate constants (Fig. 5-6), where the rate constants derived from desorption experiments were slightly higher. Considering, however, possible experimental uncertainties in the mass balance and the complex contamination history of the sample,

the results indicate that sorptive uptake for NS is reversible and that the release can be approximated by the spherical diffusion model used.

The use of Triton X-100 at the end of the experiment caused increases in the release rates. Table 5-4 shows the relative increase of PAH release rates during the Triton application. As only the final sample was purged with surfactant, the duration of the enhanced release could not be determined.

Table 5-3: Summary of the obtained diffusion rate constants D_d/a^2 , the fraction of fast desorbing PAH X_i , λ the first-order rate coefficient of the fast fraction, and t_{90} , the time until 90 % of the sorbed mass is removed by mere purging. Release/time plots for the below mentioned compounds not found in Fig. 5-5 are given in Appendix III.

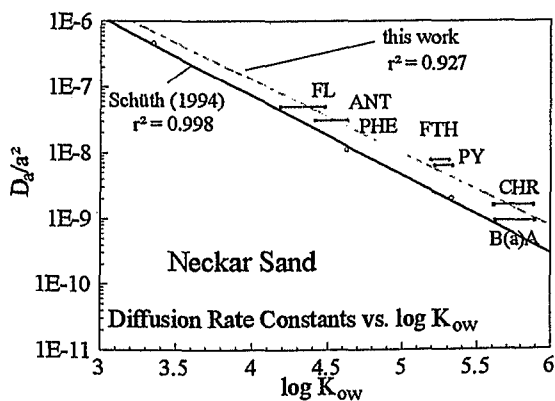


Figure 5-6: Dependency of the diffusion rate constants on the octanol/water partition coefficients. The diffusion rate constants decrease with increasing K_{ow} . Values derived from sorption and desorption experiments are in good agreement. The bars indicate the range of K_{ow} s from the literature.

Neckar Sand

	λ [1/s]	X_i [-]	D_d/a^2 [1/s]	t_{90} [d]
FL	-	-	5e-8	42
PHE	-	-	4e-8	53
ANT	-	-	4e-8	53
FTH	2e-6	0.3	8e-9	213
PY	2e-6	0.3	8e-9	223
B(a)A	-	-	9e-10	2360
CHR	-	-	1.5e-9	1415

Table 5-4: Relative increase of desorption rates in the final sample during surfactant treatment.

PAH	K_{ow}	Rel. Increase
FL	4.18	33
PHE	4.46	8.5
ANT	4.45	10.5
FTH	5.33	2.9
PY	5.33	4.6
B(a)A	5.61	30.1
CHR	5.61	25.1

However, in accordance to findings with RS (Chap. 5.1), where the flux rate for *FTH* decreased again to expected levels expected by the diffusion model, it is assumed that the increase in PAH release rates is also only a temporal one.

In addition to increases in the already monitored PAHs, the surfactant application also caused high K_{ow} compounds, which so far were below the detection limit, to appear in the effluent. Fig. 5-7 shows the comparison of the initial concentrations of PAHs in the effluent with the concentrations measured in the final sample. The relative increases in desorption rates do not show a K_{ow} dependency. As the high desorption rate

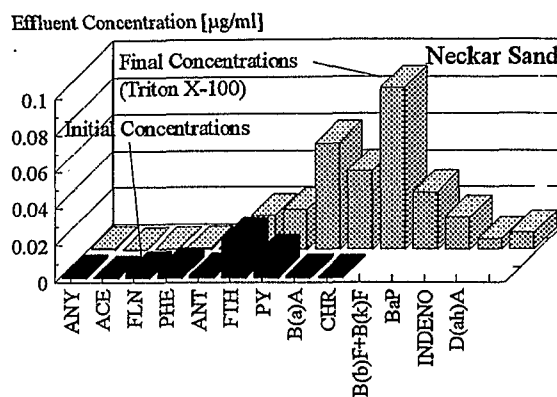


Figure 5-7: Comparison of the initial effluent concentrations and the effluent concentrations during the surfactant treatment. Surfactant treatment causes high K_{ow} compounds appear in the effluent.

increases for low K_{ow} PAHs are not reflected by high residual amounts, a mobilization of fines cannot explain this behavior.

Although the mobilization of otherwise very resistantly sorbed high K_{ow} compounds at much higher concentrations reduces their concentrations in the contaminated domain, the effluent aqueous phase carries very high concentrations of the toxically more relevant 4- and 5- ring PAHs.

5.3 Desorption from Allgäusand (AS)

5.3.1 Sorption History

The desorption behavior of PAH from AS was evaluated using 3 single component samples from SCHÜTH (1994) (*NAP*, *FTH* and *FTH II*) and 2 multicomponent samples from WILHELM (1992). According to SCHÜTH (1994), none of the samples had yet reached equilibrium conditions prior to desorption. For *NAP* approx. 70 % and for *FTH* about 30 % of the equilibrium K_d was reached in the sorptive uptake experiment (500 days). The exposure time for the sample from Wilhelm (1992) to coal tar was approx. 700 days, so similar nonequilibrium conditions could be expected. However, as none of the AS samples in the Schüth experiments reached equilibrium, the equilibrium K_d s were estimated using isotherm data derived from pulverized samples, assuming that pulverization had no influence on the sorption capacity of the material (BALL and ROBERTS, 1991; SCHÜTH and GRATHWOHL, 1996).

5.3.2 Effects of Nonequilibrium Conditions

Without prior knowledge of the degree of equilibration, data sets might be prone to be modeled with inappropriate assumptions concerning their initial conditions. Figure 3-5 depicts the differences in release behavior of an equilibrated system as compared to changing degrees of nonequilibrium prior to desorption. Unfortunately, the data obtained from desorption experiments do not necessarily provide information as to whether desorption started from an equilibrated system. As experimental data for hydrophobic compounds usually do not reach high degrees of contaminant removal during monitoring time, the typically higher slopes (-1/2--3/2) of fluxes expected from nonequilibrated systems might not yet show up prominently to be identified as such. An additional instantaneously desorbing fraction could also be responsible for a supposedly high amount of initial removal of a contaminant in the beginning of a desorption experiment, as it is expected for nonequilibrium conditions.

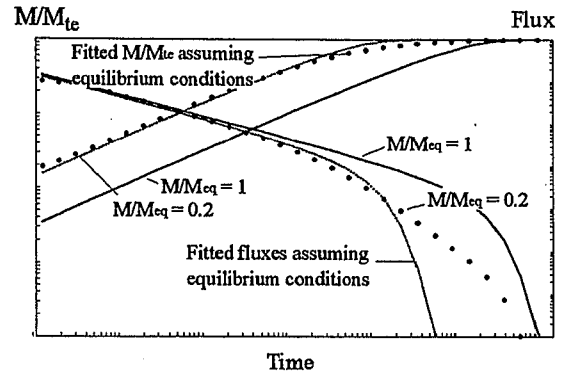


Figure 5-8: Fitting nonequilibrium data ($M/M_{eq} = 0.2$) with an equilibrium approach (using the mass sorbed (M_{te}) as M/M_{eq}) leads to higher diffusion rate constants and shorter contaminant removal times. The slopes of the fluxes of both approaches do not deviate but in a late stage of the experiment. A distinction between the two initial conditions therefore needs very long monitoring times (Fluxes = descending lines; M/M_{te} = ascending lines).

The consequence with respect to the determination of diffusion rate constants is, that experimental data fitted under an erroneous equilibrium assumption would lead to a possible introduction of an instantaneously desorbing fraction to account for the supposedly high initial removal of a compound and generally to higher diffusion rate constants. In the case shown in Fig. 5-8, the assumption of equilibrium conditions ($M/M_{eq} = 0.2$) leads to an overestimation of the diffusion rate constant of one order of magnitude and an underestimation of the removal times.

5.3.3 Desorption Behavior of Allgäu Sand

5.3.3.1 Desorption of *NAP* and *FTH*

The different experimental setup in the batch sorption experiments conducted by SCHÜTH (1994) leads to different boundary conditions than in column purge experiments. In the batch experiment aqueous concentrations decrease as a consequence of sorptive uptake. The analytical solutions (Eqs. 3-13-3-17) to model the desorption from a nonequilibrated sample however, assume constant aqueous concentrations during sorptive uptake. The effect of this mismatch of boundary conditions is documented in Figure 5-9.

The different type curves in Figure 5-9 correspond to different β 's (the ratio of solute mass dissolved to mass in solid phase at equilibrium) in batch systems during sorptive up-

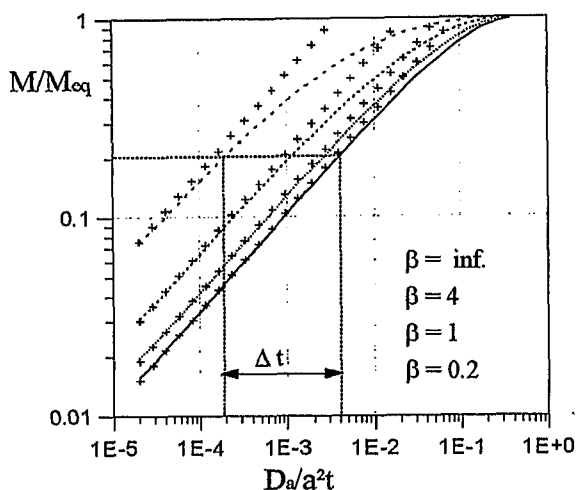


Figure 5-9: Analytical solutions of M/M_{eq} for different values of β ($\beta = \infty \rightarrow$ infinite bath); cross symbols denote the short-term approximations. $D_a t/a^2$ denotes the dimensionless time. Identical M/M_{eq} s correspond to different experimental time scales due to different boundary conditions. To account for the 'early' arrival at this M/M_{eq} , the model assuming infinite bath boundary conditions must lead to higher rate constants. (after Grathwohl, 1995)

take. For small β s, the initial rates of uptake are higher than in the case of $\beta \approx \infty$ which corresponds to an infinite bath (the boundary condition assumed for the poorly equilibrated systems in Chap. 3.1.7). At early times the degree of M/M_{eq} reached in an experiment where β is small, is higher than in the case of the infinite bath ($\beta \approx \infty$) (see Fig. 5-9). Erroneously interpreting a desorption experiment assuming $\beta \approx \infty$ would lead to an overestimation of the diffusion rate constants, as higher rate constants are needed to make up for the 'fast' arrival at the respective M/M_{eq} . The differences in time to reach equivalent M/M_{eq} with respect to the boundary conditions in column experiments increase as β gets smaller. In Figure 5-9 this time discrepancy (in terms of dimensionless time) is shown for a β of 0.25 with respect to a $\beta = \infty$.

SCHÜTH (1994) determined a β of 1.43 for *NAP*, 0.33 for *PHE* and 0.07 for *FTH*. For *NAP* with the highest β , it can be assumed that deviation in the obtained rate constant using the nonequilibrium model is minimal, as the boundary conditions are closest to that of an infinite bath. If the *NAP* desorption experiment is evaluated using the nonequilibrium approach (see Fig. 5-10), the derived diffusion rate constant ($2e-7$ 1/s), however, is by far higher (approx. 2 orders of magnitude)

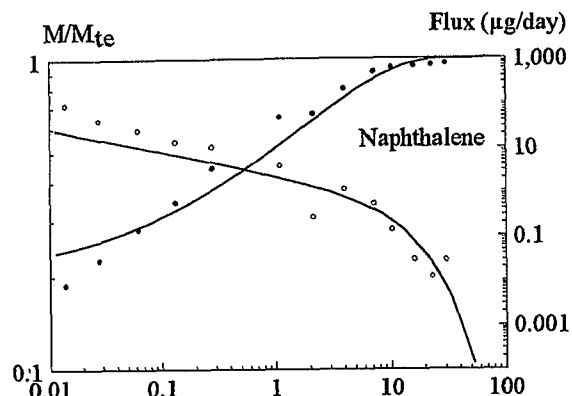


Figure 5-10: Modeling the desorption kinetics of *NAP* from AS sample using the nonequilibrium approach. The derived rate constant ($2e-7$ 1/s) is in contradiction to the one obtained in the sorption experiment (SCHÜTH, (1994).

than the one determined in the sorption experiment. This result indicates that the derived equilibrium K_{ds} by Schüth appear to be overestimated. That being the case, all three PAHs monitored by Schüth must have reached a much higher degree of equilibrium conditions, comparable to that of Neckar Sand. Consequently the equilibrium modeling approach also seems to valid for the Allgäu Sand samples and was used to determine the diffusion rate constants.

The obtained diffusion rate constants for the 3 samples and a comparison with the rate constants derived by SCHÜTH (1994) are compiled in Tab. 5-3. The diffusion rate constants for the equilibrium condition modeling show the expected discrepancy to the values from the sorption experiment in that the derived desorption rate constants are generally higher (by approx. one order of magnitude).

Fig. 5-10 shows the release behavior of the three samples (*NAP*, *FTH I* and *FTH II*). Fig.

Table 5-3: Diffusion rate constants (D_a/a^2), the fraction of instantaneous desorption X_i and first-order coefficient λ obtained from sorption (SCHÜTH, 1994) and desorption experiments (this work) modeled assuming equilibrium prior to desorption (see also Table 5-4).

	Sorption		Desorption			
	D_a/a^2 [1/s]	X_i [-]	D_a/a^2 [1/s]	X_i [-]	λ [1/s]	
<i>NAP</i>	$1.7e-9$	0.33	$2e-7$	0.2	$1e-3$	
<i>FTH</i>	$1.5e-10$	-	I	$2e-9$	0.015	$1e-3$
			II	$2e-9$	0.05	$2e-4$

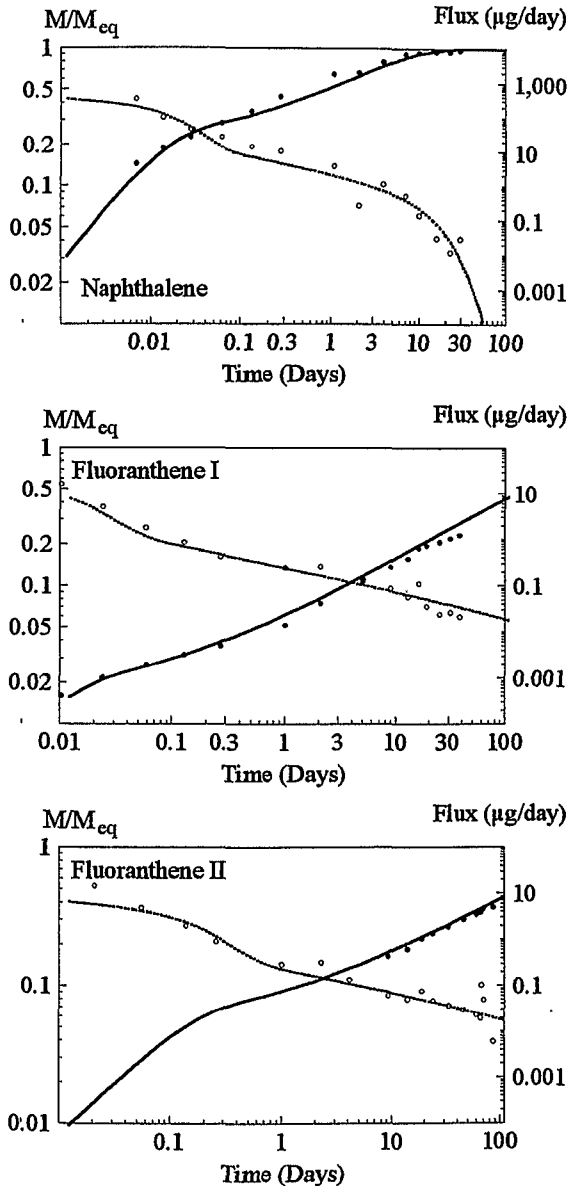


Figure 5-11: Modeling of the desorption kinetics of 3 AS samples using the equilibrium approach (Ascending lines = M/M_{eq} ; descending lines = flux). The peak in the *FTH II* release at the end of the experiment is caused by the use of Triton X-100 (2g/l). It shows only a short impact on the release rates.

5-11 shows the dependency of diffusion rate constants from the octanol/water partition coefficient. Decreasing K_{ow} s again show decreasing rate constants. The rate constants derived for both *FTH* experiments show a good reproducibility. In contrast to the RS, the effect of the fast desorbing sites is of minor importance, as the bulk mass of PAHs sorbed is associated with the intraparticle domain.

In the *FTH II* experiment a surfactant was used at the end of the experiment. The use of Triton X-100 (2g/l) led to a peak in fluxes,

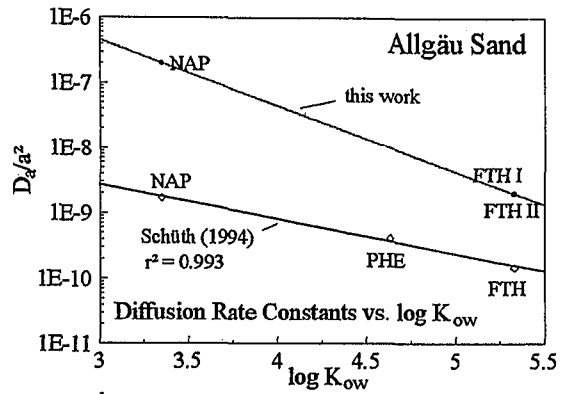


Figure 5-12: Dependency of the diffusion rate constants on the octanol/water partition coefficients. The diffusion rate constants decrease with increasing K_{ow} . The diffusion rate constants for the equilibrium condition modeling show a significant discrepancy to the values from the sorption experiment (see also Fig. 5-15).

which could be monitored for 2 samples. After this peak, the release rates dropped below the expected model flux. The short rate increasing effect is assumed to be due a limited PAH mobilization due to micelles entering the available intragranular pore space. As for RS (see Fig. 5-1) the observation indicates that there is no significant long-term effect of micelles on the release of *FTH* from the intraparticle domain of AS, as micelles with an approx. size of 5 nm (ROSEN, 1979) cannot reach the intraparticle domain and have further desorption enhancing effect. A visible mobilization of fines due to the dispersing effects of Triton X-100 was not monitored.

5.3.3.2 Desorption of PAH Mixture

The exposure of AS to PAHs was performed in a like manner as that of the NS (700 days) (see Chap. 5.2.1) with the exception of the use of surfactants. Fig. 5-13 shows the fingerprint of both the original tar oil and the AS used in the experiment. In contrast to the NS sample, the fingerprint is virtually identical with that of the source material, whereas NS had lost some of its 3-ring compounds with respect to the original coal tar. This indicates that AS might have a higher tendency to sorb PAHs than NS and the 3-ring PAHs are not subject to extensive biodegradation or volatilization.

Two experiments were conducted with the AS sample (AS I and AS II). Figure 5-14 shows

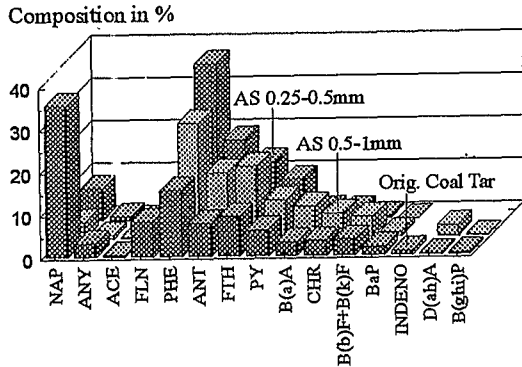


Figure 5-13: Relative abundances of the 16 EPA PAHs in the original coal tar (EBERHARDT,1995) and AS. In contrast to NS, the AS finger printing is similar to the distribution of PAHs in the original coal tar, with the exception of *NAP*.

release plots fitted with the equilibrium approach for experiment 1 and 2. Of all experiments using AS (single and multicomponent), only the AS batch used in experiment 1 showed a considerable fast desorbing fraction (0.3 - 0.21). The amount of X_i is rather constant, (see Table 5-4) which indicates no discriminating desorption from fast sites between PAHs of different K_{ow} s in the AS. Dependent on the K_{ow} , the time span over which the fast fraction is dominating grows with increasing K_{ow} . The diffusion rate constants derived for the second batch for corresponding PAHs agree well with those of batch 1. The lack of a fast desorbing fraction cannot be explained. A possible explanation could lie in a higher amount of grains at the lower limit of the grain size distribution (0.25 mm - 1 mm).

Table 5-4 gives a compilation of the diffusion rate constants for both batches. In both batches the rate constants decrease with increasing K_{ow} s. Compared to the rate constants from the sorptive uptake experiments (SCHÜTH, 1994), the rate constants from the equilibrium model for the AS are higher (in accordance with the single component samples) and reach similar values as in NS.

The first-order coefficients λ for the fast desorbing fraction do not exhibit a similar trend as the diffusion rate constant and remain constant (1e-5 - 4e-5 1/s) over whole range of octanol/water partition coefficients (see Table 5-4). Fig. 5-15 shows the rate constants of all AS samples fitted with the equilibrium model.

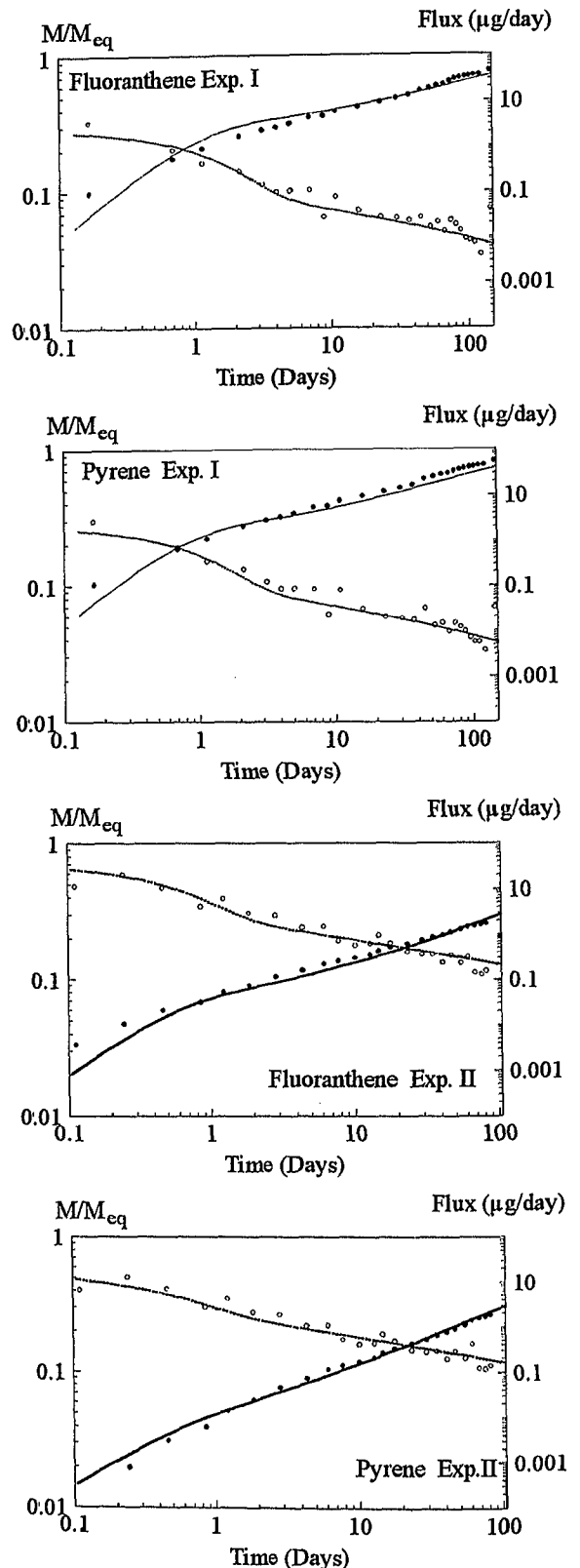


Figure 5-14: Modeling of the desorption kinetics of *PY* and *FTH* from AS (experiment 1 and 2) using the equilibrium approach. (Ascending points = M/M_{eq} ; descending points = fluxes). The spike in release rates at the end of the experiment 1 is caused by the use of Triton X-100. The model fit for experiment 2 did not require a significant amount of instantaneously desorbing fraction.

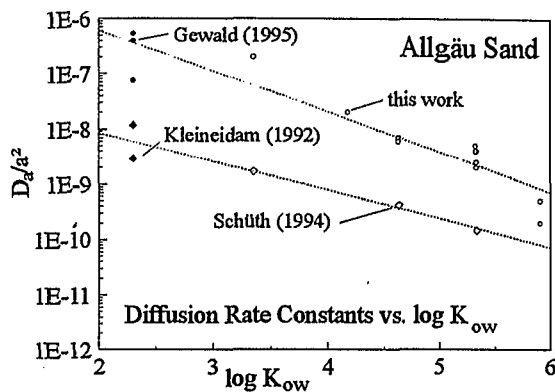


Figure 5-15: Dependency of the diffusion rate constant on the octanol/water partition coefficient in AS. The diffusion rate constants decrease with increasing K_{ow} . However, the values derived from sorption (Kleineidam and Schüth) and desorption experiments (this work and Gewald) deviate considerably from each other.

Additionally rate constants for AS with TCE ($\log K_{ow}=2.29$) derived by KLEINEIDAM (1992) and GEWALD (1995) are plotted to compare the validity of possible trends of D_a/a^2 towards lower K_{ow} s. Sorption data from Kleineidam fit well with the expected trend from Schüth, whereas desorption data from Gewald (also using the equilibrium approach) yield values that are considerably higher and fit fairly well with data of this work. Generally, the desorption data fitted with the equilibrium model yield rate constants of about one order of magnitude higher than observed during sorptive uptake.

For FTH and PY (having identical K_{ow} s) with the most experiments, the range of derived rate constants from all tests is between $5e-9$ and $2e-9$ $1/s$ and changes by a factor of 2.5.

Table 5-4: Summary of the obtained diffusion rate constants D_a/a^2 , the fraction of fast desorbing PAH X_i , the first-order rate coefficient of the fast fraction λ , and t_{90} , the time until 90 % of the sorbed mass is removed by mere purging. Release/time plots for the compounds not found in Fig. 5-13 are given in Appendix III.

Allgäu Sand				
	λ [1/s]	X_i [-]	D_a/a^2 [1/s]	t_{90} [d]
AS 1				
FL	4e-5	0.25	2e-8	90
PHE	2e-5	0.3	6e-9	285
ANT	1e-5	0.3	7e-9	245
FTH	1.5e-5	0.25	4e-9	445
PY	2e-5	0.21	5e-9	370
AS 2				
FTH	3e-5	0.08	2.5e-9	810
PY	3e-5	0.02	4e-9	525
B(a)A	4e-5	0.03	5e-10	4150
CHR	-	-	2e-10	10600

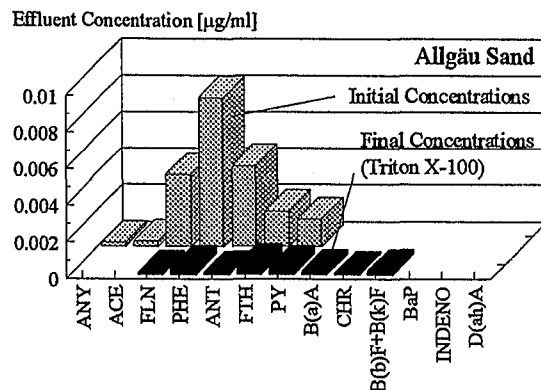


Figure 5-16: Comparison of the initial effluent concentrations and the final effluent concentrations during the surfactant treatment. In contrast to the NS samples, the final concentrations were considerably lower than the initial concentrations.

Considering possible errors in the mass balance, it can be expected that the determination of rate constants in column purge experiments will be within one order of magnitude.

As with the RS and NS, the use of Triton X-100 in experiment 1 applied to the final sample showed an increase in the release rates of all monitored compounds (see Tab. 5-5). Fig. 5-16 shows the comparison of the initial concentrations of PAHs in the effluent and the concentrations measured in the final sample. As in the NS sample, the surfactant application caused higher K_{ow} compounds, to appear in the effluent, that could not be monitored before. However, compared to the effect of the Triton application on the NS (Fig. 5-17) the concentrations were well below the respective initial effluent concentrations in the AS. As in NS, the release rate increases did not show a correlation to K_{ow} . If the enhanced release of PAH during surfactant application is due a limited access of micelles into the intraparticle domain, this less pronounced increase could be due to the smaller intraparticle porosity of AS as compared to NS.

Table 5-5: Relative increase of desorption rates in the final sample during surfactant treatment.

PAH	K_{ow}	Rel. Increase
FL	4.18	2.7
PHE	4.46	2.0
ANT	4.45	0.7
FTH	5.33	5.7
PY	5.33	5.7

5.4 Summary and Discussion

The desorption characteristics of three aquifer materials were evaluated using column purge experiments and applying an intraparticle diffusion approach. The sands showed distinct differences with respect to their physico-chemical properties, which gave rise to individual release characteristics. Generally desorption from the three sands followed the diffusion model, once a fast desorbing fraction was introduced which accounted an instantaneously removed mass of contaminant. The subsequent long-term release of PAHs could be interpreted in terms of retarded intraparticle diffusion. With the exception of AS the obtained rate constants correspond well with those derived from the sorption experiments, indicating that for the used materials sorption appears to be fully reversible. The deviation between the rate constants derived for Allgäu Sand are assumed to be the result of overestimated equilibrium K_d s in the sorption experiment.

As the derived diffusion rate constants for identical PAHs in single- and multicomponent experiments are in close agreement, competitive sorption effects do not seem to occur in the tested samples.

For all sands the obtained diffusion rate constants decreased with increasing octanol/water partition coefficient, which is in accordance to process of retarded pore diffusion. The changes in diffusion rate constants D_a/a^2 between respective PAHs depends on the distribution coefficient K_d , which is expressed as $K_{oc} f_{oc}$ (see Eq. 2-9). Considering K_{oc} - K_{ow} relationships such as $K_{oc}=0.6 K_{ow}$ (KARICKHOFF et al., 1979), a slope of approx. -1 in the $\log K_{ow}/\log D_a/a^2$ plots is expected for a regression. In contrast to AS and NS, which show the expected trend, RS hardly exhibits a dependency of the diffusion rate constants on the respective K_{ow} . This contrasting behavior is due to the different inherent physico-chemical characteristics which are addressed in detail in the following.

Table 5-6: Compilation of the derived diffusion rate constants D_a/a^2 , first-order coefficients λ , fraction of fast desorbing PAHs X_i , and the desorption time t_{90} % of 3 aquifer materials (determined using the equilibrium assumption).

Sample	PAH	Grain Size [mm]	Radius [cm]	X_i [-]	λ [1/s]	D_a/a^2 [1/s]	D_a [cm ² /s]	t_{90} [d]
RS	NAP	0.315-1	0.028	0.8	1.5e-3	1.5e-7	1.1e-10	2.6
	FTH I	0.315-1		0.5	4e-4	6e-8	4.7e-11	19.1
	FTH II	0.315-1		0.5	2e-4	8e-8	6.2e-11	24.7
NS	FL	0.25-1	0.025	-	-	5e-8	3.1e-11	42
	PHE	0.25-1		-	-	4e-8	2.5e-11	53
	ANT	0.25-1		-	-	4e-8	2.5e-11	53
	FTH	0.25-1		0.3	2.5e-6	8e-9	5e-12	213
	PY	0.25-1		0.3	5e-6	7e-9	4.3e-12	223
	B(a)A	0.25-1		-	-	9e-10	5.6e-13	2360
	CHR	0.25-1		-	-	1.5e-9	9.3e-13	1415
AS	NAP	0.315-1	0.028	0.2	1e-3	2e-7	1.5e-10	9.4
	FTH I	0.315-1		0.02	1e-3	2e-9	1.5e-12	1076
	FTH II	0.315-1		0.05	2e-4	2e-9	1.5e-12	1080
AS 1	FL	0.25-1	0.025	0.25	4e-5	2e-8	1.2e-11	90
	PHE	0.25-1		0.3	2e-5	6e-9	3.7e-12	285
	ANT	0.25-1		0.3	1e-5	7e-9	4.3e-12	245
	FTH	0.25-1		0.25	1.5e-5	4e-9	2.5e-12	445
	PY	0.25-1		0.21	2e-5	5e-9	3.1e-12	370
AS 2	FTH	0.25-1	0.025	0.08	3e-5	2.5e-9	1.5e-12	810
	PY	0.25-1		0.02	3e-5	4e-9	2.5e-12	525
	B(a)A	0.25-1		0.03	4e-5	5e-10	3.1e-13	4150
	CHR	0.25-1		-	-	2e-10	1.2e-13	10600

The applicability of the intraparticle diffusion approach in a strict sense is limited to retarded intraparticle diffusion in homogeneous samples (in size, as well as in composition). Homogeneous materials with a pronounced intraparticle domain (AS or NS) will therefore more readily follow the model than a sample showing little intraparticle porosity. Mere intraparticle diffusion can for example not account for a large fraction (min. 50%) of the released PAHs in the RS. Although this instantaneously released fraction can be fitted using a first-order approach, the fitting procedure does not render a corresponding physical process. An attempt to interpret the nature of the early time release must be limited to assumptions as to the location of the fraction on or close to the grain surface. With this caveat the intraparticle diffusion approach is limited to the description of the long-term release behavior of the Rhine Sand. This long-term release, could well be fitted using the intraparticle diffusion approach and total desorption was reached.

For NS and AS, containing a higher content of carbonate particles, the prerequisites to follow a retarded intraparticle diffusion model are better met in terms of a combined effect of higher internal porosity, organic carbon content and internal surfaces. The bulk mass sorbed could be attributed to the intraparticle domain. NS showed the highest content of PAHs sorbed which corresponds to the highest intraparticle porosity and organic carbon content. Both sands showed a considerable fraction of their pore volume and the associated internal surfaces in the lower mesopore to micropore range. This could cause steric hindrances due to reduced pore throats (BRUSSEAU ET AL, 1991), and can decrease the rate constants by a factor 2.

The application of surfactants at late times in the experiments led to increases of the monitored release rates. In addition to this general increase in PAH release rates, high K_{ow} compounds appeared in the effluent, which could not be monitored prior to the Triton application. This indicates that high K_{ow} compounds can effectively be mobilized, by micellar transport, due to an increased apparent solubility in the hydrophobic micellar core. The enhancing removal effect however, appears to be limited to a short period of time. This indicates that micelles cannot effectively reach PAHs in the intragranular pore domain.

Conclusively it can be noticed that the different aquifer materials can vary considerably in their obtained rate constants. Diffusive mass transfer limitation at the grain scale through intraparticle diffusion causes a considerable reluctance of hydrophobic compounds to remediation attempts. Once sorbed, subsurface contaminations will prevail over long periods of time; however the involved release rates are small. Fitting mixtures of lithological components with a single diffusion rate constant may lead to a fraction of instantaneous released contaminants. In such a multirate system the monitored fluxes display phases in which the bulk effect on release is transferred from fast fractions to components of slower desorption kinetics. Single rate constants therefore seem to be an oversimplification of a release behavior of such a system. A characterization of the individual components (in size as well as in material characteristics) can lead to a better understanding of the observed release behavior.

6. PAH Release from Gasworks Site Material

6.1 Desorption Experiments of the Heidenheim Materials

All materials used from the Heidenheim site had undergone wet mechanical on-site treatment prior to the desorption studies but still contained considerable amounts of PAHs. Out of the bulk material two fractions were separated and tested with respect to their desorption behavior. Representative for all PAHs five compounds were considered for monitoring (see Chap. 2.1), which covered a range of octanol/water partition coefficients from 4.18 (*FL*) to 6.84 (*B(k)F*) (SIMS and OVERCASH, 1983). As often found in aged contaminations the more soluble compounds (e.g. naphthalene and acenaphthene) were present only at low concentrations and rapidly dropped below the detection limit. This could be due to initially low concentrations or, most likely, to loss of these compounds due to prior release on the site. Figure 6-1 shows typical concentration distributions of the 16 EPA PAHs for two batches of the Heidenheim 0.25-0.5 mm fractions, which reflects this depletion of higher soluble compounds.

6.1.1 Desorption of PAH from the 'light' fraction (0.25-0.5mm)

As in some aquifer sands, the desorption behavior of the PAHs can be subdivided in two

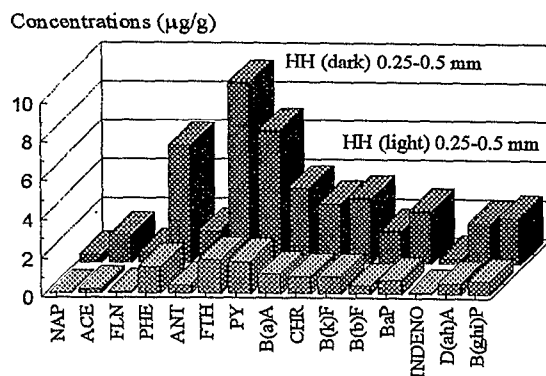


Figure 6-1: Concentrations distributions for the PAHs from Soxhlet extractions of the Heidenheim light 0.25-0.5 mm fraction and the Heidenheim 0.25-0.5 mm dark fraction. Both batches show similar fingerprints with the highest concentrations at *FTH*.

distinct time scales. A short first phase, characterized by high initial fluxes of the PAHs from fluorene (*FL*) to benzo(a)anthracene (*B(a)A*). The initial phase is followed by an extended second period of slowly decreasing release rates. Out of the monitored compounds benzo(k)fluoranthene (*B(k)F*) is the only compound that does not show the characteristic change in slope of the release rates (see Fig. 6-4).

The short-term release behavior of the HH sample shows similar characteristics as the RS (see Fig. 5-1). The duration of this initial phase increases for compounds with increasing octanol/water partition coefficients. The fast desorbing fraction of e.g. fluoranthene (*FTH*) persists over a longer period of time compared to that of phenanthrene (*PHE*). The times to reach the second phase (time period after which the PAH flux is totally controlled by the intraparticle diffusion), ranges from about 0.3 days for fluorene to 1, 3 and 10 days for phenanthrene, fluoranthene and benzo(a)anthracene, respectively.

Extrapolating the duration over which this fast desorbing fraction should prevail for *B(k)F* ($\log K_{ow}$ 6.84) by a regression of the monitored times from *FL*-*B(a)A* (see Fig. 6-2), leads to an expectation well beyond the experimental time frame of 58 days. The result indicates that for *B(k)F* the initial phase

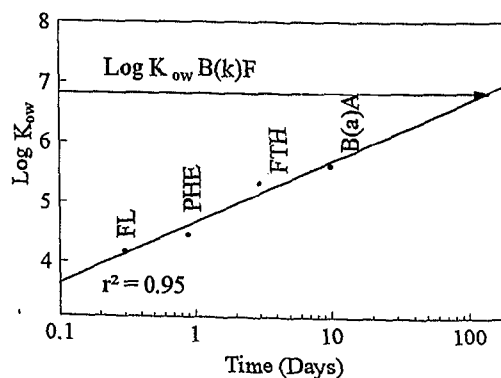


Figure 6-2: Plot of the duration of the initial phase of fast PAH release (X_i) vs. the octanol/water partition coefficient. Extrapolating for *B(k)F* indicates that monitored release still corresponds to the release of the fast fraction.

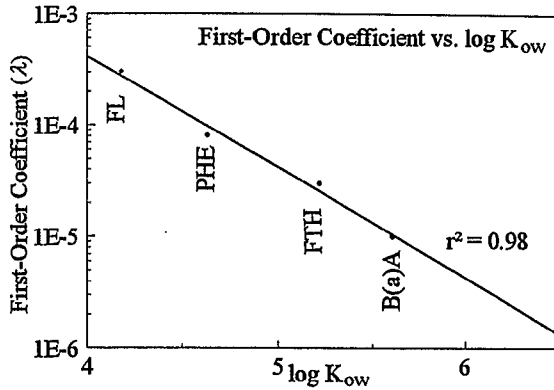


Figure 6-3: Dependency of the fitted first-order rate constants from the octanol/water partition coefficients.

of desorption with high release rates is not yet finished.

The determined diffusion rate constant for $B(k)F$ is therefore assumed to reflect the behavior of the fast desorbing fraction. The expected long-term D_a/a^2 for $B(k)F$ can be expected to be even smaller. This corresponds well to deviation of the long-term diffusion rate constant of $B(k)F$ from the trend of diffusion rate constants in Fig. 6-5 and the fact that $B(k)F$ in contrast to the other compounds monitored, does not need an instantaneously desorbing fraction. The relative amount of the fast desorbing fraction (X_i) with respect to the total mass sorbed on the particles (M_{eq}) for the higher K_{ow} is constant up to FTH at about 0.15. (see Table 6-1).

The first-order rate coefficients obtained in the fitting procedure decrease with increasing K_{ow} (see Fig. 6-3).

Table 6-1: Summary of the obtained diffusion rate constants, fractions of the fast components X_i , λ the first-order rate coefficient used to model the fast fraction, and t_{90} the time until 90 % of the sorbed mass is removed by mere purging.

	λ [1/s]	X_i [-]	D_a/a^2 [1/s]	t_{90} [d]
FL	3e-4	0.18	3e-9	630
PHE	8e-5	0.19	1e-9	1880
FTH	3e-5	0.13	2e-10	9800
B(a)A	1e-5	0.065	1e-10	20300
$B(k)F^*$	-	0.01	4e-11	52500

* The derived diffusion rate constant for $B(k)F$ most likely corresponds to the fast desorbing fraction.

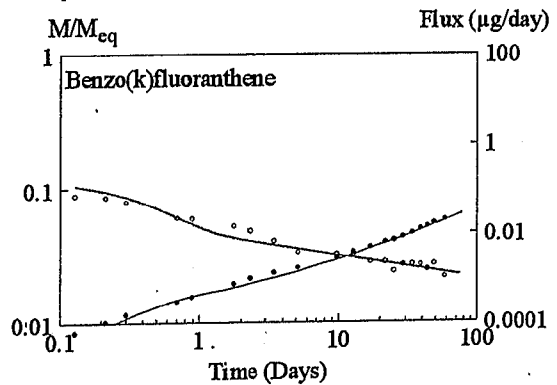
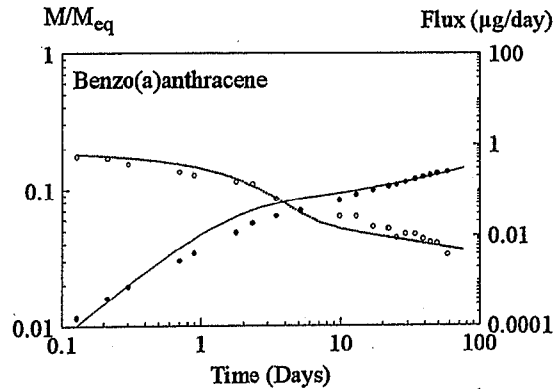
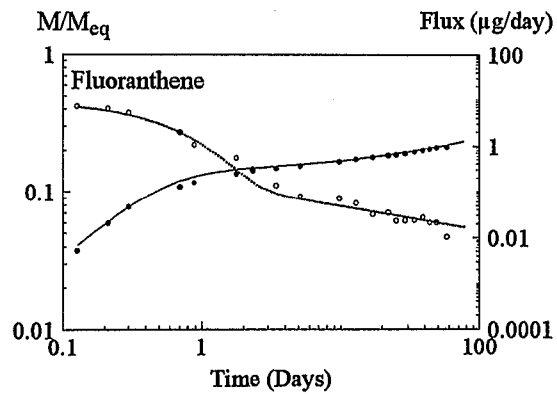
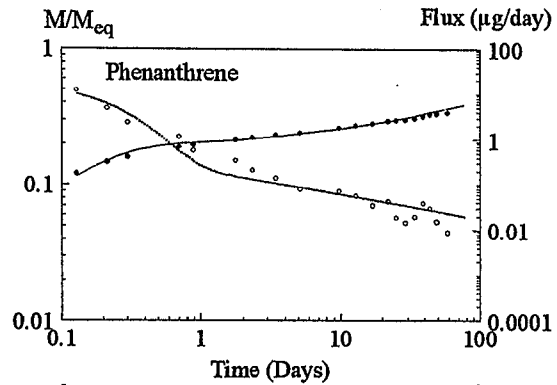


Figure 6-4: Desorption kinetics of 4 PAHs from the Heidenheim 0.25-0.5 mm fraction. Solid lines and dotted lines: M/M_{eq} and fluxes fitted with a two-site model. For the fast desorbing fraction (X_i) a simple first-order approach is used to describe the desorption kinetics, the long-term desorption is modeled using the intraparticle diffusion model.

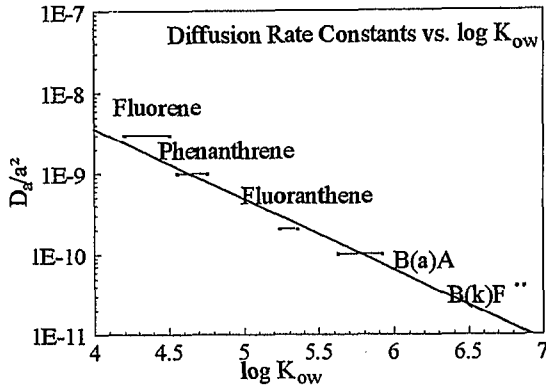


Figure 6-5: Dependency of the diffusion rate constants of HH 0.25-0.5mm from the octanol/water partition coefficients. The diffusion rate constants again typically decrease with increasing $\log K_{ow}$. The bars indicate the range of K_{ow} found in the literature.

As most of the sorbed mass can be attributed to the second period and special interest lies in the release characteristics over long periods of time, making the latter of the two phases the more relevant with respect to groundwater related risk assessments. The long-term desorption behavior generally showed a good fit between the diffusion model and the desorption data (see Fig 6-5). The resulting diffusion rate constants and the first-order rate constants are listed in Table 6-1. As could be expected, an inverse correlation between K_{ow} and the long-term diffusion rate constant was observed.

Using the obtained long-term rate constants the time to reach a 90% removal of contaminants in a hydraulic remediation can be evaluated by extending the desorption time in the model. Fig. 6-6 emphasizes the

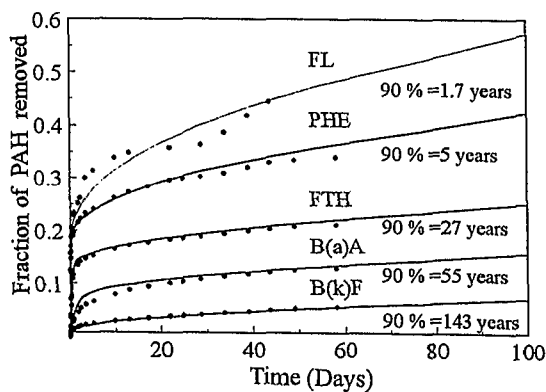


Figure 6-6: Per cent PAH removed in the column experiment vs. time. The time needed to remove 90 % of the respective PAHs varies on the order of 3 magnitudes. The fitted line resembles the expected mass release based on the diffusion model.

different time scales at which removal takes place for the respective PAHs. Effective removal times differ on the order of three magnitudes from 1.7 years for *FL* to more than 100 years for *B(k)F*. Especially the extremely long desorption times for high K_{ow} compounds, which are toxically relevant, stress the fact that rate limited processes generally oppose to remediation efforts.

The slow desorption kinetics of the bulk mass of PAHs sorbed also demonstrates that the pretreatment with surfactants did not much effect PAHs sorbed in the intraparticle domain (in the case of benzo(k)fluoranthene, release from the intraparticle domain could not at all be evaluated, due to the very low diffusion rate constants). Time scales for soil washing procedures (hours) and diffusive transport processes (days to years) differ to a degree that appears to limit the application of soil washing to materials showing surface contaminations with tar oil phase, whereas resistantly sorbed contaminants will not be efficiently removed.

6.1.2 Temperature Effects on Desorption

Diffusion limited transport seems to dominate the long-term release of sorbed PAHs from contaminated aquifer material. The time scale for remediation is correlated to the long-term apparent diffusion coefficient of the monitored compound. As the obtained rate constants in this work are generally low, the associated times to reach high levels of remediation are on the order of months to years (see Fig. 6-6). Measures to enhance PAH removal rates in order to reduce the remediation times need to be taken into consideration to arrive at more reasonable time scales.

Any attempt to enhance the mass transfer between the aqueous and solid phase will either have to effect the rate constants (see Eq. 2-17) or the concentration gradients during desorption. As the gradient in remediation attempts (e.g. pump and treat) is already close to the maximum (aqueous concentrations are reduced to a minimum), a successful enhancement of the release rates relies on increased diffusion rate constants.

One way to increase the mass transfer rates is a change in the temperature of the system. Several authors found desorption kinetics to be sensitive to temperature changes. Experiments conducted by FARRELL (1992) using TCE found increases in desorption rates on the order of a factor of 2 by increasing the temperature from 15°C to 30°C in Borden sands. HARMON (1992) reports rate increases of a factor of 3 for Mofett material (4°C-36.5°C). GEWALD (1996) found changes in release rates of a factor of 2 by either increasing or decreasing the temperature by 10° C in sandy aquifer material (Donau Sand). STEINBERG ET AL. (1987) found desorption of 1,2 dibromoethane from top soils to be highly temperature dependent.

To evaluate the effect of increased temperature on the long-term desorption of PAHs from HH light material, several temperature controlled column purge experiments were conducted at 4°C, 20°C and 40°C (for desorption plots see Appendix III).

6.1.2.1 Nature of Temperature Dependencies

Temperature dependency is generally attributed to increasing aqueous diffusion coefficients at higher temperatures, which cause increases in observed desorption rates. To quantify the change of aqueous diffusion coefficients for hydrophobic compounds in dilute aqueous solutions with temperature, HAYDUK and LAUDIE (1974) arrive at the following equation

$$D_{aq} = \frac{13.26 \cdot 10^{-5}}{\mu^{1.14} V_B^{0.589}} \quad (6-1)$$

where μ is the dynamic viscosity ($ML^{-1} T^{-1}$) and V_B is the Le Bas molar volume (LYMAN ET AL., 1990) (a temperature term is not included, as the temperature dependency is incorporated in the viscosity term).

The LeBas molar volume is calculated from the structural formulae of the respective compound (Table 1-2). Fig. 6-7 gives an example of the effect of temperature variations on the aqueous diffusion coefficient of FTH.

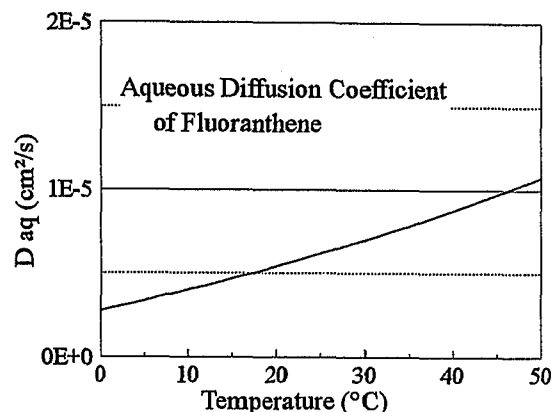


Figure 6-7: Temperature dependency of the diffusion rate constants *FTH* based on the increase of the aqueous diffusion coefficient.

If the change of aqueous diffusion coefficients was the sole reason of increasing rate constants, the monitored increases should follow the trend given by Eq. 6-1. Any further increase in measured apparent diffusion coefficients, however, must be caused by additional processes acting at the grain scale. Other than the aqueous diffusion coefficient, the capacity $\alpha (= \epsilon + K_d \rho)$ is assumed to be a possible parameter that could be subject to a temperature dependency (see Eq. 2-14). In order to increase D_a , the equilibrium partition coefficient K_d must adopt smaller values. In temperature controlled experiments HARMON (1992) found somewhat inconclusive results addressing the problem of temperature effects on K_d s. REISINGER (1995) found an inverse correlation of K_d s and temperature increase, leading to an increase of the apparent diffusion coefficient and consequently to decreasing remediation times.

An additional factor leading to temperature variant D_a s is argued by FARRELL (1992). An enhancing effect of higher temperatures on diffusion rate constants could be expected for molecules passing through pore constrictions

Table 6-2: Summary of the long-term diffusion rate constants (D_a/a^2) derived at 4°C, 20°C, and 40°C for the HH light 0.25-0.5 mm fraction.

	4°C	20°C	40°C	
FL	-	3e-9	-	-
PHE	3e-10	1e-9	3.5e-9	4e-9
FTH	6e-11	2e-10	7e-10	7e-10
B(a)A	-	1e-10	3e-10	2e-10
B(k)F	-	4e-11	7e-11	6e-11

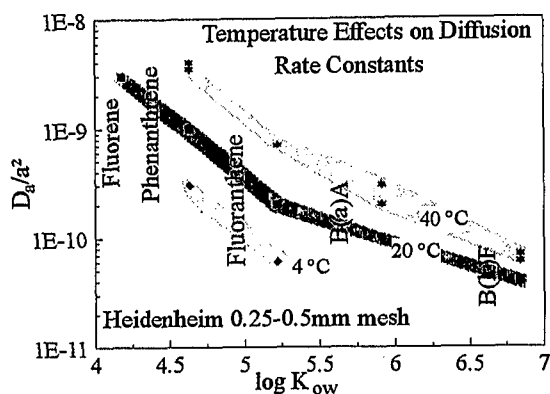


Figure 6-8: Temperature dependency of the diffusion rate constants of several PAHs. The column experiments were conducted at 4°C, 20°C and, 40°C. The increase of the diffusion rate constants for *PHE* and *FTH* exceed the expected values based on the increased aqueous diffusion coefficients.

in microporous solids, as they have to overcome an energy barrier at pore throats of the approx. size of their diameter. Increased temperatures would result in higher kinetic energy to overcome these energy barriers. Intraparticle domains exhibiting a prominent fraction of radii in the low mesopore to micropore range could therefore be subject to restricted pore diffusion and yield lower rate constants than could be expected from an unrestricted aqueous medium.

Based on the above assumption of increased aqueous diffusion coefficients only, the estimated enhancement would lead to a 1.5 respectively 1.6 fold increase in observed diffusion rate constants by changing the temperature from 4°C to 20°C and from 20°C to 40°C respectively. However, the changes in determined diffusion rate constants are higher (see Table 6-2 and Fig. 6-8). This finding indicates that an additional process must be active, which accounts for this additional increase of rate constants.

6.1.2.2 Determination of Activation Energies

Determining temperature dependent diffusion rate constants can yield an indication, as to the environment in which diffusive mass transfer takes place. The rates at which molecules move in a medium (e.g. water) depend on the energy needed to overcome the resistance imposed on the compound of interest by the medium (e.g. viscosity). Only

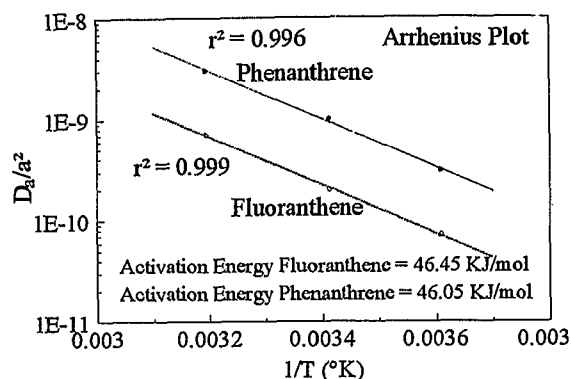


Figure 6-9: Arrhenius type plots of diffusion rate constants vs. 1/Temperature (°K) for *PHE* and *FTH*. The slope of the linear regression through the data is a measure for the inherent activation energies.

the fraction of the molecules, that has sufficient kinetic energy to overcome this resistance, is able to move downgradient and is subject to diffusive transport. This critical energy threshold is called the activation energy E_a . As the temperature rises the fraction of molecules reaching this minimum critical energy level increases.

In order to evaluate the change in diffusion rate constants as a function of temperature the Arrhenius equation is used, expressed as

$$k = A e^{-E_a/RT} \quad (6-2)$$

with k the rate constant (in this case D_a/a^2), A the preexponential factor [-], E_a the activation energy [J/mol], R the universal gas constant [$J \text{ mol}^{-1} \text{ K}^{-1}$], and T the temperature [°K]. or after finding the log

$$\log k = \log A - 2.303 E_a / RT \quad (6-3)$$

The activation energy of a compound in a liquid system can be deduced from the regression slope of rate constants plotted vs. 1/T (see Fig. 6-9). The activation energy for diffusion in an aqueous phase is approx. 20 kJ/mol (HARMON, 1992). Activation energies around 20 kJ/mol therefore, are an indication of diffusive processes taking place in an aqueous environment.

Arrhenius type plots for the Heidenheim light material are shown in Fig. 6-9. The activation energies for *FTH* and *PHE* are approx. 46 kJ/mol and are about two times higher than expected. These values support the existence

of an additional diffusion limiting process in the Heidenheim material.

As the pore size distribution and the associated internal surfaces and pore volumes show that a considerable fraction of the available intragranular pore space is located in a range of pore radii close to the critical threshold of several molecule diameters (the size of *FTH* is approx. $6.3\text{\AA} \times 4.9\text{\AA}$), the higher activation energies could be due to hindered pore diffusion in the intragranular domain, as compared to non-constricted diffusion in water filled pores. Molecules reaching such meso-microporous domains could be subject to sorption caused by the proximity of pore walls. Another mechanism that could cause higher activation energies is intrasorbent diffusion, where the mass transfer through organic polymers might need higher activation energies than simple pore diffusion.

Activation energies derived from Arrhenius type plots for Mofett and Borden materials yielded values from 24 kJ/mol to 52 kJ/mol (HARMON, 1992). REISINGER (1995) found activation energies of about 50 kJ/mol for desorption experiments using *TCE*, indicating that activation energies higher than 20 kJ/mol could be a commonly found feature in desorption of organics.

Accompanying the high activation energies found, are relatively high increases in apparent diffusion coefficients with respect to those expected in aqueous environments. These indicate that the limiting mass transfer process cannot be explained by mere aqueous

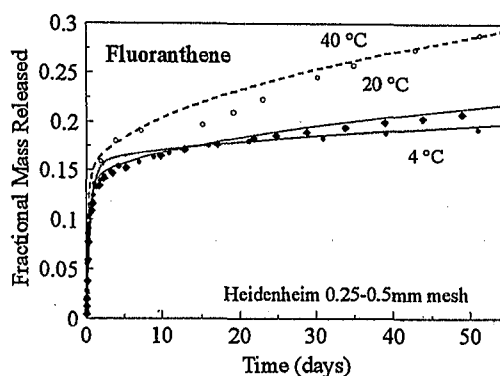


Figure 6-10: Fractional masses of *FTH* released at 4°C, 20°C and 40°C. The changes in diffusion rate constants cause considerable changes in the desorption behavior.

diffusion. The observed increase in apparent diffusion coefficients is more likely due to the combined effects of increased diffusion coefficients and decreasing K_{ds} of the samples.

The effect of temperature variation on the masses released over time for *FTH* is shown in Fig. 6-10. The plot demonstrates that considerable differences can be expected in terms of residual masses and remediation times as diffusion rate constants are evaluated at different temperatures. Desorption rate studies for contaminated sites should therefore either be conducted at approx. groundwater temperatures or if possible be evaluated from the Arrhenius plots. Release predictions that are not taking into account the temperature differences, will tend to overestimate the diffusion rate constants.

6.1.3 Desorption of the Dark Fractions

In contrast to the previously described materials, the dark samples were primarily made up of soot, cinder and coal particles. These components were found in abundance in the bulk mass and can be considered to be site specific products, formed during the carbonization process. Generally these materials exhibit high PAH concentrations and very high organic carbon contents associated with higher internal surfaces and intraparticle porosities (see Table 4-3).

6.1.3.1 Desorption from the 0.25- 0.5 mm Fraction

The desorption of 0.25-0.5 mm dark fraction was monitored for 60 days (see Fig. 6-12). In contrast to the previous HH samples, the dark fraction did not show a pronounced fast desorbing fraction. If the long-term diffusion rate constants are plotted against the octanol/water partition coefficient, a similar inverse correlation is found as with the materials tested (Fig. 6-11).

Determining the time t_{90} at which 90 % of the mass of a PAH is desorbed, also covers a time frame of up to more than 100 years, indicating the same reluctance of the sorbed compounds to remediation efforts. Table 6-4 compiles the determined diffusion rate constants and estimated time frames.

Although the 0.25-0.5 mm dark fraction generally were found to have slightly lower

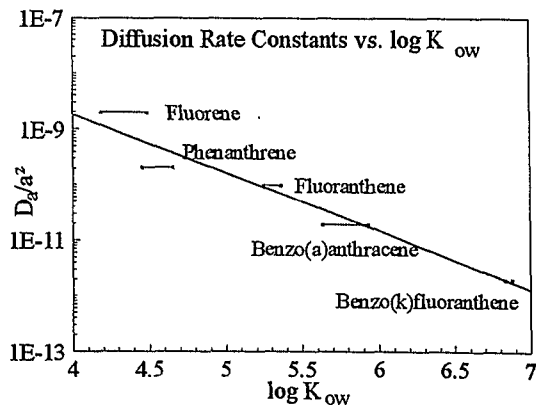


Figure 6-11: Dependency of the diffusion rate constant on the octanol/water partition coefficient. The diffusion rate constants decrease with increasing K_{ow} . Horizontal bars indicate the variations in $\log K_{ow}$ values in the literature.

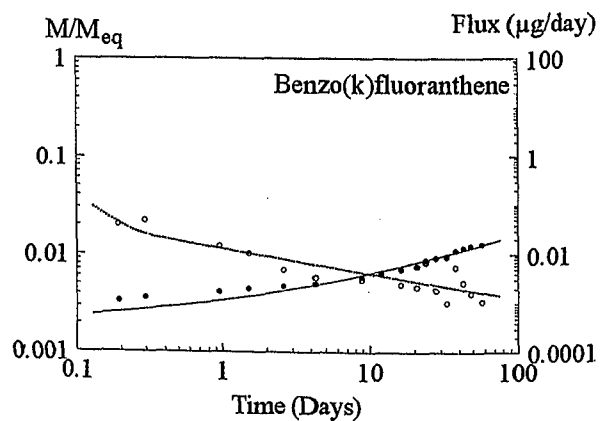
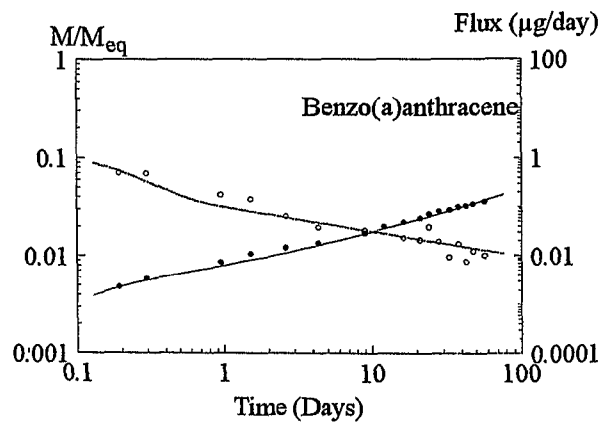
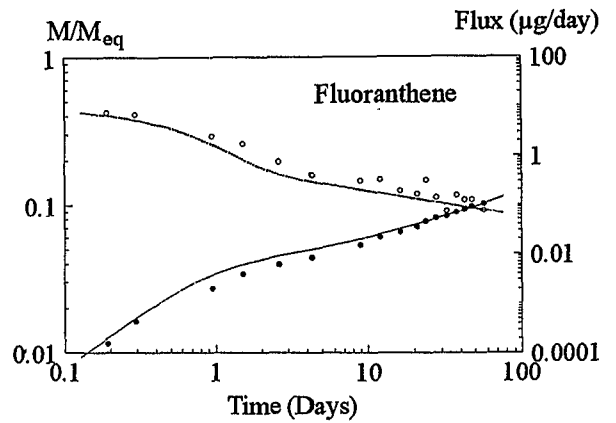
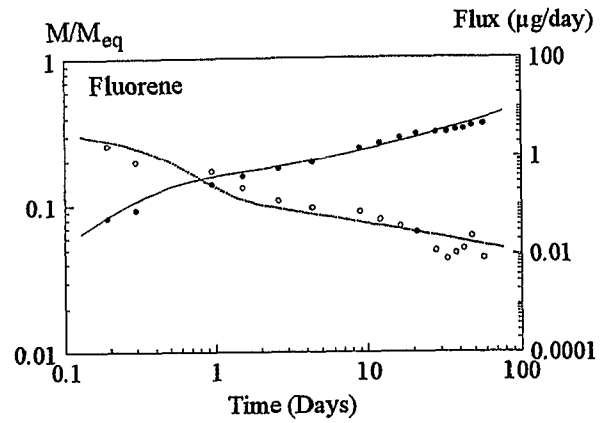


Figure 6-12: Desorption kinetics of 4 selected PAHs of the Heidenheim 0.25-0.5 mm dark fraction (solid symbols = M/M_{eq} ; circles = flux).

Table 6-3: Summary of the obtained diffusion rate constants, fractions of the fast components X_p , λ the first-order rate coefficient used to model the fast fraction, and t_{90} the time until 90 % of the sorbed mass is removed by mere purging.

	λ [1/s]	X_i [-]	D_a/a^2 [1/s]	t_{90} [d]
FL	5e-5	0.12	2e-9	980
PHE	5e-5	0.05	2e-10	10300
FTH	2e-5	0.03	1e-10	20800
B(a)A	1e-4	0.003	2e-11	105000
B(k)F	3e-4	0.002	2e-12	1060000

diffusion rates, the actual PAHs fluxes in the effluent at comparable times are higher for the dark fraction as the initial concentrations are higher.

6.1.3.2 Desorption from the 1-2 mm Fraction

The 1-2 mm fraction of the HH material showed the highest organic carbon content (~ 45 %). Although the PAH concentrations (see Figure 6-13) were very highest, the release of most components dropped below the detection limit after a short time. For these compounds an interpretation using the diffusion model was not possible. Out of the observed PAHs *FTH* and *PY* could be monitored for 100 days before dropping below the detection limit and could be interpreted using the desorption model. At the end of the experiment surfactant was applied to the sample.

Figure 6-14 shows the obtained release data for *FTH*. Although the fluxes and the cumulative mass data exhibit the typical shape of diffusion controlled release from an

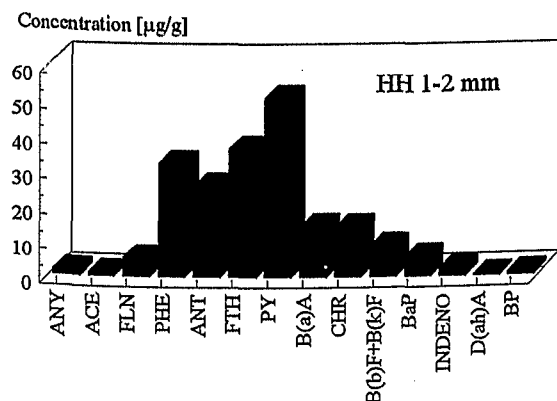


Figure 6-13: PAH concentrations of the HH 1-2 mm dark fraction. Concentrations add up to as much 200 µg/g.

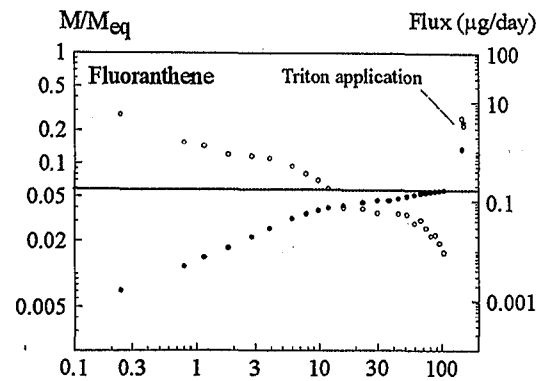


Figure 6-14: Release of *FTH* from the HH 1-2mm dark fraction (descending data (open circles) = flux; ascending symbols (solid circles = cumulative mass). Although only 6% of the total mass is removed (indicated by the horizontal line) fluxes decrease dramatically. Only a fraction of the total mass seems to be available for desorption.

intraparticle domain (e.g. -1/2 slope of the fluxes), only a small fraction of the total concentration seems to be readily available for desorption. The observed fluxes of *FTH* and *PY* at 60 days already deviate from the -1/2 slope. This indicates that desorption has already reached a high degree of removal (>90% of the respective mass). In terms of total mass found on the material (derived from the SFE extraction of the column material) only minor amounts of the mass takes part in this observed release process.

Figure 6-15 shows the model fit for *FTH*, assuming that a fraction of 6 % of the total mass follows the intraparticle diffusion model. The model fits well for both *FTH* and *PY*, indicating that the observed release can be attributed to release from an intraparticle

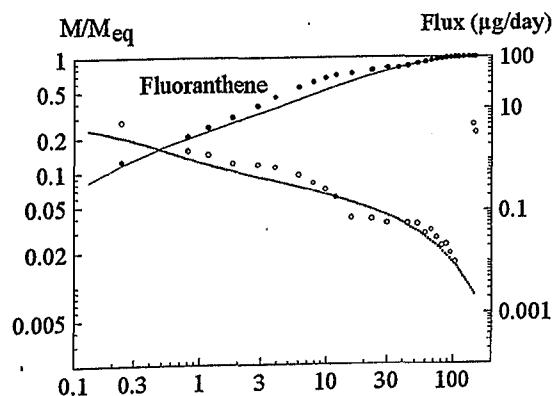


Figure 6-15: Desorption kinetics of *FTH* from the Heidenheim 1-2 mm dark fraction (solid symbols = M/M_{eq} , circles = flux). The diffusion model shows a good fit, if the mass balance is correct with regard to a much smaller M_{eq} (6%).

Table 6-4: Summary of the obtained diffusion rate constants, fractions of the fast components X_f , λ the first-order rate coefficient used to model the fast fraction, and t_{90} the time until 90 % of the sorbed mass is removed by mere purging.

	λ [1/s]	X_f [-]	D_a/a^2 [1/s]	t_{90} [d]
<i>FTH</i>	1e-5	0.05	3.5e-8	59
<i>PY</i>	-	-	4e-8	53

domain. The obtained diffusion rate constants are found in Table 6-4. Compared to rate constants from the HH_d 0.25-0.5 mm (see Table 6-3) the derived D_a/a^2 for *FTH* and *PY* are more than 2 orders of magnitude higher, leading to very short t_{90} for the modelled fraction. The desorption plot for *PY* is found in Appendix III.

These results indicate that for the HH 1-2 mm fraction only a very small fraction of the total mass is readily available for desorption. The bulk mass of the PAHs is either not available for desorption in an aqueous environment (under the experimental conditions), or the time scale involved in the removal is well beyond the used experimental time scale.

Similar findings are reported by MCGRODDY and FARRINGTON (1995). They found pore-water concentrations in sediment cores to be significantly lower than predicted by partitioning models. They hypothesize that pyrogenically derived PAHs, associated with soot particles deposited in sediments, may be less available to partition into porewater. In desorption experiments STEINER and BURTSCHER (1994) found several fractions of perylene sorbed on combustion particles, which desorbed in distinct temperature ranges. One fraction of perylene was able to withstand desorption to temperatures of up to 650° K. This also indicates fractions of PAHs that are more strongly associated with the soot particles.

As this HH sample is made up of combustion products, such as soot particles generated at high temperatures, the result is in accordance with those of the above cited authors. Although the intraparticle diffusion model could only address a minor fraction of the total mass sorbed, it was well able to describe

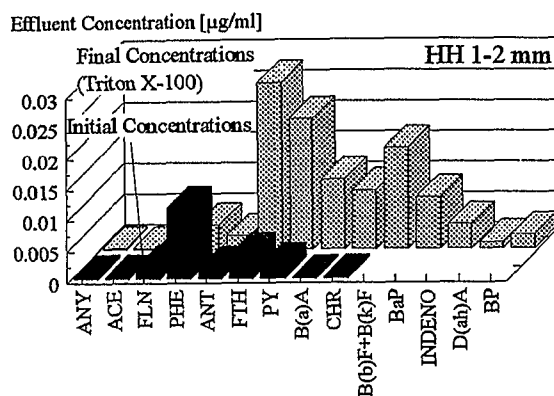


Figure 6-16: Comparison of the initial aqueous PAH concentrations and the PAH concentrations found in the samples during Triton X-100 application (2g/l).

the relevant release of PAHs during the first 100 days.

The high removal rates during the application of surfactant (Triton X-100 at 2 g/l) is assumed to be due to the removal of fines (the effluent was observed to be clouded) and their successive extraction in the cyclohexane trap. The cyclohexane extraction caused high concentrations of PAHs in the 2 final samples. In contrast to PAHs found in the effluent aqueous samples, also high K_{ow} compounds are found at high concentrations. A comparison of the initial effluent concentrations and the final concentrations during the Triton application is found in Figure 6-16.

6.1.4 Summary

As in the natural aquifer materials, the release of PAHs followed the intraparticle diffusion model. As expected, diffusion rate constants decreased with increasing K_{ow} . For the 0.25-0.5 mm light fraction rate constants again showed an approx. slope of -1 in the $\log K_{ow}/\log D_a/a^2$ plot, indicating a linear K_{oc}/K_{ow} relationship. The regression for the 0.25-0.5 mm dark fraction, however, shows a slope considerably less than -1, which cannot be explained.

The time scale to reach 90 % of removal of the PAHs therefore differs on the order of magnitudes for PAHs of different octanol/water partition coefficient. Table 6-5 shows a compilation of all derived rate constants from the HH materials.

The diffusion rate constants are temperature dependent. The observed increases in diffusion rate constants are higher than expected by a mere increase of aqueous diffusion coefficients. This is likely to be due to a decrease of the partition coefficients K_d with increasing temperature.

The determined activation energies are higher than expected for diffusion in an aqueous environment. These values might be due to intrasorbent diffusion, where molecules most likely encounter higher resistances to diffusive mass transfer than in an aqueous environment. Considering the high fraction of internal surfaces and pore volumes in the lower mesopore to micropore range, constrictivity effects may be an additional reason causing high activation energies. Both effects cause decreasing apparent diffusion coefficients.

Soot and coal particles appear to include considerable fractions of PAHs that are not readily available for desorption. This indicates that pyrogenically derived PAHs might be more strongly associated with the particles and not be available for sorption/desorption processes or only at rates that could not be resolved by these experiments.

The on-site wet mechanical treatment prior to sampling could not effectively remove the sorbed compounds. Soil washing procedures with short contact times (hours) are not capable to have an effect on the transport from the intraparticle domain at the grain scale into the mobile phase and are usually too short to remove all residual phase.

Table 6-5: Compilation of the derived diffusion rate constants D_a/a^2 , first-order coefficients λ , fraction of fast desorbing PAHs X_f , and the desorption time t_{90} % of HH materials.

Sample	PAH	Grain Size [mm]	Radius [cm]	X_f [-]	λ [1/s]	D_a/a^2 [1/s]	D_a [cm ² /s]	t_{90} [d]
20°C								
HH light	FL	0.25-0.5	0.017	0.18	3e-4	3e-9	8.6e-13	630
	PHE			0.19	8e-5	1e-9	2.8e-13	1880
	FTH			0.13	3e-5	2e-10	5.7e-14	9800
	B(a)A			0.065	1e-5	1e-10	2.8e-14	20300
	B(k)F			0.01	4e-11	1.1e-14	52500	
4°C								
HH light	PHE	0.25-0.5	0.017	0.12	3e-5	3e-10	8.6e-14	6600
	FTH			0.15	2e-5	6e-11	1.7e-14	32000
	PY			0.13	2e-5	7e-11	2e-14	32500
40°C								
HH light	PHE	0.25-0.5	0.017	0.2	1e-4	3.5e-9	1e-12	530
	FTH			0.15	3e-5	7e-10	2e-13	2750
	B(a)A			0.04	2e-4	3e-10	8.6e-14	6900
	B(k)F			0.01	1e-4	7e-11	2e-14	30000
HH light	PHE	0.25-0.5	0.017	0.19	8e-5	4e-9	1.1e-12	470
	FTH			0.13	5e-5	7e-10	2e-13	2800
	B(a)A			0.02	3e-5	2e-10	5.7e-14	14000
	B(k)F			-	-	6e-11	1.7e-14	36500
HH dark	FL	0.25-0.5	0.017	0.12	5e-5	2e-9	5.7e-13	980
	PHE			0.05	5e-5	2e-10	5.7e-14	10300
	FTH			0.03	2e-5	1e-10	2.8e-14	20800
	B(a)A			0.003	1e-4	2e-11	5.7e-15	105000
	B(k)F			0.004	3e-4	2e-12	5.7e-16	1060000
HH dark*	FTH	1-2	0.07	0.05	1e-5	3.5e-8	1.7e-10	59
	PY			-	-	4e-8	1.9e-10	53

* only a limited fraction of the total mass extracted, is assumed to take part in the release.

6.2 PAH Release from Materials Containing Residual Coal Tar

In contrast to the previous aquifer materials, the Karlsruhe samples contained considerable visible amounts of residual tar phase. The residual phase formed spherical aggregates of identical grain sizes as the aquifer material and was made up of a mixture of coal tar and aquifer particles, coated with fine particles. The coal tar aggregates were highly viscous and could easily be deformed mechanically, exposing a center of a less viscous tar phase. As the material was obtained directly from a borehole, such aggregates seem to be abundant in the subsurface of this site.

The release of PAHs from phase is, of course, the major source of any PAH input in the subsurface. Domains containing residual tar phase form a long-term input source, and the rate at which mass transfer takes place determines the risk potential originating from such a site. Recent column experiments dealing with the release of PAHs from coal tar showed a correlation between release rates and experimental flow rates (EBERHARDT, 1995). Possible reasons for such a correlation include film diffusion (mass transfer into the aqueous phase at nonequilibrium conditions), where the film thickness changes as a function of the flow velocity (see Chap. 2.3.5.1) or simply by reaching equilibrium conditions. These are achieved, if the residence time of the percolating water in a contaminated domain is sufficient to reach saturated conditions.

6.2.1 Validation of Equilibrium PAH Release

In order to evaluate data from column experiments in terms of equilibrium controlled release, it is necessary to identify this flow-flux correlation as an equilibrium release process. PAH release under equilibrium conditions reveals itself in time vs. concentration plots by showing constant effluent concentrations over extended periods of time. Further evidence to confirm the equilibrium assumption is the invariance of the effluent concentrations with respect to flow velocities in the column which results in linearly flow corre-

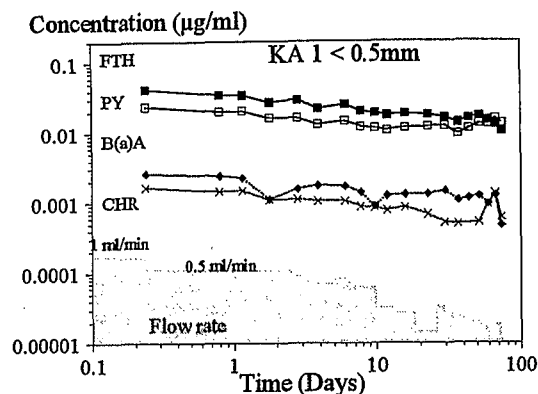


Figure 6-17: Effluent concentrations of 4 PAHs from column experiment KA 1 (<0.5 mm). The concentrations remain constant over an extended period of time, although the flow rate has been changed by approx. one order of magnitude. This indicates that the equilibrium assumption holds true for extended periods of time in the column experiment.

lated contaminant fluxes. Figure 6-17 shows effluent concentrations of several compounds from column purge experiment KA 1 (<0.5 mm). Although the flow rate in the column during the experiment is reduced by a factor of approx. 10, the effluent concentrations of these PAHs remain at a constant level over the entire monitoring period (73 days).

Under equilibrium conditions the concentration of the effluent represents the max. aqueous solubility of a compound in equilibrium with the tar phase (C_w^{sat*}) and directly delivers the necessary input parameter to calculate the expected fluxes. Figure 6-18 compares the initial aqueous concentrations from 3 column experiments (KA 1-3) aqueous saturation concentrations of single pure compounds and the calculated solubilities applying Raoult's Law (1-2 mm tar aggregates were used to derive the composition of the residual phase and to determine the respective molar fractions (see Figure 6-19 and Eq. 6-3)).

The respective molar fractions χ_i are calculated as

$$\chi_i = \frac{m_i MW_T}{MW_i m_T} \quad (6-3)$$

where m_i = mass of a compound i , MW_T = the molar weight of the tar, MW_i the molar weight of the compound i , and m_T , the mass of the complex organic mixture.

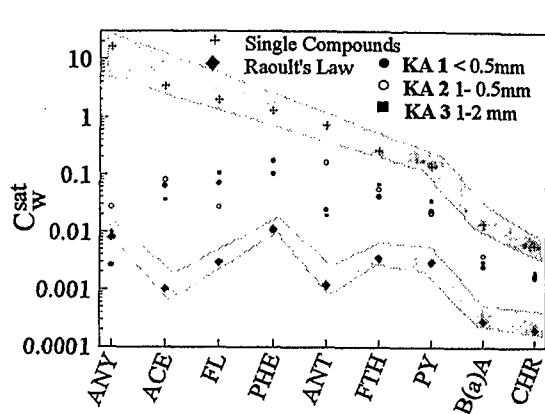


Figure 6-18: Initial aqueous concentrations in three column experiments of PAHs compared to C_w^{sat*} of the single compounds (see Table 1-2) and solubilities calculated from Raoult's Law. The observed values of the column experiments agree reasonably well with each other. The solubilities calculated using Raoult's Law show the same trend, but are consistently lower than the measured data.

The solubilities are calculated assuming a MW_T of 350 g/mol (LOYEK, pers. com). The fact, that derived values for Raoult's solubilities are presumably smaller than the measured values, are due to an uncertainty with respect to the amount of aquifer material included within the tar aggregates.

If m_T is overestimated, the molar fractions of all compounds are consequently underestimated. Introducing the underestimated molar fractions in Raoult's Law (Eq. 3-18) to determine the solubility of a compound, it will

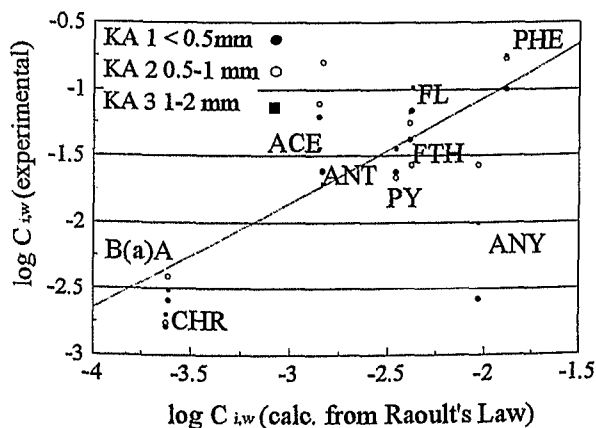


Figure 6-19: Measured initial aqueous concentrations $C_{i,w}$ for 3 column purge experiments (KA 1-3) compared to $C_{i,w}$ calculated from Raoult's Law (using 1-2 mm tar aggregates to determine the molar fractions of the individual PAHs). Measured concentrations are consistently lower than solubilities determined by Raoult's Law, due to an error in the determination of the mass of the organic phase.

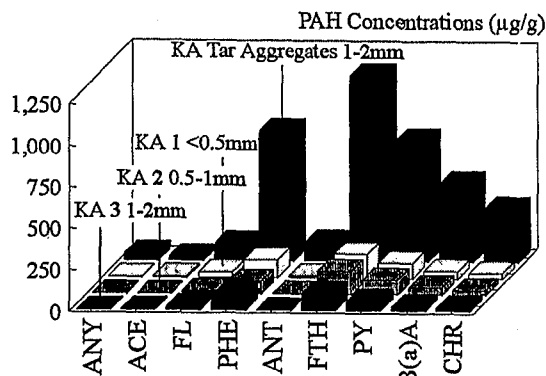


Figure 6-20: Concentrations of the three grain sizes used in the KA column experiments. The individual fractions show the same finger print as the original coal tar. Concentrations show a trend to decrease with increasing grain size.

also be underestimated, as is the case with those obtained for the tar aggregates.

6.2.2 PAH Release from Karlsruhe Material

As the residual tar aggregates are the prime source of PAH release, the volume of phase present and the available interfacial area determine the release rates. Fig. 6-19 shows the concentration distributions of PAHs up to *CHR* for the respective grain sizes. The finger prints of the KA samples closely follow that of the residual tar phase aggregates. As with the Heidenheim samples, the coal tar aggregates exhibit low concentrations for the more soluble compounds, and *FTH* is the most abundant PAH present. The more soluble compounds, e.g. *NAP*, and *ANY*, must have been already removed, as coal tars generally contain considerable amounts of these constituents (see Fig. 5-4).

With the 1-2 mm grain size fraction showing only slightly smaller concentrations than the <0.5 mm and 0.5-1 mm fraction, the same volumes of coal tar are present in the respective bulk masses. This, however, would lead to different surfaces available for mass transfer in the columns.

Equivalent volumes of coal tar would lead to an increase in surface of 5.6 times for the <0.5 mm fraction and a twofold increase for the 0.5-1 mm fraction with respect to the 1-2 mm fraction (assuming mean radii of 0.125, 0.35, and 0.7 for the respective samples) (see

Table 6-6: Surfaces and volumes of single sphere and equivalent surfaces for identical volumes.

	KA 1 [<0.5 mm]	KA 2 [0.5-1 mm]	KA 3 [1-2 mm]
Single Spheres			
Radius [mm]	0.125	0.35	0.70
Surface [mm ²]	0.19	1.57	6.28
Volume [mm ³]	0.008	0.18	1.48
Equivalent Surface			
	5.6	2	1

Table 6-6). In terms of an interpretation with respect to expected effluent concentrations, KA 1 and KA 2 with their higher interfacial areas have better prerequisites to meet equilibrium conditions in the effluent than KA 3 (shortest contact time).

Table 6-7 gives the relevant column parameters of the 3 samples. The effective flow velocities lie in the order of several m/day at late times and correspond to velocities found in sandy gravel aquifers. If equilibrium conditions are reached at these flow velocities, it can be assumed, that the saturation length for the KA material on site is also on the order of several cm. If this holds true, even small contaminated domains can therefore cause maximum effluent concentrations, and emission of PAH out of such a domain could be approximated by the C_w^{sat*} .

6.2.2.1 Modeling Equilibrium PAH Release

As the initial effluent concentrations in the 3 experiments KA1 - KA 3 can be considered to correspond to the solubility of the respective PAHs, the release behavior should be linearly correlated to the flow rates in the columns (as long as saturation is reached). Figure 6-22 shows the release behavior for *FTH* and *B(a)A* from the KA 1 and KA 2 samples. A compilation of equilibrium release of monitored PAHs is found in Appendix III. In all experiments the flow rates were changed by approx. one order of magnitude in 3 consecutive steps of decreasing flow rates. In the case of KA 1, the flow rates deviated considerably from those expected by the change induced by the peristaltic pump. This irregular flow behavior (see Fig. 6-17) is attributed to the mobilization of fines (as KA 1 represents the smallest grain size fraction <0.5mm) which

Table 6-7: Relevant column parameters and flow conditions for 3 grain sizes of the Karlsruhe material (KA 1 ≤ 0.5 mm, KA 2=0.5-1 mm, KA 3=1-2 mm)

Sample	Column length [cm]	Porosity [%]	flow rates	
			ml/min	m/d
KA 1	7	38.2	1-0.07	50-3.5
KA 2	9	41.0	1-0.07	44-3.0
KA 3	5	40.2	1-0.07	46-3.2

also caused the premature end of the experiment due to a blocked capillary after 73 days.

An arrival at equilibrium conditions for individual PAHs in column experiments and the duration over which equilibrium conditions can be maintained (time at which the saturation front leaves the column) in the experiment depends on the K_{ow} and the grain size (resulting in different surface/volume ratios of the tar aggregates). For more soluble PAHs (e.g. *PHE*) effluent concentrations start to deviate from max. solubility after only a few days, whereas for high K_{ow} compounds equilibrium conditions can be maintained much longer (see Figure 6-23).

The differences in the concentration developments over time for identical PAHs, due to different surface/volume ratios, in the 3 experiments is representatively shown in Fig. 6-21, for effluent *FTH* concentrations.

In experiment KA 3 (1-2 mm) equilibrium conditions could not be established for PAHs with a K_{ow} less than that of *B(a)A* and the release behavior shows considerable deviations from the equilibrium release assumption

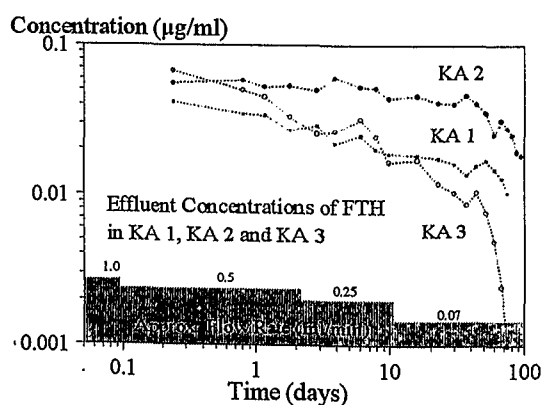


Figure 6-21: Effluent concentrations of *FTH* from the 3 column purge experiments (KA 1 KA 3). The concentrations in KA 2 remain constant over an extended period of time. KA 3 shows considerable deviations from the equilibrium assumption.

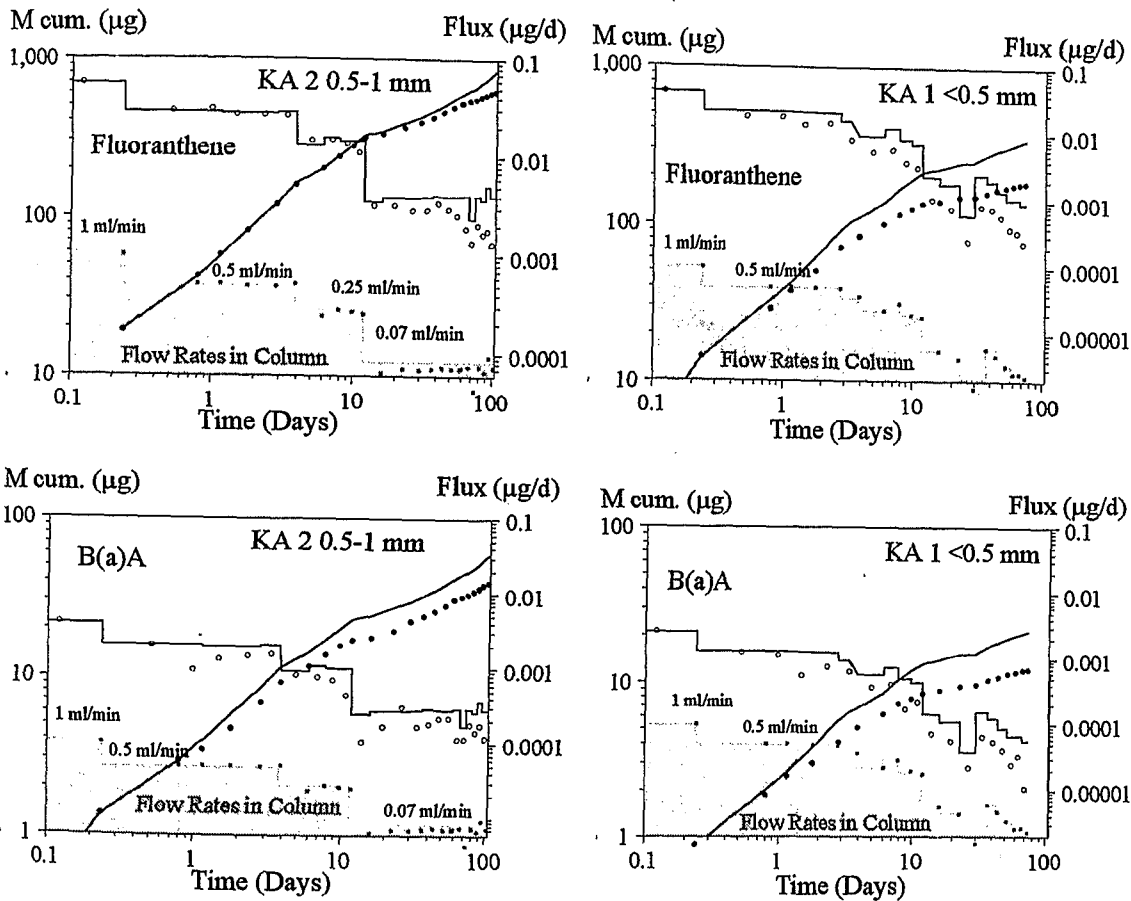


Figure 6-22 Equilibrium release of 2 PAHs (*FTH* and *B(a)A*) from the KA 1 <0.5 mm fraction (right panels) and KA 2 0.5-1 mm fraction (left panels). Breaks in contaminant fluxes coincide with flow conditions. (Ascending curve = cum. mass release, descending curve = PAH flux).

even at early times (see Appendix III). This corresponds to view that KA 3 has the lowest surface/volume ratio and the available tar/water interface cannot facilitate PAH release at rates that reach equilibrium conditions in this column.

For KA 1 and KA 2 equilibrium conditions were reached for PAHs starting at a K_{ow} of *FTH*. KA 2 (0.5-1 mm) with the longest column length shows the best fits for an equilibrium release assumption. KA 1 with its frequent changes in flow rates conclusively demonstrates the correlation of flow and flux rates, as fluxes closely mimic the ups and downs of the flow rates.

Small deviations of the predicted flow rates from the expected rates at late times could be due to changing saturation concentrations C_w^{sat*} , as the PAHs are constantly removed and are being depleted in the tar phase (causing changing molar fractions see Eq. 6-3). This deviating trend is revealed by the in-

creasing gap of the cumulative mass curve (adding up all deviations over time) for the late time data, whereas at early times both fluxes and masses show a good fit.

At late times in the experiment KA 3 (and to a lesser degree in KA 2) effluent concentrations dropped drastically (see Figure 6-23), even for high K_{ow} PAHs that so far showed equilibrium release. A reason for this decline can only partly lie in above mentioned changing saturation concentrations, due to changing molar fractions in the tar phase.

As the decline in effluent concentrations effects several PAHs of different K_{ow} s simultaneously (e.g. *B(a)A* and *FTH* in KA 3 and KA 2), a possible change in the mass transfer characteristics inside the tar aggregates, such as formation of diffusion limiting films, seems possible. LUTHY ET AL. (1993) observed skin-like films that developed at the coal tar-water interface and argue that mass transfer coefficients might well vary as the coal tar ages.

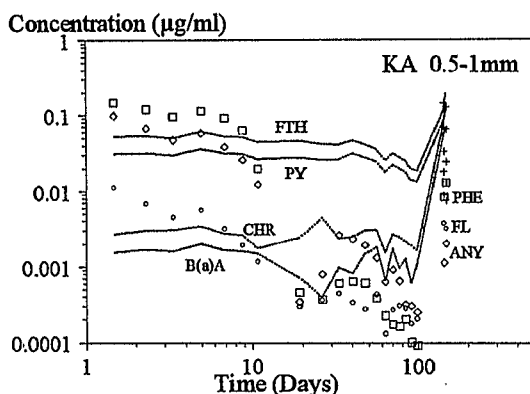
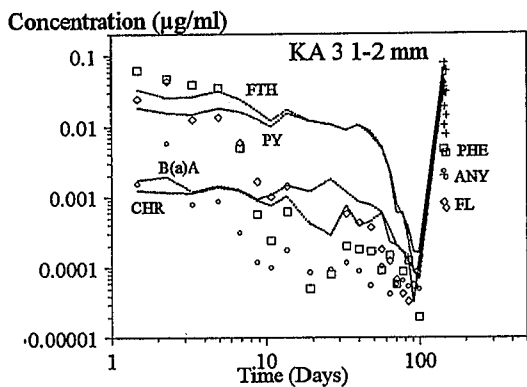


Figure 6-23: Development of effluent concentrations in KA 3 (upper frame) and KA 2 (lower frame). Dotted lines represent PAHs that establish equilibrium conditions during extended periods of time (*FTH*, *PY*, *B(a)A*, *CHR*). Open symbols denote a selection of 3 PAHs of low K_{ow} (*ANY*, *FL*, and *PHE*) which could not maintain equilibrium conditions. Crosses indicate high K_{ow} PAHs which could only be monitored during the surfactant application in final stage of the experiment. The dramatic increase of effluent concentrations at the end of KA 3 experiment is due to the application of Triton X-100 (2g/l).

Similar to previous column purge experiments, Triton X-100 was applied to experiments KA 2 and KA 3, to evaluate the effect on the release of PAHs from coal tar aggregates. Figure 6-23 shows the impact on effluent concentrations of PAHs during the application of Triton X-100 (2g/l). Measured concentrations of the effluent increased drastically. PAHs that had dropped below the detection limit in KA 3 early in the experiment could be monitored again (e.g. *ACE*) and high K_{ow} compounds that could not be monitored prior to the surfactant application (e.g. *BP*, *IP*, *(D(a,h)A)*) were detected (see Figure 6-23).

The effluent however, was clouded, indicating the removal of fines from the columns, due to the dispersing qualities of

the surfactant. The high removal rates are therefore attributed to the extraction of fine particles in the cyclohexane phase, rather than the increased solubility of PAHs due to micellar effects. The appearance of high concentrations of PAHs of very high octanol/water partition coefficients (indicated by crosses in the Fig. 6-23) can also serve as an indication of the extraction of fines, as the corresponding concentrations more soluble PAH, is less pronounced, as they are depleted. However, as the solubilizing effect of surfactants is the more pronounced the more hydrophobic a compound is, a similar effect could also occur without a mobilization of fines.

In order to better understand long-term release from and the effect of surfactants on residual coal tar phase however, specially designed experiments need to be performed.

6.2.2.2 Nonequilibrium PAH Release from KA Material

Saturation distances are controlled by a combination of factors such as flow velocity, transfer rates, and tar/water interfacial area. The superimposed effects of all these factors determine, whether the effluent leaving a contaminated domain (column) reaches saturation. In order to reach distinct non-equilibrium conditions in an experiment, it is necessary to reduce the contact time of the aqueous phase and the residual organic phase. This scenario was mimicked by purging a column, in which hand-picked coal tar aggregates (1-2 mm) were packed at the far end of a column, so that the saturation length was minimal (approx. 3 mm) and the distribution of the aggregates, in contrast to the mixed bulk material, was not dispersed between aquifer material over the column length (KA 4).

In order to investigate the effects of changing flow conditions, the flow rates were reduced by approx. one order of magnitude. Effluent concentrations did not reach equilibrium conditions even for high K_{ow} PAHs as in experiments KA 1-3 and were well below saturation. As flow rates were reduced, the effluent concentrations continuously increased

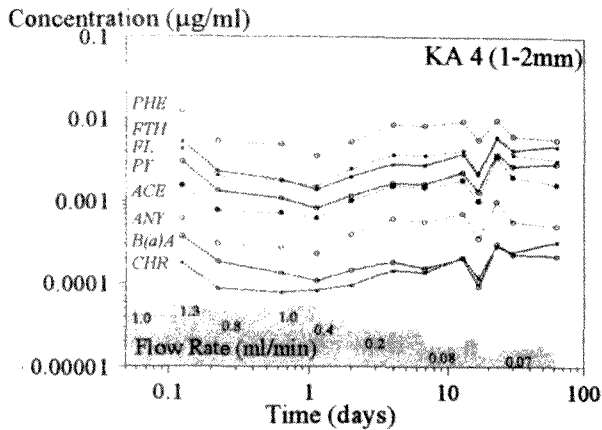


Figure 6-24: Development of effluent concentrations over 63 days. As flow rates are reduced the concentrations show an inverse trend, indicating that mass transfer occurs under nonequilibrium conditions.

(see Fig. 6-24). These increasing effluent concentrations rule out a process equivalent to an intraparticle release of PAHs from the tar aggregates (where concentrations are expected to decrease with time and are independent of flow velocities). It is, however, in accordance with the view of increasing contact time between the aqueous phase and the residual NAPL, which leads to higher degree of saturation in the effluent (see Fig. 6-24). POWERS (1992) found similar interactions of aqueous flow velocities and effluent concentrations for the release of entrapped NAPL phase.

The instantaneous changes in flow rates can be interpreted in terms of reduced film thicknesses at higher flow rates (see Chap. 3.3), causing a higher gradient (Eq. 3-24) at the tar/water interface and a consequent decline

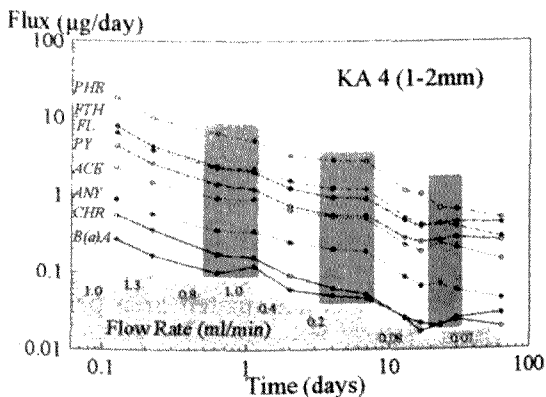


Figure 6-25: Plot of contaminant fluxes of several PAHs vs. time. As flow rates are decreased during the experiment the fluxes show concomitant drops in removal rates. Fluxes in the shaded area are used to evaluate the correlation between flow rate and contaminant release.

of contaminant fluxes. Fig. 6-25 shows the down-stepping contaminant fluxes immediately after a change in flow velocities, with a subsequent consolidation of the fluxes at a lower (constant) level. Film thicknesses could however not be determined, as the tar/water interface was unknown.

The relative increases in contaminant fluxes do not follow a linear trend as the velocities are reduced (as required by the equilibrium assumption), but show higher decreases at low flow rates. EBERHARDT (1995) found similar relations for column experiment with coal tar. The relative flux increases observed are also on the same order of magnitude as those observed by EBERHARDT (1995) (see Tab. 6-4).

The relative changes in release rates with respect to flow velocities for KA 4 are plotted in Fig. 6-26, where fluxes and flow rates are normalized with respect to the lowest flow rates, corresponding to 0.07 ml/min. The data used for the correlation are found in the shaded domains of the flux vs. time plot of Fig. 6-25 and were selected from sections, where flow rates remained constant for a respective flow velocities.

Mass transfer coefficients for film diffusion (in contrast to those of intraparticle diffusion) are dependent on the flow conditions in an observed system (e.g. column experiment). Correlations for their estimation are generally presented in terms of the dimensionless Sherwood number (POWERS, 1992) which is defined as

Table 6-4: Relative increase in PAH release rates with respect to relative increases in flow rates. (# = Data from EBERHARDT, 1995).

PAH	Relative Increases in Flowrates			
	3	14	2 [#]	8 [#]
ANY	3	5.4	2.7	3.2
ACE	2.2	4.0	1.7	2.6
FL	2.9	5.59	2.1	2.9
PHE	4.2	8.6	2.6	3.0
FTH	2.1	5.0	2.0	5.1
PY	2.0	4.8	2.1	5.8
B(a)A	2.0	5.0	1.9	4.7
CHR	2.5	7.4	3.0	6.2

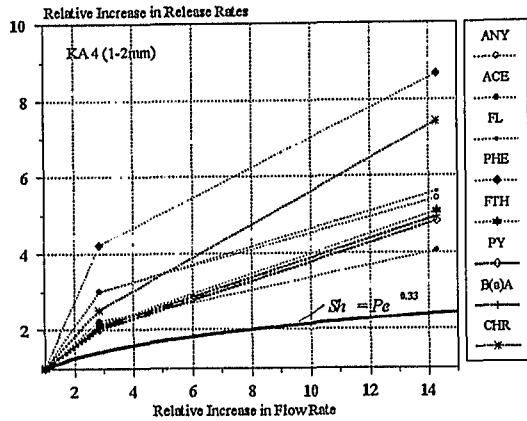


Figure 6-26: Plot of the relative release rates vs. relative flow rates. As the flow velocity is decreased the release rates of the various PAHs drop. The relative changes however do not follow a linear trend as expected by the equilibrium assumption.

$$Sh = \frac{K_L l}{D} \quad (6-4)$$

with K_L , the mass transfer coefficient [LT^{-1}], l , a characteristic length [L] and D the diffusion coefficient of a compound in water [L^2T^{-1}].

Mass transfer coefficient correlations have been derived for certain particular flow systems (see POWERS, 1991). For the release of compounds from solid spheres several authors empirically arrived at correlations in the form of

$$Sh = a + b Pe^{0.33} \quad (6-5)$$

where a and b are empirical constants and Pe is the dimensionless Peclet number, defined as

$$Pe = \frac{v l}{D} \quad (6-6)$$

where v is the pore velocity [LT^{-1}], D is the aqueous diffusion coefficient [LT^{-2}], and l a characteristic length [L].

If similar correlations hold true for the column experiment KA 4, the effluent PAH fluxes should be correlated to the increase of the flow rate to the power of 1/3. Expressing the mass transfer coefficient in terms of Sherwood numbers (solving Eq. 6-4 for K_L) the flux can be expressed as

$$F = \frac{Sh D}{l} \Delta C \quad (6-7)$$

Figure 6-26 shows the relative changes of the release rates of several PAHs with relative changes in flow velocities in the KA 4 experiment and the expected flow/flux correlation.

Although the data exhibits similar non linear trends of changing contaminant fluxes, the used correlation cannot describe the release behavior, as the data constantly plots above the expected values.

6.2.3 Summary and Discussion

Residual coal tar, as in the Karlsruhe samples, shows a clear correlation between flow velocities and PAH release rates. High velocities cause high release rates. Two different general scenarios were found. PAH release under equilibrium conditions will render max. effluent aqueous concentrations (following Raoult's Law) and the release rates accompanying changing velocities, will tend to follow this trend linearly. Whether equilibrium conditions are present depends on parameters such as the interfacial contact area of the residual coal tar and the contact time and the K_{ow} . For the monitored PAHs reaching equilibrium over extended periods of time, the available saturation distances were on the order of few centimeters. The observed flow rates correspond to 50 - 3 m/day and are in the range that can be expected in a sandy-gravel aquifer.

This indicates that already small domains contaminated with residual phase can locally cause max. concentrations for PAHs in effluent water. In such cases the total release of contaminants out of a domain containing residual coal tar depends on the transmissivity of this domain, which controls the volume of water purging the contaminated area per unit time.

In the course of the experiment the release rates show a gradual decline independent from changing flow velocities. These small deviations are assumed to be caused by changing aqueous solubilities of the

respective compound as it is depleted in the tar phase. Both processes are superimposed on each other. The external flow conditions however, are dominating the release behavior during that time.

At late times the PAH release decreased drastically. These effects affect several PAHs of different K_{ow} simultaneously, indicating changes in the tar phase which influence the transfer of PAHs from the core of the aggregate to the tar/water surface. Mass transfer from the tar phase (especially at late times) to the tar water interface appeared to introduce a second rate limiting effect on the release of PAHs.

The effect of surfactants on the release of PAHs from residual phase could not be determined, as the measured increases in effluent concentrations at the end of the experiments were due to fine particles being removed from the column.

Nonequilibrium conditions also show a correlation between fluxes and flow velocities. The PAH concentrations measured in the effluent were below the respective concentrations measured under equilibrium

conditions. The rate limiting process is considered to be film diffusion, where the release rate fluctuations are due to changing film thicknesses. Film thicknesses decrease with increasing flow velocities and the expected effective gradient changes are linearly correlated. In contrast to PAH release from the intraparticle domain, the changing film thicknesses form a flow dependent 'external resistance' to mass transfer of PAHs into the aqueous phase, which affects all PAHs alike. PAH release rates however are not linearly correlated to flow velocities. The attempt to describe the dependency of PAH mass transfer and flow conditions using dimensionless a Sherwood number approach however, could not fit the obtained data.

A contaminated domain can successively be subject to both scenarios. Time variant mass transfer coefficients of the PAHs from the residual phase and/or changing flow regimes can alter the necessary saturation length to reach saturation in the effluent concentrations. As the dimensions of the contaminated domain becomes smaller than the saturation length, the concentrations of PAHs in the collected effluent depends on the flow rate.

7. Conclusions

The desorption and release behavior of several aquifer materials containing 'aged' contaminants (PAHs sorbed on aquifer particles, as well as in residual phase) was monitored in column purge experiments. Monitoring the release rates, leads to a more realistic picture of the impact of a subsurface contamination on groundwaters and offers a means to evaluate the potential risk.

The release of PAHs into the aquatic environment is subject to diffusion limited release rates. High degrees of contaminations in the aquifer materials therefore do not necessarily lead to high contaminant concentrations in the aqueous phase, unless residual coal tar is present (saturation within short distances). Actual aqueous concentrations depend on the type of contamination (residual coal tar or sorbed constituents) and the physico-chemical properties of the contaminant, as well as of those of the aquifer material.

The observed release rates in a column purge experiments give maximum values, as the boundary conditions can be set to reach maximum concentration gradients for PAH release.

Desorption. Release of PAHs sorbed in aquifer particles can be described by a retarded spherical intraparticle diffusion model.

Desorption of PAH takes place under non-equilibrium conditions. The time scale for remediation depends on the respective desorption rate constants of the PAHs. For sorbed PAHs remediation times can reach years to decades.

Diffusion rate constants decrease with increasing octanol-water partition coefficients (growing hydrophobicity), which is in accordance to the process of retarded pore diffusion.

Sorption of PAHs on the tested natural aquifer materials appears to be completely reversible.

Speeding up remediation efforts is linked to the ability of the enhancement of diffusion coefficients and a decrease of K_d s respectively e.g. by temperature increase.

Increases in temperature cause higher diffusion rate constants. The increases in the observed rate constants are higher than expected by a mere increase due to growing aqueous diffusivity. This is likely to be due to a decrease of the K_d with increasing temperatures.

Surfactant application. Surfactant application at the end of an experiment always causes an increase in PAH fluxes. For the release of PAHs from the intraparticle domain surfactant application only temporarily caused increased release rates (possibly due to colloid mobilization). This indicates that the intraparticle domain is only partly effected by solubilizing effects of micelles as size exclusion effects limit the accessibility of intragranular porosity.

Although the combined two-site first-order/diffusion model for the prediction of PAH release will tend to oversimplify natural systems, it was able to describe the observed PAH release rates over extended periods of time. With the initial fraction of fast released PAHs (X_i) described by the first-order approach, the much more important diffusion limited long-term desorption controls the contaminant release.

Soot and coal particles. Based on measured PAH concentrations in soot and coal particles formed during carbonization processes, only a small fraction of PAHs seems to be readily available for desorption in an aqueous environment. The bulk fraction of the mass seems to be strongly associated with the particles.

Residual coal tar. Trapped in the subsurface residual coal tar can act as long-term source for groundwater contamination. Effluent concentrations in column experiments containing coal tar aggregates were found to

reach the maximum aqueous solubilities for PAHs having a K_{ow} of FTH or higher.

Saturation distances for these blobs (distance to reach max. solubilities) were found to be in the decimeter range for flow velocities that could well be expected in a sand-gravel aquifer.

The observed max. concentrations are a function of the composition of the residual phase under consideration and can be determined using Raoult's Law.

Depending on the surface/volume ratio of the tar aggregates and the column length, these equilibrium conditions could be maintained over extended periods of time.

In terms of a field interpretation, these results show that even small domains containing residual coal tar can lead to max. PAH concentrations (solubility). Release rates of PAHs from such a site, could therefore be approximated by simply determining the solubilities of the respective PAH using Raoult's Law and by determining the volumetric flow rate passing through the domain.

If nonequilibrium conditions are established, the flow conditions have a significant impact on the amount of PAHs leaving a coal tar contaminated domain. Increasing flow velocities cause a thinning out of the water film at the tar/water interface, therefore increasing the gradient across it.

Changes in PAH release by changed flow velocities are not linearly correlated. An attempt to interpret the obtained data in terms of a correlation based on literature Sherwood numbers did not lead to satisfactory results.

Observed declines in effluent concentrations at late times in the experiments, which affect all monitored PAHs simultaneously, is an indication that the residual tar phase might undergo an alteration, which results in a mass transfer limitation into the aqueous phase and can considerably decrease the release of PAHs into the aquatic environment.

Depending on flow conditions and surface/volume ratios the release of PAHs can take place under equilibrium or nonequilibrium conditions. In order to quantitatively describe PAH release from complex mixtures such as coal tar however, more detailed studies are needed to understand the complex processes involved in their release.

With respect to remediation efforts the results of this work can be summarized as follows:

Column experiments lead to a more realistic interpretation of the release characteristics of contaminated material. The obtained release rates are a conservative means to evaluate the amount of PAHs leaving a site, as the boundary conditions such as concentration gradients into the mobile phase or flow velocities can be considered to be at a maximum level. In-situ PAH release will most likely find less favorable conditions with respect to desorption and dissolution rates.

Having characterized the max. release rates under favorable conditions (max. gradient, high flow rates) makes it possible to arrive at a more meaningful interpretation of the potential risk of a site. The limited public financial resources available for remediation efforts could be spent on sites of high risk potential, and remediation efforts more efficiently be adjusted to the specific site characteristics.

8. Bibliography

- Abdul, A.S., Gibson, T.L., Rai, D.N. (1990):** Selection of Surfactants for the Removal of Petroleum Products from Shallow Sandy Aquifers.- *Ground Water*, 28 (6): 920-926.
- Anders, T. (1995):** Extraktion PAK-haltiger Bodenproben mit überkritischem CO₂.- Diplomarbeit, Geologisches Institut der Universität Tübingen: 54.
- Bahr, J.M., Rubin, J. (1987):** Direct Comparison of Kinetic and Local Equilibrium Formulations for Solute Transport Affected by Surface Reactions.- *Wat. Res. Res.*, 32 (3): 438-452.
- Ball, W.P., Roberts, P.V. (1991, a):** Long-Term Sorption of Halogenated Organic Chemicals by Aquifer Material. 1. Equilibrium.- *Environ. Sci. Technol.*, 25 (7): 1223-1237.
- Ball, W.P., Roberts, P.V. (1991, b):** Long-Term Sorption of Halogenated Organic Chemicals by Aquifer Material. 2. Intraparticle Diffusion.- *Environ. Sci. Technol.*, 25 (7): 1237-1249. -
- Bjørseth, A. (1983):** Handbook of Polycyclic Aromatic Hydrocarbons.- Marcel Dekker, Inc., New York: 727.
- Brown, M.S. Burris, D.R. Cherry, J.A., Mackay, D. (1992):** Enhancement of Organic Contaminant Retardation by the Modification of Aquifer Material with Cationic Surfactants.-In: Subsurface Restoration, Third International Conference on Groundwater Quality Research, June 21-24,1992, Dallas: 194-196.
- Brunauer, S., Emmett, P.H., Teller, E. (1938):** Adsorption of Gases in Multimolecular Layers.- *J. Am. Chem. Soc.*, 60: 309-319.
- Brusseau, M.L., Jessup, R.E., Rao, P.S.C. (1991):** Nonequilibrium Sorption of Organic Chemicals: Elucidation of Rate-Limitation Processes.- *Environ. Sci. Technol.*, 25 (1): 134-142.
- Brusseau, M.L., Jessup, R.E., Rao, P.S.C. (1992):** Modeling Solute Transport Influenced by Multiprocess Nonequilibrium and Transformation Reactions.- *Wat. Res. Res.*, 28 (1): 175-182.
- Brusseau, M.L. (1992):** Rate-Limited Mass Transfer and Transport of Organic Solutes in Porous Media That Contain Immobile Immiscible Organic Liquid.- *Wat. Res. Res.*, 28 (1): 33-45.
- Brusseau, M.L. (1993):** The Influence of Solute Size, Pore Water Velocity, and Intraparticle Porosity on Solute Dispersion and Transport in Soil.- *Wat. Res. Res.*, 29 (4): 1071-1080.
- Burris, D.R., Antworth, C.P. (1992):** In Situ Modification of an Aquifer Material by a Cationic Surfactant to Enhance Retardation of Organic Contaminants.- *J. Cont. Hydrol.*, (10): 325-337.
- Caroll, K.M., Harkness, M.R. Bracco, A.A., Balcarcel, R.R. (1994):** Application of a Permeant/Polymer Diffusional Model to the Desorption of Polychlorinated Biphenyls from Hudson River Sediments.- *Environ. Sci. Technol.*, 28 (2): 253-258.
- Chantong, A., Massoth, F.E. (1983):** Restrictive Diffusion in Aluminas.- *AIChE Journal*, 29 (5): 725-731.
- Chiou, C.T., Porter, P.E., Schmedding, D.W. (1983):** Partition Equilibria of Nonionic Organic Compounds Between Soil Organic Matter and Water.- *Environ. Sci. Technol.*, 17 (4): 227-231.
- Connaughton, D.F. Stedinger, J.R. Lion, L.W., Shuler, M.L. (1993):** Description of Time-Varying Desorption Kinetics: Release of Naphthalene from Contaminated Soils.- *Environ. Sci. Technol.*, 27 (12): 2397-2403.
- Crank, J. (1975):** The Mathematics of Diffusion.- 2nd Edition, Clarendon Press, Oxford, London: 414.

- Domenico, P.A., Schwartz, F.W. (1990):** Physical and Chemical Hydrogeology.- John Wiley & Sons, New York: 824.
- Eberhardt, C. (1995):** Freisetzung von polyzyklischen aromatischen Kohlenwasserstoffen aus Teer und Teer und Creosot.- Diplomarbeit, Geologisches Institut der Universität Tübingen: 74.
- Farrell, J. (1993):** Desorption Equilibrium and Kinetics of Chlorinated Solvents on Model Solids, Aquifer Sediments, and Soil.- Ph.D.Dissertation, Department of Civil Engineering, Stanford University: 190.
- Fetter, C.W. (1993):** Contaminant Hydrogeology.- Macmillan Publishing Company, New York: 458.
- Frank, H., Evans, M. (1945):** Free Volume and Entropy in Condensed Systems. III. Mixed Liquids.- *J. Chem. Phys.*, 13: 507-532.
- Fountain, J.C. (1992):** Field Tests of Surfactant Flooding.- In: Sabatini & Knox (Eds.) Transport and Remediation of Subsurface Contaminants, *ACS Symposium Series 491*: 182-194.
- Freeze, A.R., Cherry, J.A. (1979):** Groundwater.- Prentice-Hall Inc., Englewood Cliffs, New York: 604.
- Freudenthal, R.I., Jones, P.W. (1978):** Carcinogenesis- A Comprehensive Survey, Vol.1.- Raven Press, New York: 1978.
- Freundlich, H. (1903):** Kapillarchemie.- Leipzig, Akademische Verlagsgesellschaft m.b.H.: 591.
- Gewald, T. (1995):** Der Einfluß der Desorptionskinetik bei der Freisetzung von Trichlorethen (TCE) aus verschiedenen Aquifersanden.- *Tübinger Geowissenschaftliche Arbeiten (TGA) Reihe C (in print)*
- Grathwohl, P. (1989):** Verteilung unpolarer organischer Schadstoffe in der ungesättigten Bodenzone am Beispiel leichtflüchtiger chlorierter Kohlenwasserstoffe - Modellversuche.- *Tübinger Geowissenschaftliche Arbeiten (TGA) Reihe C, Nr.1*: 102.
- Grathwohl, P., Farrell, J., Reinhard, M. (1990):** Desorption Kinetics of Volatile Organic Contaminants from Aquifer Materials.- In: Arendt, F., Hinsenveld, M., van den Brink, W.J. (Eds.): Contaminated Soil '93, Kluwer Academics: 343-350.
- Grathwohl, P. (1990):** Influence of Organic Matter from Soils and Sediments from Various Origins on the Sorption of Some Chlorinated Aliphatic Hydrocarbons: Implications on K_{OC} Correlations.- *Environ. Sci. Technol.*, 24 (11): 1687-1693.
- Grathwohl, P. (1992):** Persistence of Contaminants in Soils and Sediments Due to Diffusion-Controlled Desorption.- In: Proceedings of the International Symposium on Environmental Contamination in Central and Eastern Europe: 604-606.
- Grathwohl, P., Gewalt, T., Pyka W., Schüth, C. (1993):** Gefährdung des Grundwassers durch Elution organischer Schadstoffe aus kontaminierten Erdreich.- Zwischenbericht PW 92 113.
- Grathwohl, P., Reinhard, M. (1993):** Desorption of Trichloroethylene in Aquifer Material: Rate Limitation at the Grain Scale.- *Environ. Sci. Technol.*, 27 (12): 2360-2366.
- Grathwohl, P., Pyka, W., Merkel, P. (1994):** Desorption of Organic Pollutants (PAHs) from Contaminated Aquifer Material.- In Dracos, T.H., Stauffer, F.(Eds.): Proceedings of the IAHR/AIRH Symposium on Transport and Reactive Processes in Aquifers Zürich: 469-474.
- Grathwohl, P., Kleineidam, S. (1995):** Impact of Heterogeneous Aquifer Materials on Sorption Capacities and Sorption Dynamics of Organic Contaminants. In Kovar, K., Krasny, J. (Eds.): Groundwater Quality: Remediation and Protection, Prague 15-18 May 1995, IAHS Publ. No. 225:79-86.
- Gregg, S.J., Singh, K.S.W. (1982):** Adsorption, Surface Area and Porosity.- 2nd Edition, Academic Press, New York: 303.

- Grimmer, G. (1985):** Vorkommen, Analytik und Bedeutung der PAH als Umweltcarcinogene.- Erdöl und Kohle - Ergas - Petrochemie vereinigt mit Brennstoff-Chemie, 38 (7): 310-314.
- Gutsche, H., Heike, T. (1990):** Altlasten auf ehemaligen Gaswerksgeländen - Einführung in die Problematik.- In: Altlasten auf ehemaligen Gaswerksgeländen - Probleme und Lösungen.- DVGW-Symposium am 9. und 10. März 1989 in Karlsruhe. *DVGW Schriftenreihe Gas* (45): 7-16.
- Harmon, T.C. (1992):** Determining and Modeling Diffusion-Limited Desorption Rates in Heterogeneous Aquifer Solids.- Ph.D Dissertation, Department of Civil Engineering, University of Stanford: 274.
- Harmon, T.C., Roberts, P.V. (1992):** The Effect of Equilibration Time on Batch Desorption Rate Measurements with Aquifer Particles.- Symposium on Fundamental and Applications of Adsorption Processes to Environmental Problems.
- Harmon, T.C., Roberts, P.V. (1994):** Comparison of Intraparticle Sorption and Desorption Rates for a Halogenated Alkene in a Sandy Aquifer Material.- *Environ. Sci. Technol.*, 28 (9): 1650-1660.
- Hassett, J.J., Means, J.C., Banwart, W.L., Wood, S.G. (1980):** Sorption Properties of Sediments and Energy-Related Pollutants.- *U.S. Environmental Protection Agency*, EPA-600/3-80-041.
- Hassett, J.J., Banwart, W.L. (1989):** The Sorption of Nonpolar Organics by Soils and Sediments.- In: Sawhney B.L., Brown, K. (Eds.): Reactions and Movements of Organic Chemicals in Soils.- *Soil Sci. Soc. Am. Inc., Am. Soc. of Agronomy Inc.*, Madison, Wi.:31-44.
- Hayduk, W., Laudie, H. (1974):** Prediction of Diffusion Coefficients For Nonelectrolytes in Dilute Aqueous Solutions.- *A.I.Ch.E.J.* 29 (3): 611-615.
- Herbert, M. (1992):** Sorptions- und Desorptionsverhalten von ausgewählten polyzyklischen aromatischen Kohlenwasserstoffen (PAK) im Grundwasserbereich.- *Tübinger Geowissenschaftliche Arbeiten (TGA) Reihe C, Nr.12*: 112.
- IARC (1985):** IARC Monographs on the Evaluation of the Carcinogenic Risk of the Chemicals to Humans.- Polynuclear Aromatic Compounds, Part 4, Bitumens, Coal Tars and Derived Products, Shale-Oils and Soots, Vol 35: 159.
- James, R.V., Rubin, J. (1979):** Applicability of the Local Equilibrium Assumption to Transport Through Soils of Solutes Affected by Ion Exchange. In: E.A. Jenne(Ed.): Chemical Modeling in Aqueous System.- *Am. Chem. Soc. Symp. Ser.*, (93): 225-235.
- Kärger, J., Ruthven, D.M. (1992):** Diffusion in Zeolites and other Microporous Solids.- John Wiley & Sons, Inc.: 605.
- Karickhoff, S.W., Brown, D.S., Scott, T.A. (1979):** Sorption of Hydrophobic Pollutants on Natural Sediments.- *Wat. Res. Res.*, 13: 241-248.
- Karickhoff, S.W. (1984):** Organic Pollutant Sorption in Aquatic Systems.- *J. Hydraulic. Eng., ASCE*, 10 (6): 707-735.
- Kile, D.E., Chiou, C.T. (1989):** Water Solubility Enhancements of DDT and Trichlorobenzene by Some Surfactants Below and Above the Critical Micelle Concentration.- *Environ. Sci. Technol.*, 23 (7): 832-838.
- Kleineidam, S. (1992):** Vergleichende Untersuchungen zur Sorption organischer Verbindungen in Löß, Torf und Sand am Beispiel des Trichlorethen.- Diplomarbeit, Geologisches Institut der Universität Tübingen: 41.
- Knipes, C.R., Miles, W.S., Rowland, F., Randall, L.G. (1993):** Designing a Sample Preparation Method That Employs Supercritical Fluid Extraction.- Hewlett-Packard Comp., Wilmington, DE: 134.

- Lambert, S.M., Porter, P.E., Schieferstein, H. (1965): Movement and Sorption of Chemicals Applied to the Soil.- *Weeds*, 13: 185-190.
- Lee, L.S, Rao, P.S.C., Brusseau, M.L., Ogwada, R.A. (1988): Nonequilibrium Sorption of Organic Contaminants During Flow Through Columns of Aquifer Material .- *Environ. Tox. Chem.*, 7: 779-793.
- Lee, L.S, Rao, P.S.C., Okuda, I. (1992): Equilibrium Partitioning of Polyaromatic Hydrocarbons from Coal Tar into Water.- *Environ. Sci. Technol.*, 26 (): 2110-2115.
- Lee, L.S., Hagwall, M., Delfino, J.J., Rao, P.S.C. (1992): Partitioning of Polycyclic Aromatic Hydrocarbons from Diesel Fuel into Water.- *Environ. Sci. Technol.*, 26 (): 2104-2110.
- Liedl, R. (1994): Pers. Com
- Lion, L.W., Stauffer, T.B., MacIntyre, W.G. (1990): Sorption of Hydrophobic Compounds on Aquifer Materials: Analysis Methods and the Effect of Organic Carbon.- *J.Cont.Hydrol.*, 5: 215-234.
- Liu, H., Amy, G. (1993): Modeling Partitioning and Transport Interactions Between Natural Organic Matter and Polynuclear Aromatic Hydrocarbons in Groundwater.- *Environ. Sci. Technol.*, 27 (8): 1553-1562.
- Loyek, D. (1995): Pers. Com.
- Luthy, R.G., Ramaswami, A., Ghoshal, S., Merkel, W. (1993): Interfacial Films in Coal Tar Nonaqueous-Phase Liquid-Water Systems. - *Environ. Sci. Technol.*, 27 (13): 2914-2918.
- Lyman, W.L, Reehl, W.F., Rosenblatt, D.H. (Eds.) (1990): Handbook of Chemical Property Estimation Methods: Environmental Behaviour of Organic Compounds.- 2nd Edition, Mc Graw-Hill, New York.
- Mackay, D., Roberts, P.V., Cherry, J.A. (1985): Transport of Organic Contaminants in Groundwater.- *Environ. Sci. Technol.*, 19 (5): 384-392.
- Mackay, D., Shiu, W.Y., Maijanen, A., Feenstra, S. (1991): Dissolution of Non-Aqueous Phase Liquids in Groundwater.- *J. Cont. Hydrol.*, 8: 23-42.
- Magee, B.R., Lion, L.W., Lemley A.T. (1991): Transport of Dissolved Organic Macromolecules and Their Effect on the Transport of Phenanthrene in Porous Media.- *Environ. Sci. Technol.*, 25 (2): 323-331.
- McCarty, P.E., Rheinhard, M., Rittmann, B.E. (1981): Trace Organics in Groundwater.- *Environ. Sci. Technol.*, 15 (1): 40-48.
- McGinley, P.M., Katz, L.E., Weber Jr, W.J. (1993): A Distributed Reactivity Model for Sorption by Soils and Sediments. 2. Multicomponent Systems and Competitive Effects.- *Environ. Sci. Technol.*, 27 (8): 1524-1531.
- McGroddy, S.E., Farrington, J.W. (1995): Sediment Porewater Partitioning of Polycyclic Aromatic Hydrocarbons in Three Cores from Boston Harbor, Massachusetts.- *Environ. Sci. Technol.*, 29 (6): 1542-1550.
- Means, J.C., Wood,S.G., Hassett, J.J., Banwart W.L. (1980): Sorption of Polynuclear Aromatic Hydrocarbons by Sediments and Soils.- *Environ. Sci. Technol.*, 14 (12): 1524-1528.
- Mercer, J.W., Cohen, R.M. (1990): A Review of Immiscible Fluids in the Subsurface: Properties , Models, Characterization and Remediation.- *J. Cont. Hydrol.*, (6): 107-163.
- Mercer, J.W., Cohen, R.M. (Eds.) (1993): DNAPL Site Evaluation.- C.K. Smoley.
- Mersmann, A. (1986): Stoffübertragung.- Springer, Berlin, Heidelberg, New York, Tokyo: 245.

- Meyer, V. (1979):** Praxis der Hochleistungs-Flüssigchromatographie.- Verlag Moritz Diesterweg Frankfurt a.M.
- Miller, C.T., Pedit, J.A. (1992):** Use of a Reactive Surface-Diffusion Model to Describe Apparent Sorption-Desorption Hysteresis and Abiotic Degradation of Lindane in a Subsurface Material.- *Environ. Sci. Technol.*, 26 (7): 1417-1427.
- Niimi, A.J. (1991):** Solubility of Organic Chemicals in Octanol, Triolein and Cod Liver Oil and Relationships Between Solubility and Partition Coefficients.- *Water Res.*, 25 (12): 1515-1521.
- Nishioka, M., Chang, H-C., Lee, M.L. (1986):** Structural Characteristics of Polycyclic Aromatic Hydrocarbon Isomers in Coal Tars and Combustion Products.- *Environ. Sci. Technol.*, 20 (10): 1023-1027.
- Nkedi-Kizza, P., Biggar, J.W., Selim, H.M., Van Genuchten, M. TH. Wierenga, P.J. Davidson, J.M., Nielsen, D.R. (1984):** On the Equivalence of Two Conceptual Models for Describing Ion Exchange During Transport Through an Aggregated Oxisol.- *Wat. Res. Res.*, 20 (8): 1123-1130.
- Pignatello, J.J. (1990):** Slowly Reversible Sorption Of Aliphatic Hydrocarbons in Soils. II. Mechanic Aspects.- *J. Envrion. Qual.*: 1117-1126.
- Pignatello, J.J., Ferrandino, F.J., Huang, L.Q. (1993):** Elution of Aged and Freshly Added Herbicides From a Soil.- *Environ. Sci. Technol.*, 27 (8): 1563-1571.
- Powers, S.E. (1992):** Dissolution of Nonaqueous Phase Liquids in Saturated Subsurface Systems. Ph.D. Dissertation, Environmental Engineering, University of Michigan: 180.
- Powers, S.E., Loureiro, L.M., Abriola, L.M., Weber Jr.,W.J. (1991):** Theoretical Study of the Significance of Nonequilibrium Dissolution of Nonaqueous Phase Liquids in the Subsurface Systems.- *Wat. Res. Res.*, 27 (4): 463-477.
- Pyka, W. (1994):** Freisetzung von Teerinhaltstoffen aus residualen Teerphase in das Grundwasser: Laboruntersuchungen zur Lösungsrate und Lösungsvermittlung.- *Tübinger Geowissenschaftliche Arbeiten (TGA) Reihe C, Nr.17:* 76.
- Rao, P.S.C., Hornsby, A.G., Kilcrease, D.P., Nkedi-Kizza, P. (1985):** Sorption and Transport of Hydrophobic Organic Chemicals in Aqueous and Mixed Solvent Systems: Model Development and Preliminary Evaluation.- *J. Envrion. Qual.*, 14 (3): 376-383.
- Reid, R.C., Prausnitz, J.M., Poling, B.E. (1987):** The Properties of Liquids and Gases.- 4th Edition, Mc Graw-Hill.
- Reisinger, Csaba (1995):** Vergleichende Untersuchungen zur diffusionskontrollierten Desorption von Trichlorethen aus Böden, Tonsteinen und Aquifermaterial.- Diplomarbeit, Geologisches Institut der Universität Tübingen: 65
- Rutherford, D.W., Chiou, C.T., Kile, D.E. (1992):** Influence of Soil Organic Matter Composition on the Partition of Organic Compounds.- *Environ. Sci. Technol.*, 26 (2): 336-340.
- Rosen, M.J. (1989):** Surfactants and Interfacial Phenomena. 2nd Edition.- Wiley & Sons, New York: 431.
- Sanns, M. (1990):** Experimentelle Untersuchungen zum Ausbreitungsverhalten von leichtflüchtigen Chlorkohlenwasserstoffen (LCKW) in der wassergesättigten Zone.- *Tübinger Geowissenschaftliche Arbeiten (TGA) Reihe C, Nr.5:* 121.
- Schüth, C. (1994):** Sorptionskinetik und Transportverhalten von polyzyklischen aromatischen Kohlenwasserstoffen (PAK) im Grundwasser - Laborversuche.- *Tübinger Geowissenschaftliche Arbeiten (TGA) Reihe C, Nr.19:* 80.

- Schüth, C., Grathwohl, P.: Nonequilibrium Transport of PAHs in Groundwater. 1. Longterm Sorption Kinetics (submitted *Environ. Sci. Technol.*).
- Schwarzenbach, R. P., Westall, J. (1981): Transport of Nonpolar Organic Compounds from Surface Water to Groundwater- Laboratory Sorption Studies.- *Environ. Sci. Technol.*, 15 (11): 1360-1367.
- Schwarzenbach, R. P., Gschwend, P.M., Imboden, D.M. (1993): Environmental Organic Chemistry.- John Wiley & Sons Inc, New York: 681.
- Severson, R.F, Snook M.E., Howard, H.C., Chortyk, O.T., Akin, F.J. (1976): Isolation, Identification, and Quantification of Polynuclear Aromatic Hydrocarbons in Tobacco Smoke.- In: Freudenthal & Jones (Eds.): Carcinogenesis- A Comprehensive Survey Vol.1,- Raven Press, New York: 253-269.
- Shiau, B.J., Sabatini, D.A., Gupta, A., Harwell, J.H. (1991): Enhanced Solubilization and Mobilization of Subsurface DNAPL Contamination Using Edible Surfactants.-In: Subsurface Restoration. Third International Conference on Groundwater Quality Research, June 21-24, 1992, Dallas: 266-268.
- Sontheimer, H., Cornel, P., Seym, M. (1983): Untersuchungen zur Sorption von aliphatischen Chlorkohlenwasserstoffen durch Böden aus Grundwasserleitern.- Veröffentl. des Ber. und Lehrstuhls für Wasserchemie und DVGW- Forschungsstelle am Engler Bunte Institut, Karlsruhe, 21: 1-46
- Steinberg, S.M., Pignatello, J.J., Sawhney, B.L. (1987): Persistence of 1,2-Dibromethane in Soils: Entrapment in Intraparticle Micropores.- *Environ. Sci. Technol.* 21 (12): 1201-1208.
- Steiner, D., Burtscher, H.K. (1994): Desorption of Perylene from Combustion, NaCl, and Carbon Particles.- *Environ. Sci. Technol.*, 28 (7): 1254-1259.
- Vallocchi, A.J. (1985): Validity of the Local Equilibrium Assumption for Modelling Sorbing Solute Transport Through Homogeneous Soils.- *Wat. Res. Res.*, 21 (6): 808-820.
- Voice, T.C., Weber Jr, W.J. (1983): Sorption of Hydrophobic Compounds by Sediments, Soils and Suspended Solids - I. Theory and Background.- *Water Res.*, 17 (10): 1433-1441.
- Walz, A. (1994): Erfassung der ubiquitären Bodenbelastung durch polycyclische aromatische Kohlenwasserstoffe in der Umgebung eines ehemaligen Gaswerksgeländes.- Diplomarbeit, Geologisches Institut der Universität Tübingen: 73.
- Weber Jr, W.J., McGinley, P.M., Katz, L.E. (1991): Sorption Phenomena In Subsurface Systems: Concepts, Models and Effects on Contaminant Fate and Transport.- *Water Res.*, 25 (5): 499-528.
- Weber Jr., W.J., McGinley, P.M., Katz, L.E. (1992): A Distributed Reactivity Model for Sorption by Soils and Sediments. 1. Conceptual Basis and Equilibrium Assessments.- *Environ. Sci. Technol.*, (26): 1955-1962.
- Wilhelm, T. (1992): Säulenexperiment zum Transport von Teeröl in Phase und zur Elution von Teerinhaltstoffen.- Diplomarbeit, Geologisches Institut der Universität Tübingen: 56.
- Wu, S.C., Gschwend, P.M. (1986): Sorption Kinetics of Hydrophobic Organic Compounds to Natural Sediments and Soils.- *Environ. Sci. Technol.*, 20 (7): 717-725.
- Yalkowski, S.H., Pinal, R. (1993): Estimation of the Aqueous Solubility of Complex Compounds.- *Chemosphere*, 26 (7): 1239-1261.
- Young, D.F., Ball, W.P. (1993): Intraparticle Diffusion During Tetrachloroethene Transport Through Aquifer Material: A Priori Prediction of Column Behaviour from Batch Data.- *Environmental Progress*,
- Zander, M. (1980): Polycyclic Aromatic and Heteroaromatic Hydrocarbons.- In: Hutzinger, O.(Ed.): The Handbook of Environmental Chemistry, Vol. 3, Part A, Springer Verlag, Berlin: 109-131.

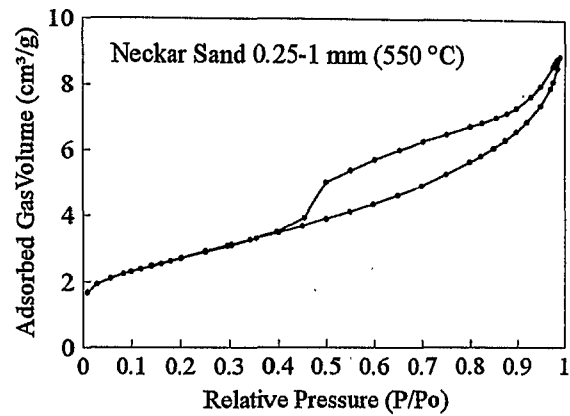
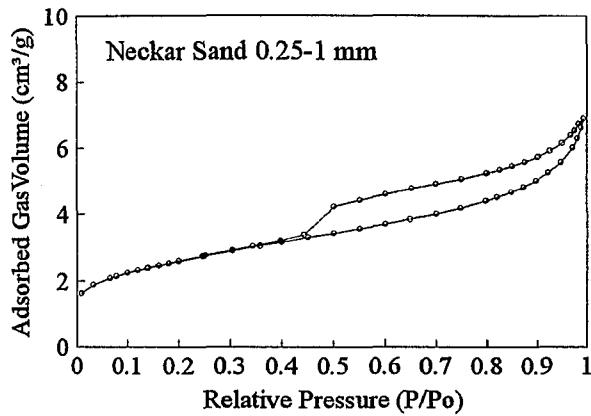
APPENDIX I

Complete Listing of HPLC Methods Used for PAH Quantification

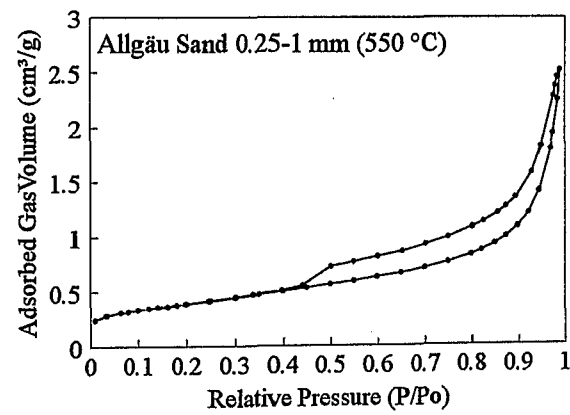
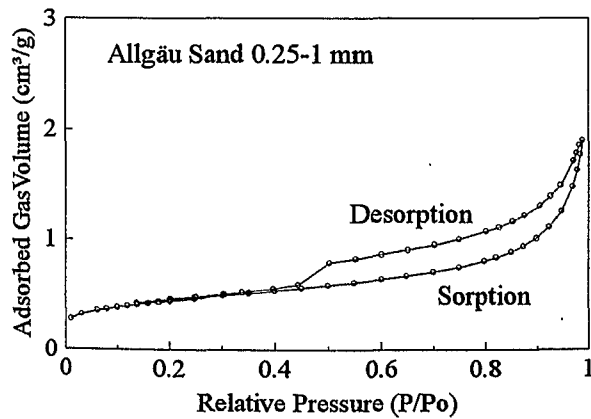
Method 1 6 PAHs			
Internal Standard: Benzo (b) naphtho(2,1-d) thiophene		Gradient: non-isocratic	H ₂ O / Acetonitrile:30/70-0/100
Runtime: 25 min		Injection Volume: 20 µl	
Wavelength (nm)	Extinction	Emission	
Naphthalene	275	350	
Fluorene	275	350	
Phenanthrene	275	350	
Fluoranthene	284	463	Used for complex mixtures of contaminated aquifer material
Benzo (a) anthracene	286	387	
Benzo (k) fluoranthene	305	403	
Int. Standard	234	366	
UV detection	254		
Method 2 Naphthalene			
Internal Standard : Phenanthrene		Gradient: isocratic	H ₂ O / Acetonitrile: 30/70
Runtime: 9 min		Injection Volume: 5 µl	
Wavelength	Extinction	Emission	
Naphthalene	278	324	
Phenanthrene	249	345	Used for spiked samples
Method 3 Fluoranthene			
Internal Standard : Phenanthrene		Gradient: isocratic	H ₂ O / Acetonitrile: 30/70
Runtime: 9 min		Injection Volume: 20 µl	
Wavelength	Extinction	Emission	
Phenanthrene	249	345	
Fluoranthene	249	345	Used for spiked samples
Method 4 16 EPA PAHs			
Internal Standard (-)		Gradient : non isocratic	H ₂ O/Acetonitrile:50/50-0/100
Run Time: 35 min		Injection Volume: 20 µl	
Wavelength (nm)	Extinction	Emission	
Naphthalene	278	324	
Acenaphthylene	*	*	* Acenaphthylene cannot be analyzed using a fluorescent detector
Acenaphthene	290	320	
Fluorene	290	320	
Phenanthrene	245	370	
Anthracene	245	370	
Fluoranthene	332	420	
Pyrene	332	420	
Benzo(a)anthracene	255	403	
Chrysene	255	403	
Benzo(b)fluoroanthene	270	455	Used for samples from Soxhlet extractions
Benzo(k)fluoranthene	270	455	
Benzo(a)pyrene	270	455	
Dibenzo(ah)anthracene	290	430	
Benzo(ghi)perylene	290	430	
Ideno(123-cd)pyrene	300	500	

APPENDIX II

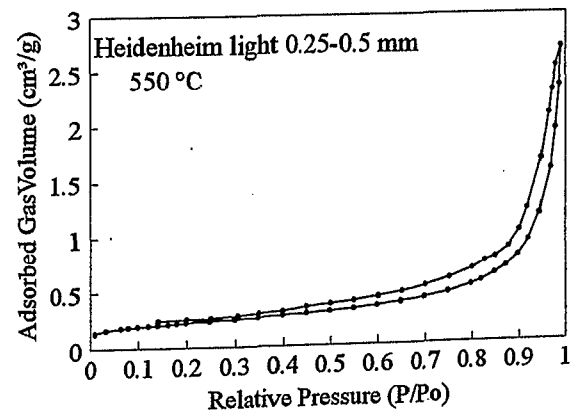
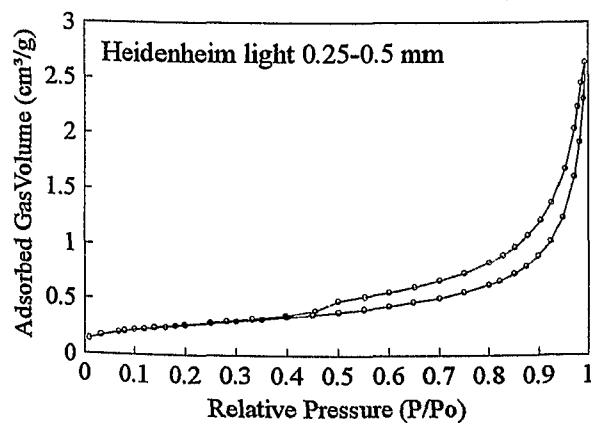
N_2 BET Isotherms for Neckar Sand (0.25-1mm)



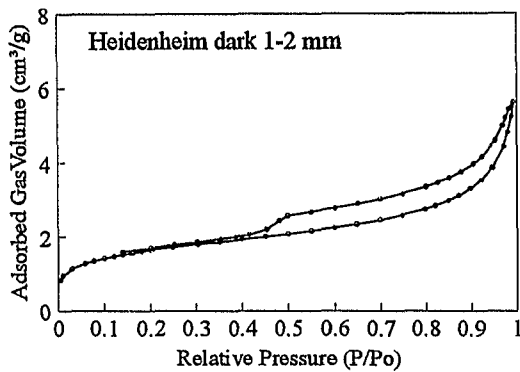
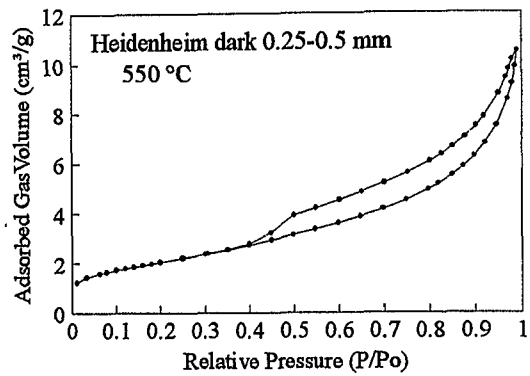
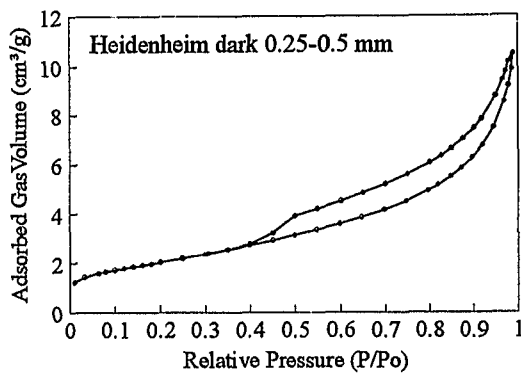
N_2 BET Isotherms for Allgäu Sand (0.25-1mm)



N_2 BET Isotherms for Heidenheim (light) (0.25-0.5mm)

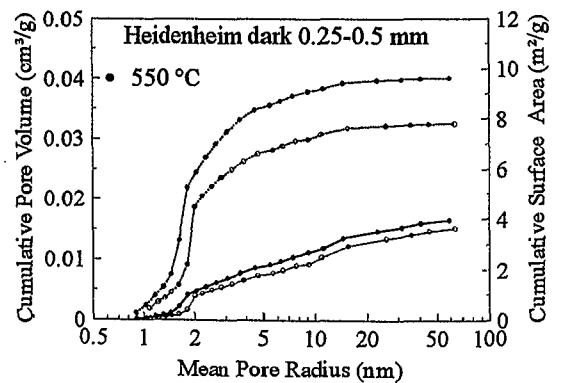
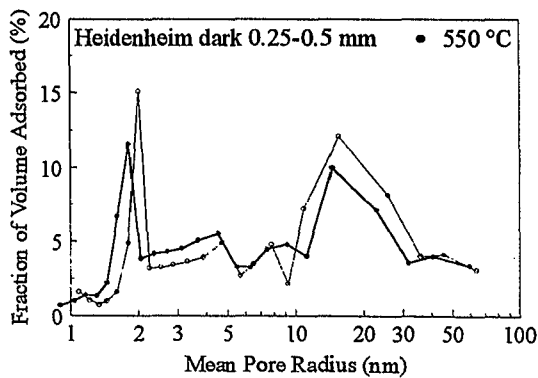


N₂ BET Isotherms for Heidenheim (dark) (0.25-0.5mm)

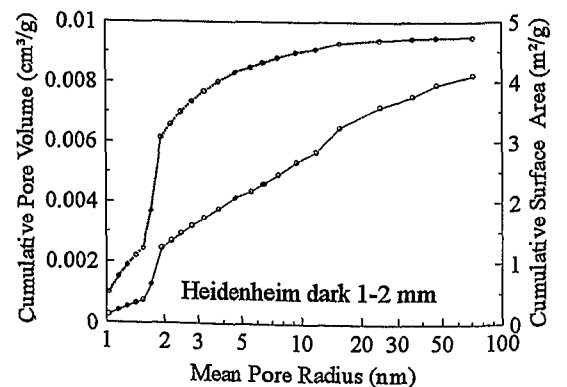
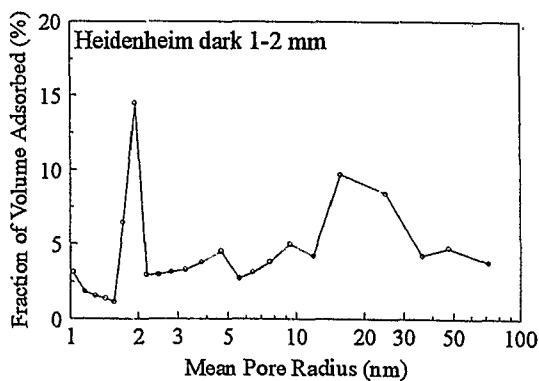


N₂ Isotherm for Heidenheim (dark) (1-2mm)

Pore Volumes/Internal Surfaces vs.Pore Radii Heidenheim dark (0.25-0.5 mm)

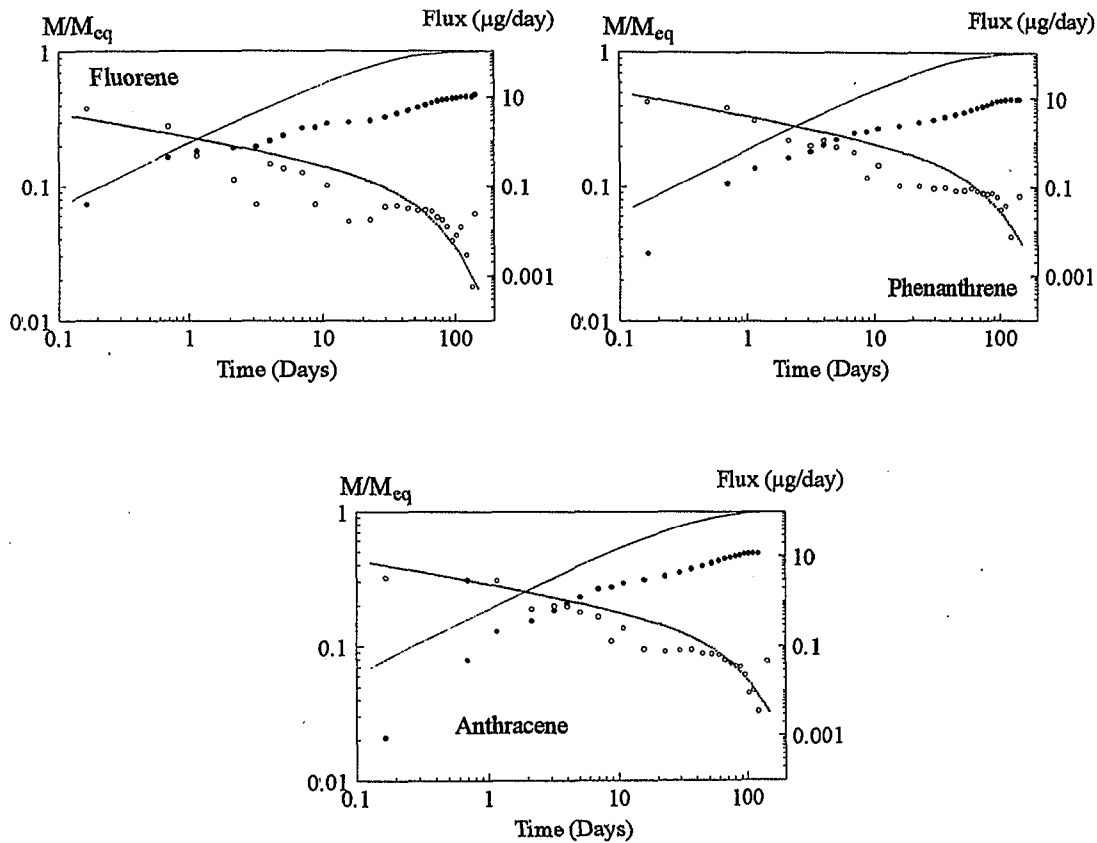


Pore Volumes/Internal Surfaces vs.Pore Radii Heidenheim dark (1-2 mm)

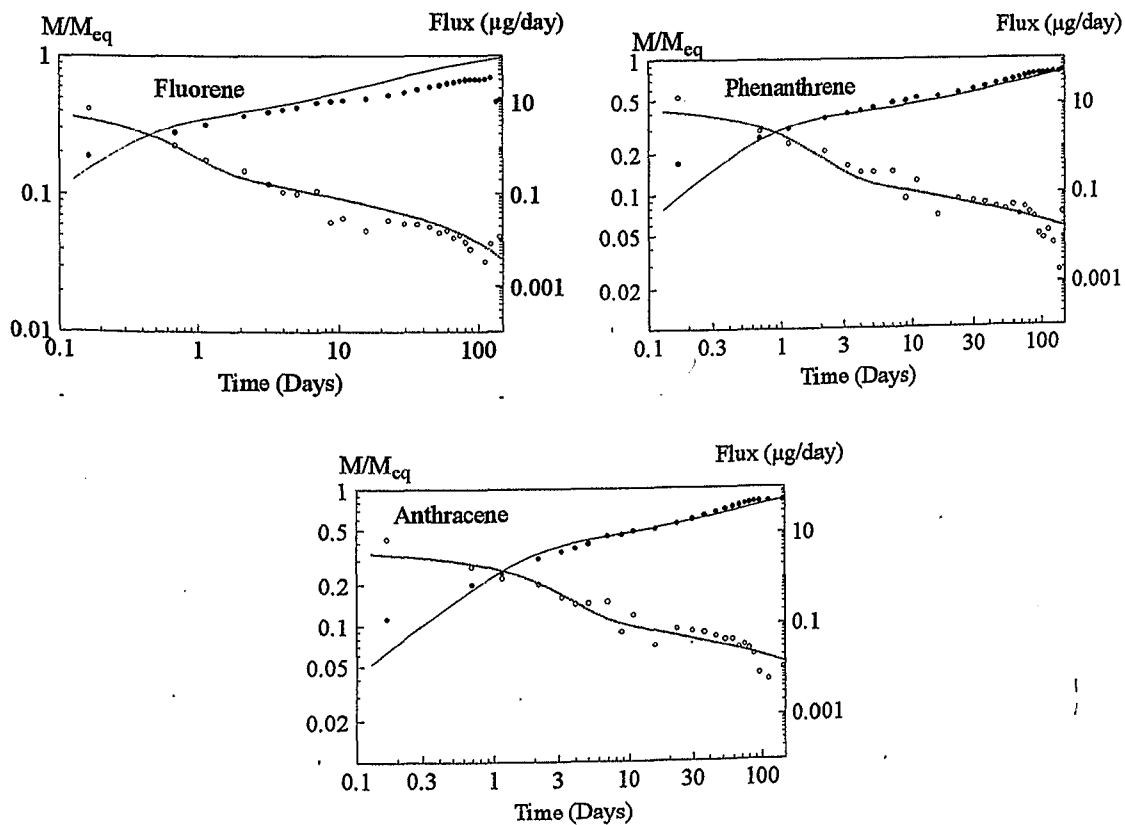


APPENDIX III

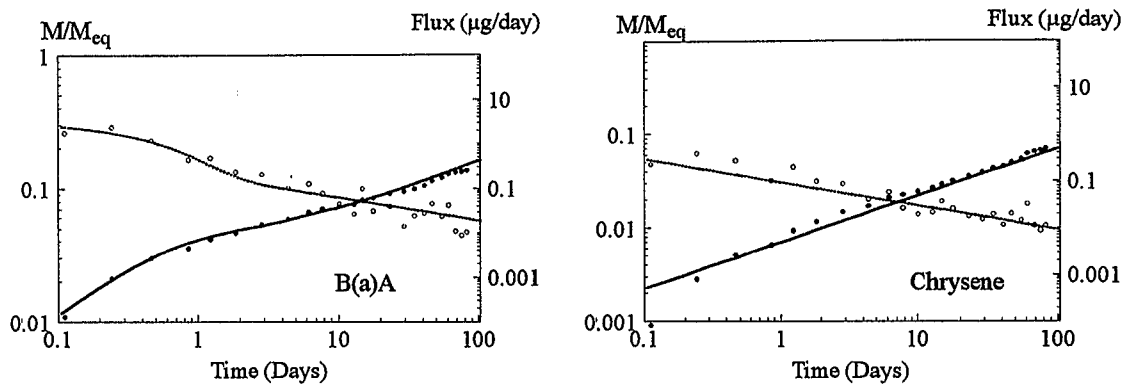
Desorption Plots of Neckar Sand 0.25-1 mm



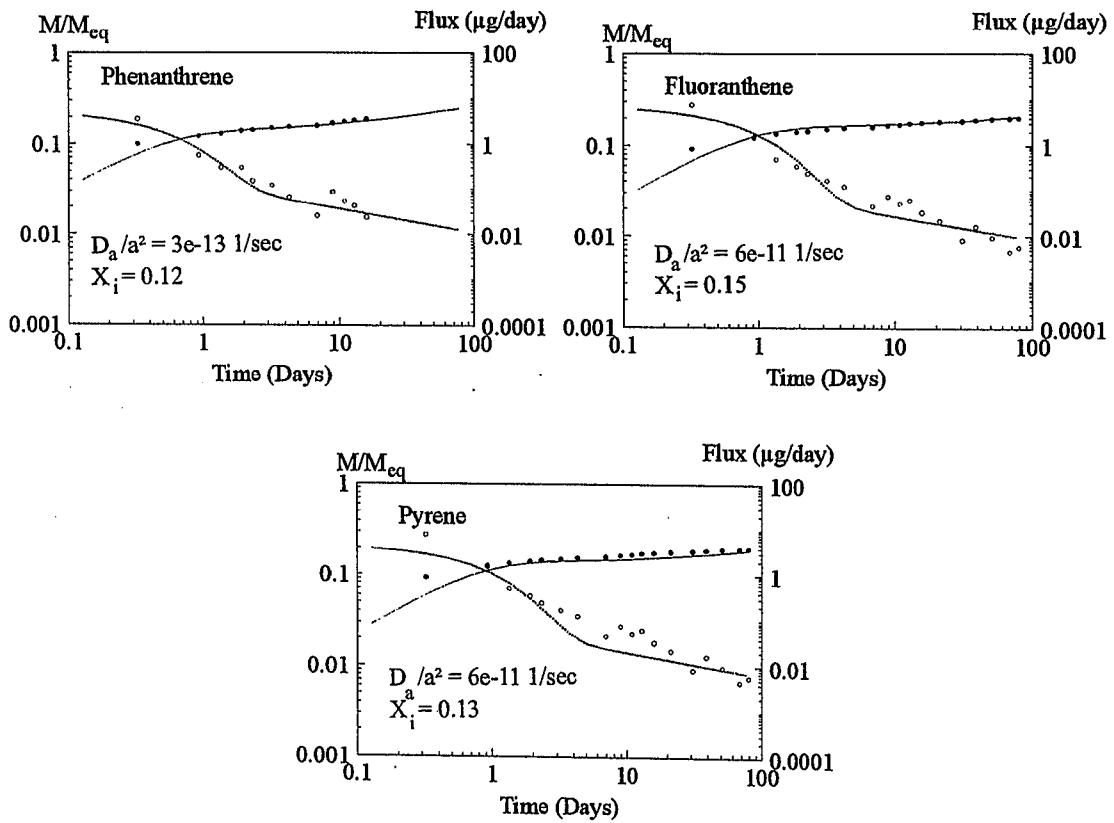
Desorption Plots of Allgäu Sand 0.25-1 mm (Experiment 1)



Desorption Plots of Allgäu Sand 0.25-1 mm (Experiment 2)



Desorption Plots of Heidenheim (light) 0.25-0.5 mm (4°C)

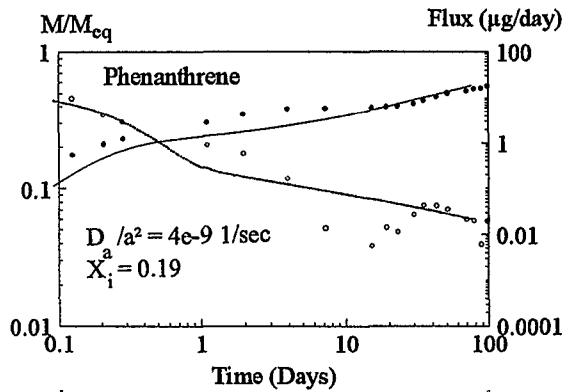


Desorption Plots of Heidenheim (light) 0.25-0.5 mm (40°C)

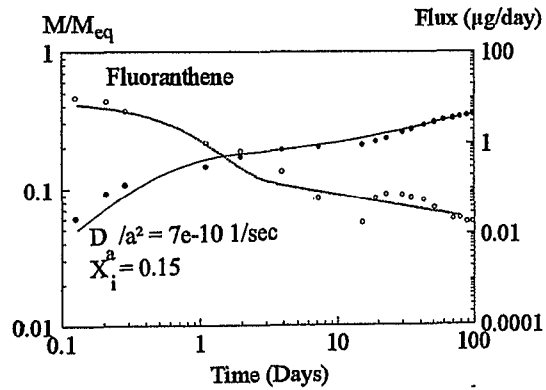
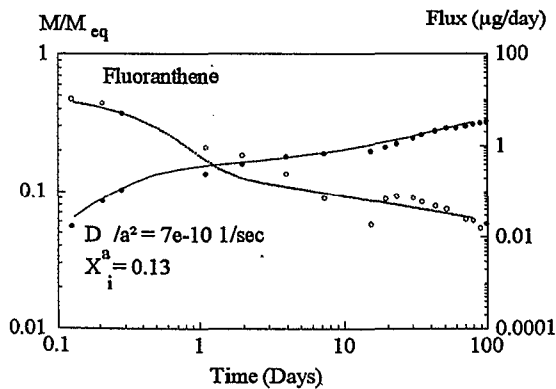
Experiment 1

Experiment 2

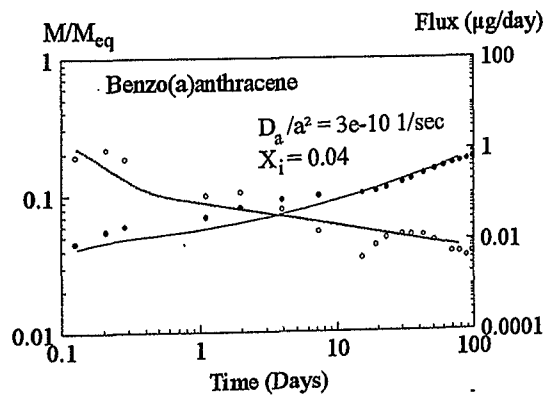
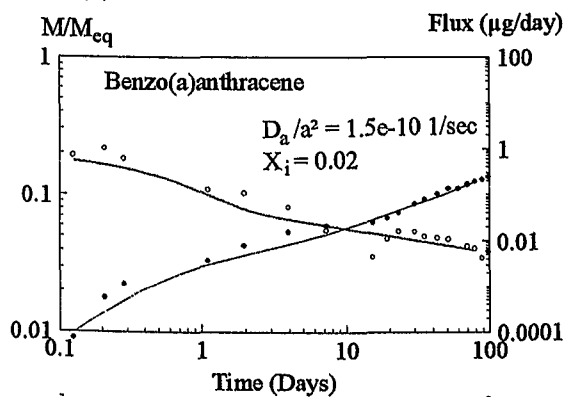
Phenanthrene



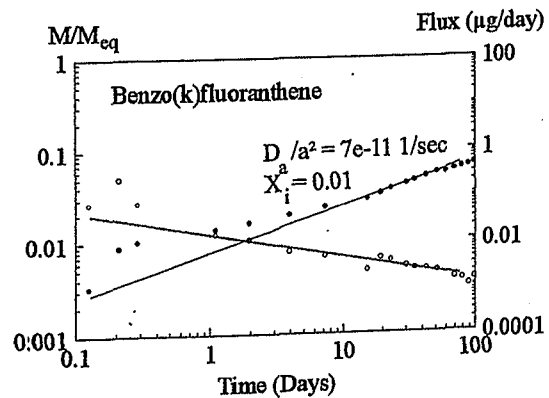
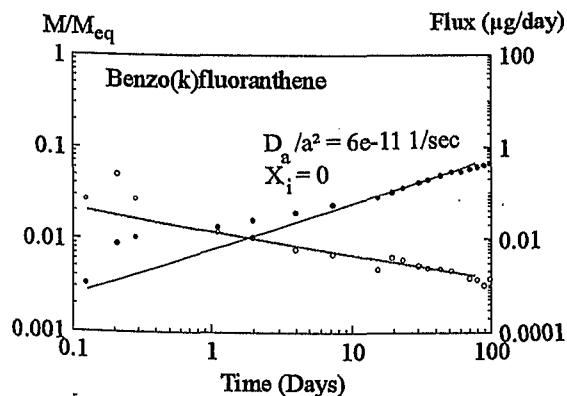
Fluoranthene



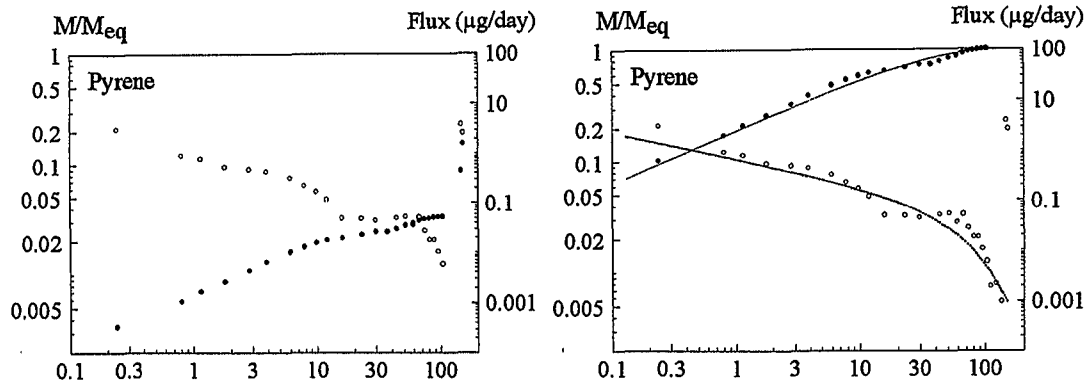
Benzo(a)anthracene



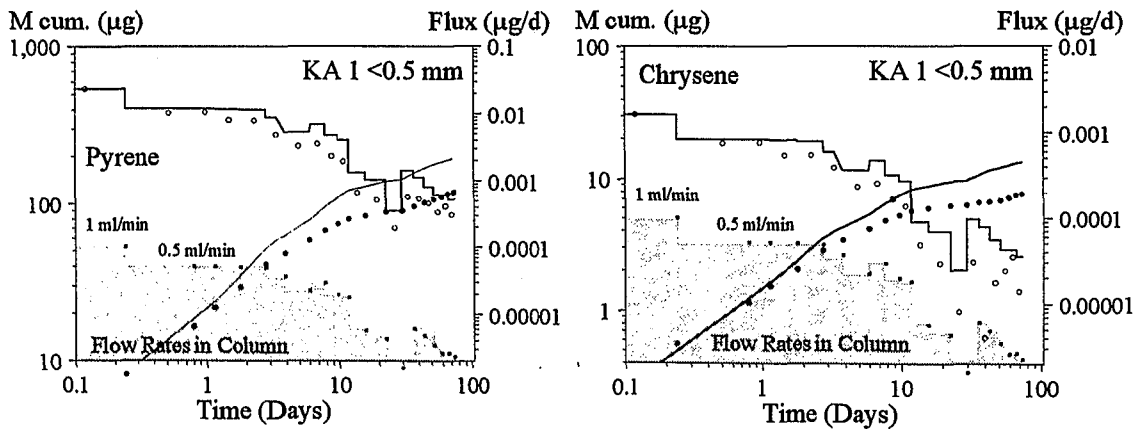
Benzo(k)fluoranthene



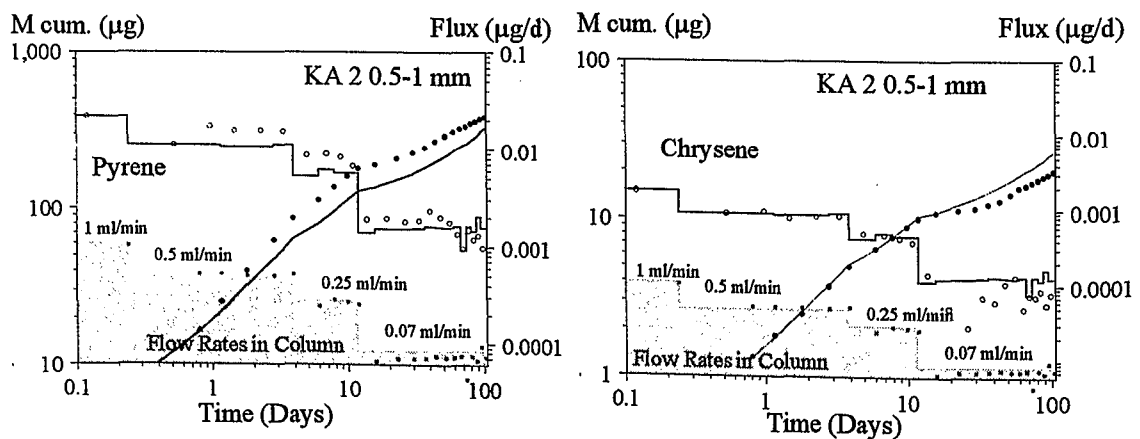
Desorption Plots of PY from HH 1-2mm (dark) Release Data (left) and Desorption Model Fit (right)



Release Plots and Concentrations Development of Karlsruhe Material (<0.5 mm)



Release Plots and Concentrations Development of Karlsruhe (0.5 -1 mm)



In der Reihe C der Tübinger Geowissenschaftlichen Arbeiten (TGA) sind bisher erschienen:

- Nr. 1: Grathwohl, Peter (1989): Verteilung unpolarer organischer Verbindungen in der wasserungesättigten Bodenzone am Beispiel der leichtflüchtigen aliphatischen Chlorkohlenwasserstoffe. 102 S.
- Nr. 2: Eisele, Gerhard (1989): Labor- und Felduntersuchungen zur Ausbreitung und Verteilung leichtflüchtiger chlorierter Kohlenwasserstoffe (LCKW) im Übergangsbereich wasserungesättigte/wassergesättigte Zone. 84 S.
- Nr. 3: Ehmann, Michael (1989): Auswirkungen atmogener Stoffeinträge auf Boden- und Grundwasser sowie Stoffbilanzierungen in drei bewaldeten Einzugsgebieten im Oberen Buntsandstein (Nordschwarzwald). 134 S.
- Nr. 4: Irouschek, Thomas (1990): Hydrogeologie und Stoffumsatz im Buntsandstein des Nordschwarzwaldes. 144 S.
- Nr. 5: Sanns, Matthias (1990): Experimentelle Untersuchungen zum Ausbreitungsverhalten von leichtflüchtigen Chlorkohlenwasserstoffen (LCKW) in der wassergesättigten Zone. 122 S.
- Nr. 6: Seeger, Thomas (1990): Abfluß- und Stofffrachtseparation im Buntsandstein des Nordschwarzwaldes. 154 S.
- Nr. 7: Einsele, Gerhard & Pfeffer, Karl-Heinz (Hrsg.) (1990): Untersuchungen über die Auswirkungen des Reaktorunfalls von Tschernobyl auf Böden, Klärschlamm und Sickerwasser im Raum von Oberschwaben und Tübingen. 151 S.
- Nr. 8: Douveas, Nikon G. (1990): Verwitterungstiefe und Untergrundabdichtung beim Talsperrenbau in dem verkarsteten Nord-Pindos-Flysch (Projekt Pigai-Aoos, NW-Griechenland). 165 S.
- Nr. 9: Schlöser, Heike (1991): Quantifizierung der Silikatverwitterung in karbonatfreien Deckschichten des Mittleren Buntsandsteins im Nordschwarzwald. 93 S.
- Nr. 10: Köhler, Wulf-Rainer (1992): Beschaffenheit ausgewählter, nicht direkt anthropogen beeinflusster oberflächennaher und tiefer Grundwasservorkommen in Baden-Württemberg. 144 S.
- Nr. 11: Bundschuh, Jochen (1991): Der Aquifer als thermodynamisch offenes System. - Untersuchungen zum Wärmetransport in oberflächennahen Grundwasserleitern unter besonderer Berücksichtigung von Quellwassertemperaturen (Modellversuche und Geländebeispiele). 100 S.
- Nr. 12: Herbert, Mike (1992): Sorptions- und Desorptionsverhalten von ausgewählten polyzyklischen aromatischen Kohlenwasserstoffen (PAK) im Grundwasserbereich. 111 S.
- Nr. 13: Sauter, Martin (1993): Quantification and forecasting of regional groundwater flow and transport in a karst aquifer (Gallusquelle, Malm, SW-Germany). 150 S.
- Nr. 14: Bauer, Michael (1993): Wasserhaushalt, aktueller und holozäner Lösungsabtrag im Wutachgebiet (Südschwarzwald). 130 S.
- Nr. 15: Einsele, Gerhard & Ricken, Werner (Hrsg.) (1993): Eintiefungsgeschichte und Stoffaustag im Wutachgebiet (SW-Deutschland). 215 S.

- Nr. 16: Jordan, Ulrich (1993): Die holozänen Massenverlagerungen des Wutachgebietes (Südschwarzwald). 132 S.
- Nr. 17: Krejci, Dieter (1994): Grundwasserchemismus im Umfeld der Sonderabfalldeponie Billigheim und Strategie zur Erkennung eines Deponiesickerwassereinflusses. 121 S.
- Nr. 18: Hekel, Uwe (1994): Hydrogeologische Erkundung toniger Festgesteine am Beispiel des Opalinustons (Unteres Aalenium). 170 S.
- Nr. 19: Schüth, Christoph (1994): Sorptionskinetik und Transportverhalten von polyzyklischen aromatischen Kohlenwasserstoffen (PAK) im Grundwasser - Laborversuche. 80 S.
- Nr. 20: Schlöser, Helmut (1994): Lösungsgleichgewichte im Mineralwasser des überdeckten Muschelkalks in Mittel-Württemberg. 76 S.
- Nr. 21: Pyka, Wilhelm (1994): Freisetzung von Teerinhaltstoffen aus residualer Teerphase in das Grundwasser: Laboruntersuchungen zur Lösungsrate und Lösungsvermittlung. 76 S.
- Nr. 22: Biehler, Daniel (1995): Kluftgrundwässer im kristallinen Grundgebirge des Schwarzwaldes - Ergebnisse von Untersuchungen in Stollen. 103 S.
- Nr. 23: Schmid, Thomas (1995): Wasserhaushalt und Stoffumsatz in Grünlandgebieten im württembergischen Allgäu. 145+ 92 S.
- Nr. 24: Kretzschmar, Thomas (1995): Hydrochemische, petrographische und thermodynamische Untersuchungen zur Genese tiefer Buntsandsteinwässer in Baden-Württemberg. 142 S.
- Nr. 25: Hebestreit, Christoph (1995): Zur jungpleistozänen und holozänen Entwicklung der Wutach (SW-Deutschland). 88 S.
- Nr. 26: Hinderer, Matthias (1995): Simulation langfristiger Trends der Boden- und Grundwasserversauerung im Buntsandstein-Schwarzwald auf der Grundlage langjähriger Stoffbilanzen. 175 S.
- Nr. 27: Körner, Johannes (1996): Abflußbildung, Interflow und Stoffbilanz im Schönbuch Waldgebiet. 206 S.
- Nr. 28: Gewalt, Thomas (1996): Der Einfluß der Desorptionskinetik bei der Freisetzung von Trichlorethen (TCE) aus verschiedenen Aquifersanden. 67 S.
- Nr. 29: Schanz, Ulrich (1996): Geophysikalische Untersuchungen im Nahbereich eines Karstsystems (westliche Schwäbische Alb). 114 S.
- Nr. 30: Renner, Sven (1996): Wärmetransport in Einzelklüften und Kluftaquiferen - Untersuchungen und Modellrechnungen am Beispiel eines Karstaquifers. 89 S.
- Nr. 31: Mohrlök, Ulf (1996): Parameter-Identifikation in Doppel-Kontinuum-Modellen am Beispiel von Karstaquiferen. 125 S.



ATTEMPTO SERVICE GmbH
Wilhelmstraße 7 · 72074 Tübingen
Telefon: 0 70 71 / 29 7 59 95 / 29 7 35 58